Electrochemical Energy Reviews (2023) 6:11
https://doi.org/10.1007/s41918-023-00181-x

REVIEW ARTICLE

Carbon-Based Electrodes for Advanced Zinc-Air Batteries: Oxygen-Catalytic Site Regulation and Nanostructure Design

Wenjie Shao[1] · Rui Yan[1] · Mi Zhou[2] · Lang Ma[3] · Christina Roth[4] · Tian Ma[1,3] · Sujiao Cao[1,3] · Chong Cheng[1,5] · Bo Yin[1] · Shuang Li[1,6]

Received: 19 April 2022 / Revised: 18 July 2022 / Accepted: 5 February 2023 / Published online: 23 March 2023

Abstract

Zn-air batteries are highly attractive for direct chemical-to-electrical energy conversion and for solving the energy crisis and environmental problems. Designing efficient oxygen electrodes has been considered one of the most critical steps in the development of advanced Zn-air batteries because of the sluggish kinetics of the oxygen reduction reaction and the oxygen evolution reaction. In recent years, nanostructured carbon-based electrodes with large surface areas, efficient oxygen-catalytic centers, and hierarchically porous matrices have provided significant opportunities to optimize the performance of the oxygen electrodes in both primary and rechargeable Zn-air batteries. In this review, we provide a comprehensive summary of the reported nanostructured carbon-based electrodes for advanced Zn-air batteries in terms of tailoring the oxygen-catalytic sites and designing carbon supports. The versatile synthetic strategies, characterization methods, and in-depth understanding of the relationships between the oxygen-catalytic sites/nanostructures and the oxygen electrode performance are systematically summarized. Furthermore, we also briefly outline recent progress in engineering flexible and high-power Zn-air batteries. Ultimately, a thorough discussion of current primary challenges and future perspectives on the rational design of nanostructured carbon-based oxygen electrodes is given, thus providing inspiration for the future prosperity of fast-kinetic and efficient Zn-air batteries in a broad range of energy fields.

Keywords Zn-air batteries · Carbon nanostructures · Electrocatalysts · Oxygen-catalytic catalysts · ORR · OER

✉ Tian Ma
matian1991@scu.edu.cn

✉ Sujiao Cao
caosujiao@scu.edu.cn

✉ Shuang Li
s.li@tu-berlin.de

[1] College of Polymer Science and Engineering, State Key Laboratory of Polymer Materials Engineering, Sichuan University, Chengdu 610065, Sichuan, China

[2] College of Biomass Science and Engineering, Sichuan University, Chengdu 610065, Sichuan, China

[3] Department of Ultrasound, West China Hospital, Sichuan University, Chengdu 610041, Sichuan, China

[4] Electrochemical Process Engineering, Engineering Sciences, University of Bayreuth, Universitätsstr. 30, 95447 Bayreuth, Germany

[5] Med-X Center for Materials, Sichuan University, Chengdu 610065, Sichuan, China

[6] Functional Materials, Department of Chemistry, Technische Universität Berlin, Hardenbergstraße 40, 10623 Berlin, Germany

1 Introduction

The ever-increasing energy consumption and related environmental concerns are driving the consistent development of electrochemical energy storage and conversion technologies [1]. Various advanced renewable electricity devices, such as primary batteries, rechargeable batteries, fuel cells, and supercapacitors, have been proposed and applied in the commercial market. Among these diverse energy devices, metal-air batteries are a kind of electrochemical device in which the electricity is produced by metal oxidation and oxygen (from air) reduction. Owing to the facile fabrication, natural abundance, favorable safety, and eco-friendliness of Zn metal, Zn-air batteries with a high theoretical energy density of 1 086 Wh kg^{-1} (fivefold larger than that of traditional lithium-ion batteries [2, 3]) have attracted increasing attention in recent years (Fig. 1a, b) [4, 5].

However, despite the advantages of Zn-air batteries, their commercialization is still hindered by several drawbacks, such as the insufficient mass transport of oxygen electrodes

and the intrinsically sluggish reaction kinetics of the oxygen evolution reaction (OER) and the oxygen reduction reaction (ORR), resulting in low cyclability of Zn-air batteries. To enhance the intrinsically sluggish kinetics, oxygen electrodes loaded with efficient oxygen catalysts are required to accelerate the ORR and/or the OER [6]. Currently, both ORR and OER catalysts are mostly based on noble metals (Pt, Ru, Ir, and so on), which usually exhibit excellent activities [7, 8]. However, their relatively low stability and high cost still hinder their large-scale application in the air cathodes of Zn-air batteries. Therefore, most reports on oxygen catalysts for Zn-air batteries have focused on designing non-noble metal–based catalytic sites with efficient and intrinsically stable catalytic activities. Furthermore, unlike the rotating disk electrode (RDE) technique used in laboratories for ORR testing, practical Zn-air batteries are susceptible to the influence of mass and air transport. Since the oxygen-catalytic reactions in Zn-air batteries generally occur at the solid (active catalysts)–liquid (electrolytes)–gas (O_2) three-phase interface, accelerating O_2 transport and enlarging their contact areas play key roles in boosting their performance [9]. Overall, the design of air cathodes with well-defined oxygen-catalytic centers and nanostructured supports is of great importance in providing a wide range of possibilities for designing advanced Zn-air batteries [10].

In recent decades, nanostructured carbon-based electrodes with enormous potentials, such as larger surface areas, efficient oxygen-catalytic centers, hierarchically porous matrices, superior durability, and low cost, were regarded as the most promising oxygen electrodes for Zn-air batteries systems [17–20]. Stimulated by the above-mentioned superiority and the necessary pursuit of structural design for carbon electrodes, several previous reviews have summarized this research field in recent years. As early as 2017, the design of a hierarchical and freestanding structured air cathode was discussed by the Shen group, with a specific emphasis on the reaction mechanism and optimization strategies of air cathodes for Zn-air batteries [9]. Later, the Zhang group reviewed fundamental studies on the structural design of oxygen catalysts in Zn-air batteries [21]. In another review, they presented the advanced progress in the atom-scale modulation and nanostructure design

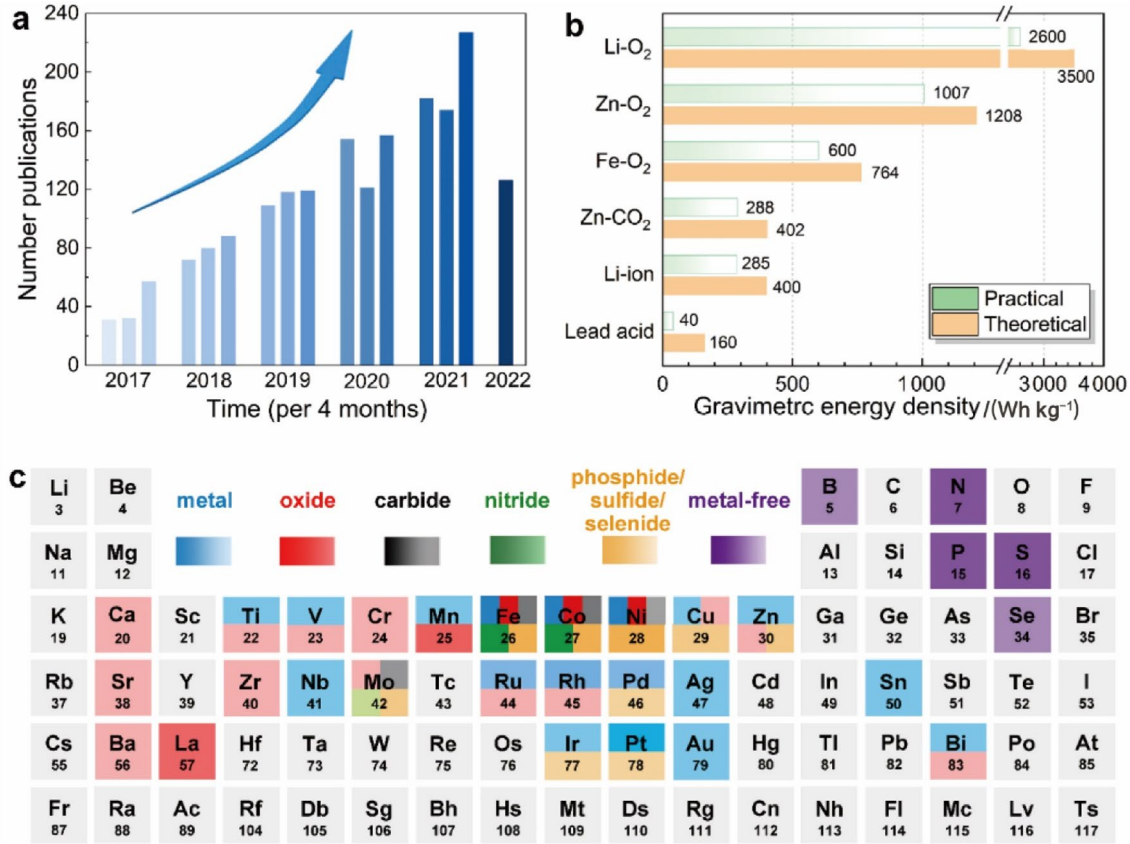

Fig. 1 Current progress in Zn-air battery research. **a** The number of publications about Zn-air batteries in the past five years. **b** Comparison of practical and theoretical energy densities for a range of batteries (the cell level refers to all anode (Zn) materials without any packaging materials or leads) [11–16]. **c** Reported electrocatalysts in Zn-air batteries to date. The different species of metal compounds are marked with different colors; more intense colors indicate more reported literature, whereas lighter colors indicate fewer reports. Updated on March 15, 2022

of carbon-based bifunctional oxygen-catalytic materials for metal-air batteries [22]. Recently, the advances of flexible Zn-air batteries were reviewed by the Huang group, who mainly focused on 3D self-supporting oxygen catalysts, types of solid-state electrolytes, and the rational design of Zn anodes [23]. However, a comprehensive review of all carbon-based oxygen catalysts, including catalytic sites, nanostructures, synthesis methods, precursor design, and developments for advanced Zn-air batteries, is still lacking. Thus, the advanced applications of flexible Zn-air batteries and high-power Zn-air batteries are summarized herein. More importantly, a comprehensive perspective with insight into the advantages, key problems, and further promising solutions of carbon-based oxygen catalysts for Zn-air batteries is provided in this review.

Herein, we present a timely and comprehensive review that summarizes the reported nanostructured carbon-based electrodes for advanced Zn-air batteries in terms of tailoring oxygen-catalytic sites and designing carbon supports. First, the working mechanisms and principles of oxygen electrodes for primary and rechargeable Zn-air batteries are briefly introduced. Subsequently, we systematically summarize the methods applied for tailoring different types of oxygen-catalytic sites, including (i) metal-free heteroatoms, (ii) metal single-atom sites, and (iii) metal alloys and compounds. Then, we outline the strategies used for designing carbon supports for advanced oxygen electrodes, such as conventional carbon nanomaterials, porous carbon, and organic precursors-derived carbon. In this review, we pay particular attention to the versatile synthetic strategies, characterization methods, and in-depth understanding of the relationships between oxygen-catalytic sites/nanostructures and electrode performance. Moreover, we also briefly comment on recent progress in the development of flexible and high-power Zn-air batteries for practical applications. Finally, we thoroughly discuss future development directions, challenges, and perspectives on the rational design of nanostructured carbon-based electrodes in Zn-air batteries. It is believed that this review can inspire future developments of fast-kinetic and efficient Zn-air batteries for use in a broad range of energy fields.

2 Principles and Mechanisms of Oxygen Electrodes in Zn-Air Batteries

2.1 Battery Components and Working Principles

The main structure of a primary Zn-air battery, which is composed of a Zn anode, an electrolyte, an air cathode with active materials to promote the ORR [24], and a gas diffusion layer that allows air to enter into the electrolyte, is illustrated in Fig. 2a. The basic working principle of a primary Zn-air battery during the discharge process in an alkaline electrolyte is illustrated in Fig. 2b.[25, 26] Specifically, the Zn anode first liberates two e^- and is oxidized to zinc ions (Zn^{2+}). The released e^- migrates via an external circuit to the air cathode, where it contacts O_2 on the surface of the catalysts. Then, the O_2 is reduced through the ORR to form hydroxide ions (OH^-) at the solid (active catalysts)–liquid (electrolytes)–gas

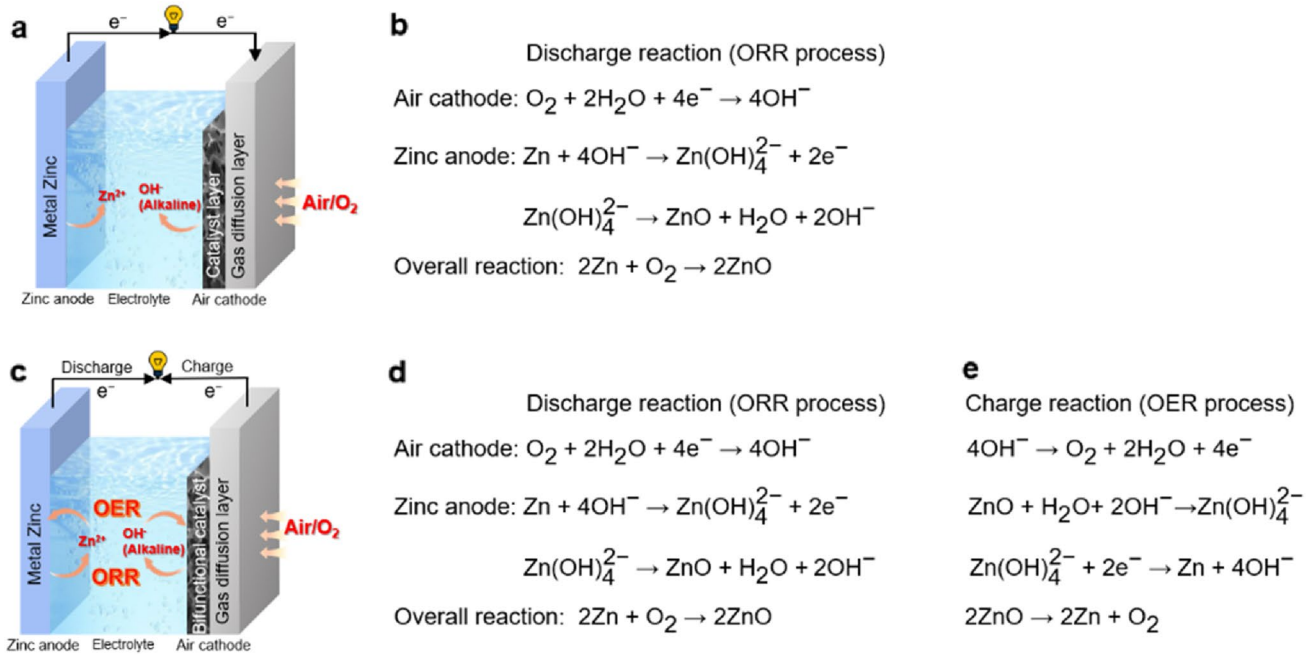

Fig. 2 **a** Schematic working principle and **b** discharge reaction equations of a primary Zn-air battery in an alkaline medium. **c** Schematic working principle, **d** discharge reaction equations, and **e** charge reaction equations of a rechargeable Zn-air battery in an alkaline medium

(O_2) three-phase interface [25], and the full battery reaction is $Zn + O_2$ to ZnO.

Theoretically, the ORR in a Zn-air battery is fully reversible. Therefore, a bifunctional (ORR and OER) oxygen-catalytic electrode will allow realization of a rechargeable Zn-air battery, where the charging process is promoted by the OER on the cathode, and ZnO is reduced back to Zn and deposited on the anode [27]. Generally, the properties of rechargeable Zn-air batteries are particularly dependent on the kinetics of both the ORR and the OER, which are closely related to the natural activities of the bifunctional catalysts, as well as the reactant diffusion efficiency at the reaction interface, as mentioned above [12]. The main structure of a rechargeable Zn-air battery, which is similar to that of a primary battery but with different electrolytes and catalyst layers, is illustrated in Fig. 2c. The working principle of a rechargeable Zn-air battery during the discharging and charging processes in an alkaline electrolyte is illustrated in Fig. 2d, e [6].

2.2 The ORR and OER in Zn-Air Batteries

The ORR, a crucial reaction on the oxygen cathode in Zn-air batteries, is a multielectron ($2e^-$ or $4e^-$) transfer reaction. As summarized in Table 1, in alkaline electrolytes, the ORR can proceed either by a two-step $2e^-$ pathway with the formation of H_2O_2 or by a more efficient $4e^-$ process to directly reduce O_2 to OH^-. Therefore, the $4e^-$ process possesses the highest O_2 utilization efficiency and is remarkably favorable for practical Zn-air battery applications [28–32].

To better understand the mechanism of the ORR, the four elementary reaction steps of the $4e^-$ pathway in an alkaline electrolyte are listed below and in Fig. 3a:[33]

$$* + O_2(g) + H_2O(l) + e^- \rightarrow OOH^* + OH^-(aq) \quad (1)$$

$$OOH^* + e^- \rightarrow O^* + OH^-(aq) \quad (2)$$

$$O^* + H_2O(l) + e^- \rightarrow OH^* + OH^-(aq) \quad (3)$$

$$OH^* + e^- \rightarrow OH^-(aq) + * \quad (4)$$

where * is the catalytic site of the catalyst and OOH*, O*, and OH* are the intermediates adsorbed on the catalytic sites. It has been reported that the free energies of all intermediates can be used to evaluate the selectivity and activity of ORR electrocatalysts. Therefore, researchers have evaluated the binding energies of O*, OH*, and OOH* on different metal surfaces by density functional theory (DFT) calculations, and a volcano plot correlating the theoretical ORR activity and the binding energies (ΔG_{OH}) was constructed, as shown in Fig. 3b [34, 35], optimizing ΔG_{OH} is the key to effectively improving the ORR activity [36, 37].

Table 1 The fundamental reaction equations of the ORR in alkaline aqueous solution

Reaction pathways	Reaction equations
$2e^-$	$O_2 + 2H_2O + 2e^- \rightarrow 2H_2O_2$
$4e^-$	$O_2 + 2H_2O + 4e^- \rightarrow 4OH^-$

The OER is the reverse of the ORR and also involves different reactive species in an alkaline medium (OH^-) [38]. The well-accepted reaction mechanism of the OER under alkaline conditions involves the formation and transformation of OH*, O*, and OOH* intermediates at a catalytic site (M) as well as electron and proton transfer, as shown in Fig. 3c. During the OER, the M–O bonding interactions play a key role in each step. Thus, researchers have related the OER performance of catalysts with a general descriptor, namely, the binding energy difference between O* and OH* ($\Delta G_O - \Delta G_{OH}$), and a volcano plot between the theoretical overpotential of the OER and the free energy $\Delta G_O - \Delta G_{OH}$ has been constructed (Fig. 3d) [34, 39]. Generally, noble metals and metal oxides of Ru/Ir are the best for the acidic OER, while catalysts derived from transition metals are more favorable for catalyzing the OER in an alkaline medium.

3 Regulation of Oxygen-Catalytic Sites

3.1 Metal-Free Heteroatoms

3.1.1 Heteroatoms for the ORR

In designing oxygen-catalytic sites, metal-free heteroatom (i.e., N, B, P, O, or S)-doping of carbon is often regarded as a promising method to optimize electrocatalytic activity by perturbing the charge/spin distribution of the sp^2 carbon plane [43–46]. In particular, N-doped carbon catalysts are widely studied for use in the ORR because their doped sites have greater electronegativity than the C sites, which can help change the electronic state of adjoining carbon atoms and the chemical adsorption mode of intermediates during the catalytic process. Representative NC-based oxygen electrocatalysts can date back to 2009; the Dai group developed a N-doped carbon nanotube (CNT) as an efficient catalyst for the ORR [47]. Since then, different NC catalysts have been designed by controlling the different types of N species, i.e., graphitic N, pyridinic N, pyrrolic N, oxidic N, triazinic N [48], and the previously reported sp-hybridized N [49], as summarized in Fig. 4a. It has been reported that the ORR catalytic activity of these N species decreases in the order pyridinic N > pyrrolic N > graphitic N > oxidized N > C (carbon) [50]. However, several N species coexist in N-doped carbon catalysts, and the individual contribution

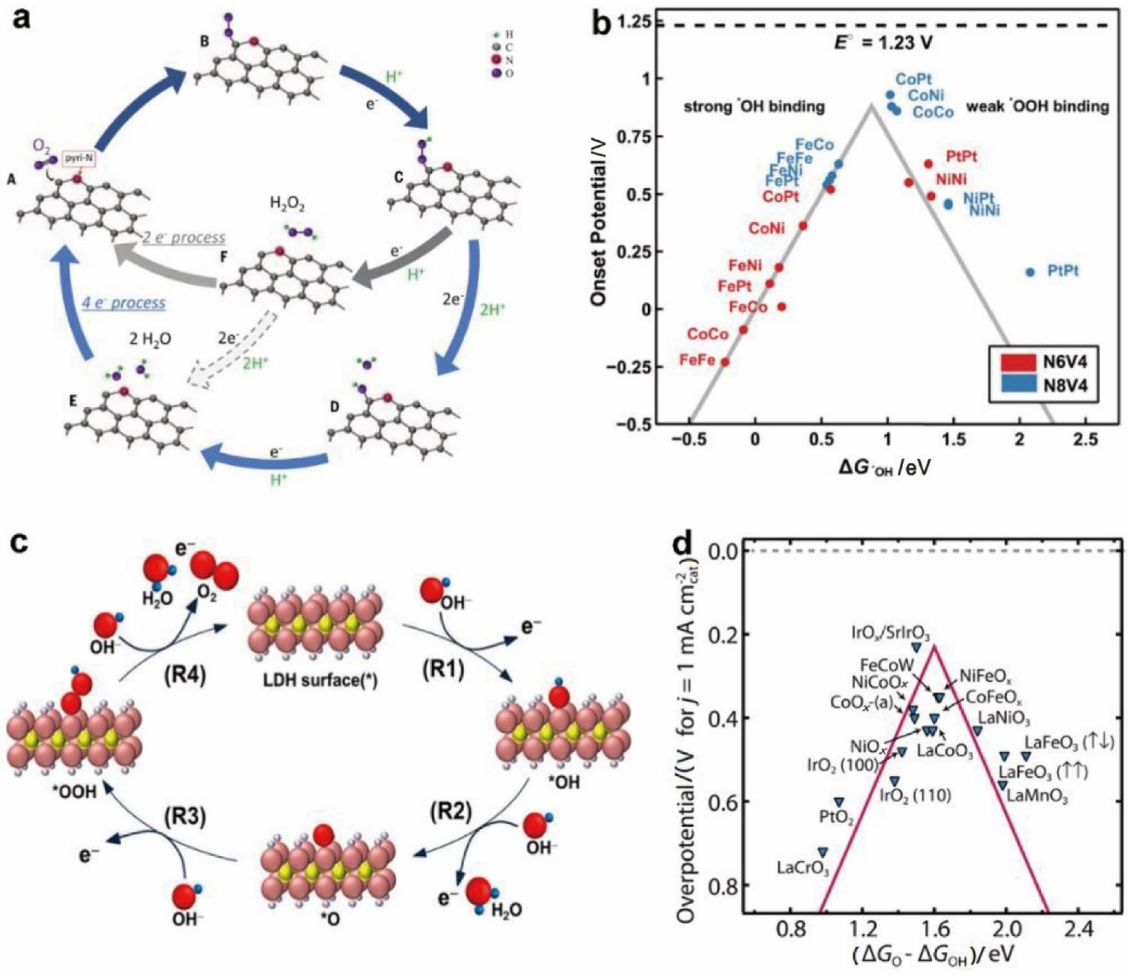

Fig. 3 **a** The ORR mechanism of N-doped carbon (NC) catalysts in an alkaline electrolyte. Reproduced with permission from Ref. [40]. Copyright 2016, National Academy of Sciences. **b** ORR volcano relationship based on metal alloys in the N-doped four-atom vacancy of graphene (denoted as N8V4 (blue) and N6V4 (red)). Reproduced with permission from Ref. [41]. Copyright 2019, American Chemical Society. **c** The OER mechanism on a layered double hydroxide (LDH) surface in an alkaline electrolyte. Reproduced with permission from Ref. [42]. Copyright 2018, Springer Nature. **d** OER volcano relationship based on metal oxides. Reproduced with permission from Ref. [34]. Copyright 2017, National Academy of Sciences

to the ORR is difficult to define. To date, various N-doped carbon catalysts, such as N-doped CNT, N-doped graphene (graphene) [51, 52], N-doped graphitic arrays [53], N-doped carbon [54, 55], and carbon nitride (C_3N_4)-based carbon materials [56, 57], have been extensively investigated for ORR applications. For example, a N-doped carbon nanofiber (N-CNF) with an abundantly N-doped active site and a N atom content of 5.8% showed an onset potential (E_{onset}) of 0.85 vs. the reversible hydrogen electrode (RHE), a high electron-transfer number (3.97 at 0.8 V vs. RHE), and good durability in an alkaline electrolyte [58].

In addition, carbon catalysts codoped with other heteroatoms (B, S, O, P, etc.) with different electronegativities (Fig. 4b), such as N/S- [59], B/N- [60], N/P- [61, 62], N/F- [63], and P/C_3N_4-codoped carbon catalysts [64], have been further explored and generally exhibited better ORR performance owing to their synergetic effects [65, 66]. In particular, boron carbon nitride (BCN) nanosheets with a large surface area of 817 m^2 g^{-1} displayed a higher E_{onset} of 0.94 V and better durability than a commercial Pt/C catalyst in an alkaline solution [67]. This outstanding ORR activity may be ascribed to the complementary effects of B/N-codoping and the tunable electronic structure of carbon. In another effort, the S,N-codoped bamboo carbons (SNBCs) displayed a high half-wave potential ($E_{1/2}$) of 0.850 V vs. RHE and superior stability. A primary Zn-air battery equipped with an SNBC12 cathode presented a high cell performance of 156 mW cm^{-2} [68]. Furthermore, triply doped carbon catalysts have also been fabricated. A typical example is a N/P/S triply doped graphene-like carbon (NPS-G, Fig. 4c) electrocatalyst with appropriate N, P, and S percentages, which displayed

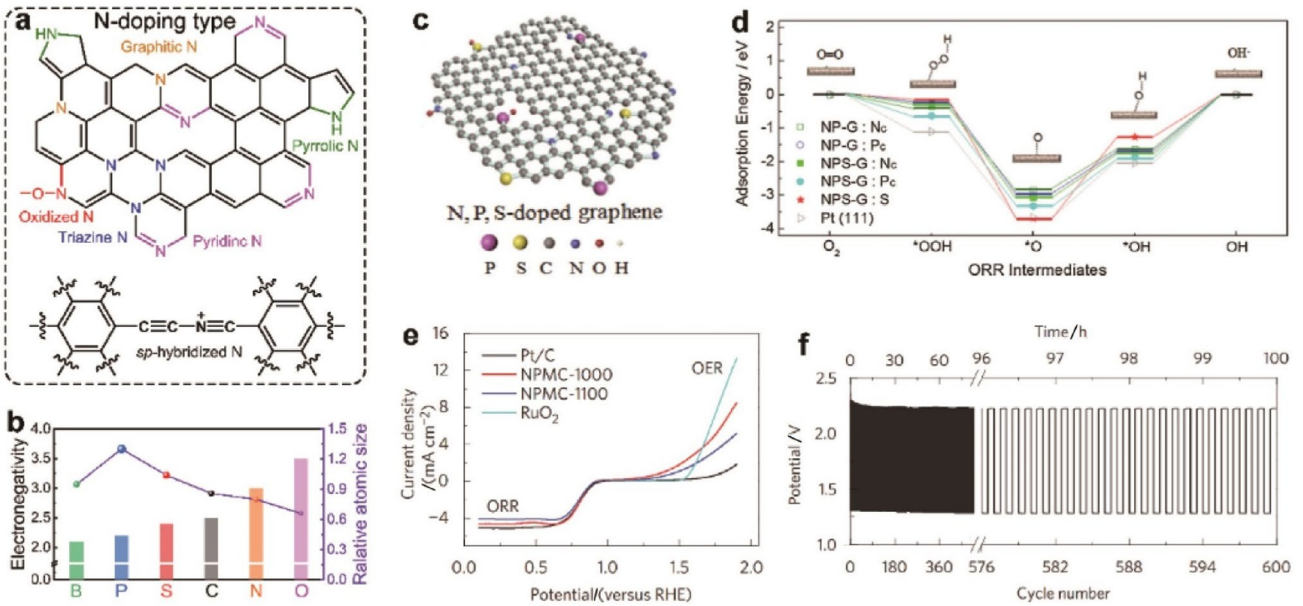

Fig. 4 **a** The typical doping type of N catalytic centers in N-doped carbon materials [48, 49]. **b** Comparison of the electronegativity and relative atomic radius of heteroatoms doped in carbon materials [71]. **c** Schematic diagram of NPS-G. **d** Calculated adsorption energies of ORR intermediates on NPS-G [69]. **c**–**d** Reproduced with permission from Ref. [69]. Copyright 2018, Elsevier B.V. **e** Linear sweep voltammetry (LSV) plots of NPMC, RuO_2, and Pt/C catalysts in 0.1 M (1 M = 1 mol L^{-1}) KOH. **f** Discharge/charge cycling stability of Zn-air batteries assembled with NPMC-1000 cathodes at 2 mA cm^{-2}. **e**–**f** Reproduced with permission from Ref. [74]. Copyright 2015, Springer Nature

better ORR performance than any singly doped counterparts in an alkaline medium. Such improved ORR performance was derived from the facilitated chemisorption of oxygen-containing intermediates on the heteroatoms of the NPS-G electrocatalysts that decreased the charge transfer resistance (Fig. 4d). Furthermore, the primary Zn-air battery prepared by using an NPS-G cathode presented a large power density and specific capacity [69].

3.1.2 Heteroatom Sites for Bifunctional Oxygen Catalysis

Despite their favorable ORR activity, the application of NC catalysts in rechargeable Zn-air batteries is still hindered by their inactivity for the OER [70, 71]. To date, very few B-doped and P-doped carbon–oxygen catalysts have been reported for rechargeable Zn-air batteries [72, 73]. Moreover, multi-doped carbon materials are promising as bifunctional oxygen catalysts for rechargeable Zn-air batteries. As a representative example, the Dai group fabricated N/P-codoped mesoporous carbon (NPMC-1000) foam with a high surface area (~1 663 m^2 g^{-1}), which exhibited high activities for both the ORR and OER owing to the N/P-codoping, edge effects, and highly porous network (Fig. 4e). The rechargeable Zn-air battery assembled with metal-free NPMC-1000 cathodes cycled steadily for 600 cycles at 2 mA cm^{-2} (Fig. 4f) [74].

3.2 Metal Single-Atom Sites

3.2.1 Single-Atom Sites for the ORR

In addition to the metal-free heteroatom-containing catalytic centers, carbon-supported single-atom catalysts have emerged as promising ORR catalysts, which are great for Zn-air batteries owing to their high intrinsic activity and maximum atom efficiency [75–78]. Currently, the most widely investigated and effective single-atom catalysts for Zn-air batteries are Fe [77, 79–83], Co [84–87], Cu [88, 89], Mn [90, 91], supported on an N-doped carbon substrate. Among them, Fe-N_4 [79, 81, 92] and Co-N_4 [85, 87], have been found to be the most active ORR centers under alkaline conditions, with ORR activity and Zn-air battery performance comparable or even superior to those of Pt/C. For example, the 3D hierarchically ordered porous NC with abundant FeN_4 active sites displayed a more positive $E_{1/2}$ of 0.875 V than the state-of-the-art Pt/C catalyst (0.845 V) [81]. The primary Zn-air battery equipped with this catalyst as the air cathode showed a higher power density (235 mW cm^{-2}) and specific capacity (~768 mAh g^{-1}) at 20 mA cm^{-2} than those of Pt/C (192 mW cm^{-2}, 737 mAh g^{-1}). Another example is that a N-doped graphitic nanosheet distributed with CoN_4 species (CoN_4/NG) showed outstanding ORR performance, with an $E_{1/2}$ of 0.870 V [87]. Simultaneously, CoN_4 species can generally achieve an improved OER

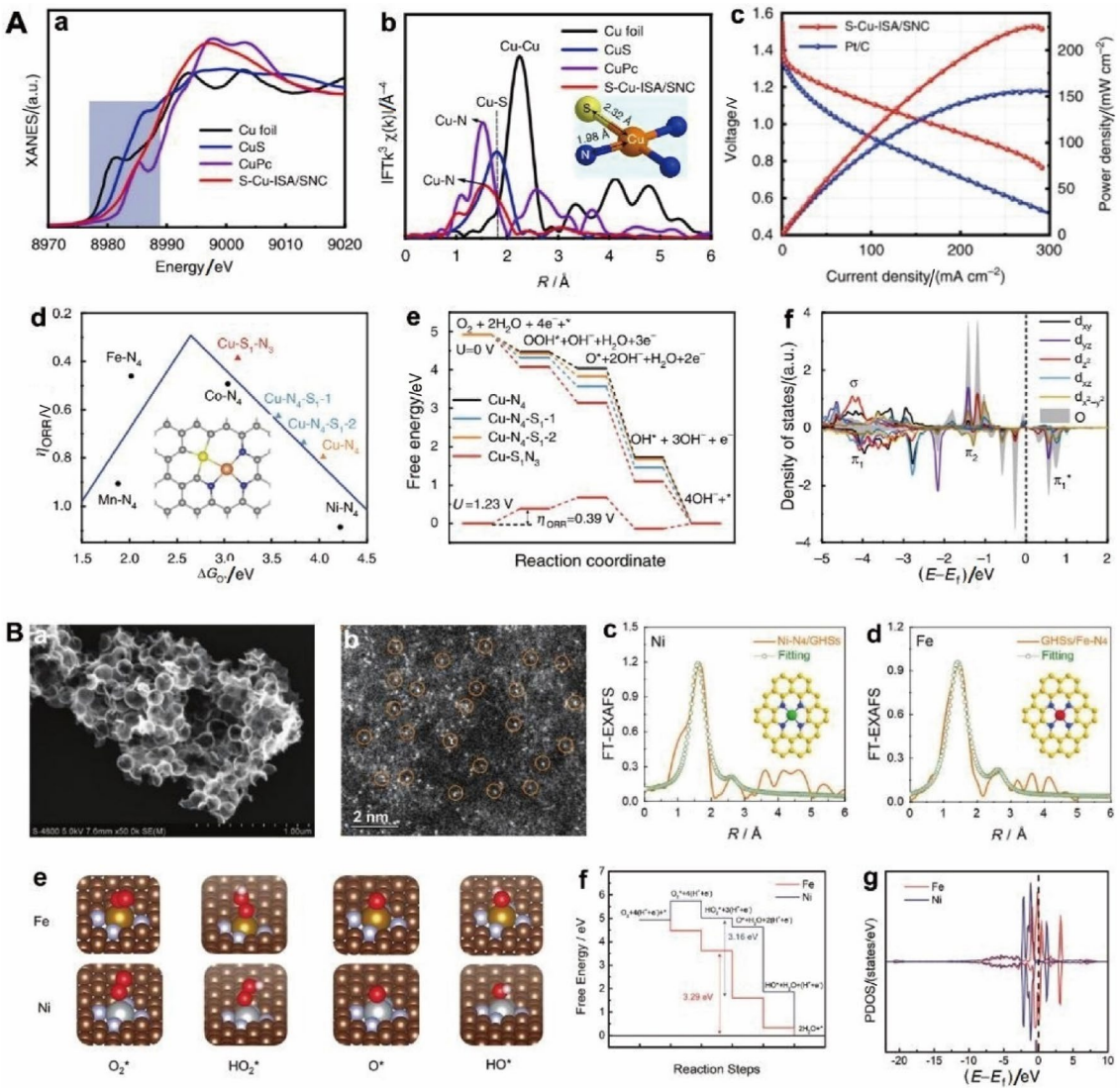

Fig. 5 **A**. **a** XANES spectra of S-Cu-ISA/SNC and reference materials at the Cu K-edge. **b** FT-EXAFS spectra of S-Cu-ISA/SNC and reference materials at the k^3-weighted Cu K-edge; the inset shows a schematic of the structure of S-Cu-ISA/SNC. **c** Discharge polarization plots and power density curves of Zn-air batteries assembled with S-Cu-ISA/SNC and Pt/C cathodes. **d** The ORR volcano plot and **e** the free energy diagram of distinct Cu-centered active sites. **f** The PDOS of Cu and O* after O* adsorption onto the Cu-S_1N_3 active center. **a**–**f** Reproduced with permission from Ref. [89]. Copyright 2020, Springer Nature. **B**. **a** SEM and **b** AC HAADF-STEM images of the Ni-N_4/GHSs/Fe-N_4 catalyst. EXAFS fitting curves of **c** Ni-N_4/GHSs and **d** GHSs/Fe-N_4 in R space; the insets in (**c**) and (**d**) show atomic structure models of Ni-N_4/GHSs and GHSs/Fe-N_4. **e** The optimal adsorption configurations of intermediates on Fe-N_4 and Ni-N_4. **f** Reaction-free energies of Fe-N_4 and Ni-N_4 for the ORR and OER, **g** PDOS of Fe-N_4 and Ni-N_4 sites. **a**–**g** Reproduced with permission from Ref. [97]. Copyright 2020, Wiley–VCH GmbH

activity for rechargeable Zn-air batteries. Thus, the CoN_4/NG catalyst as an air cathode can be incorporated into a rechargeable Zn-air battery, yielding a specific capacity and an energy density (730 mAh g_{Zn}^{-1} and 671 Wh kg^{-1}) better than those of Pt/C + IrO_2-based batteries (711 mAh g_{Zn}^{-1} and 618 Wh kg^{-1}).

Furthermore, the doping of other heteroatoms (i.e., P, S, or O) on M-N_x/C can further improve their ORR activity [75]. As shown in Fig. 5A a–b, a Cu-S_1N_3 active site stabilized in MOF-derived CNs (S-Cu-ISA/SNC) was identified by aberration-corrected high-angle annular dark-field scanning transmission electron microscopy (AC HAADF-STEM) and Fourier transform extended X-ray absorption fine structure (FT-EXAFS) spectroscopy [89]. The S-Cu-ISA/SNC with low-valent Cu-S_1N_3 exhibited outstanding ORR activity, with an $E_{1/2}$ of 0.918 V vs. RHE, outperforming Cu-ISA/SNC (in which S was separated from Cu, 0.87 V) and Cu-ISA/NC (S free, 0.86 V). Thus, the primary Zn-air battery assembled with the S-Cu-ISA/SNC cathode catalyst exhibited a higher power density of 225 mW cm^{-2} than that of a

Pt/C-based catalyst (155 mW cm^{-2}) and a specific capacity as high as 735 mAh g^{-1} at a discharge of 10 mA cm^{-2} (Fig. 5A c). DFT calculations and a volcano diagram of the ORR potential and free energy ΔG_{O*} revealed that the Cu-N_4 site with weakened bonding for ORR intermediates showed inferior ORR activity, which could be optimized by the substitution of a S atom for coordinated N (Cu-S_1N_3) because S atoms have larger atomic radii and lower electronegativity than N atoms, causing the Cu in S-Cu-ISA/SNC to lose fewer valence electrons than the Cu in Cu-ISA/NC (Fig. 5A d–f). Recently, a ZnCo with two single atoms bonded to a NC matrix (named Zn/CoN-C) was fabricated and demonstrated a higher $E_{1/2}$ of 0.861 V than CoN-C (0.793 V) and ZnN-C (0.706 V), as the dual single-atom sites more effectively accelerated the dissociation of O–O bonds to achieve improved ORR activity [93].

3.2.2 Single-Atom Sites for Bifunctional Oxygen Catalysis

Moreover, the doping of other heteroatoms is expected to improve the OER activity of M-N_x/C, which enables achieving bifunctional application in rechargeable Zn-air batteries [94–96]. This conjecture was first confirmed by the introduction of Fe-N_x moieties onto N and S co-decorated CNTs (S, N-Fe/N/C-CNTs), as reported by the Xie group [95]. Compared with N-Fe/N/C-CNT catalysts, S, N-Fe/N/C-CNTs exhibited decreased free energy for the ORR pathway and also greatly improved OER activity. The rechargeable Zn-air battery integrated with the S,N-Fe/N/C-CNT cathode showed high cycling stability over 100 h without obvious voltage gap fading. Recently, bimetallic single-atom site-doped carbon catalysts also showed great potential in enhancing the OER activity to realize rechargeable Zn-air batteries [97–99]. To further enhance the OER performance of one catalyst for rechargeable Zn-air batteries, composites of two different single-atom compounds were developed. Chen et al. designed nonadjacent dual single-atom sites (Ni-N_4 and Fe-N_4) doped graphene hollow nanospheres (Ni-N_4/GHSs/Fe-N_4) by integrating Fe(II) phthalocyanine (FePc) onto the surface of a Ni-N_4 precursor (SiO_2@$[Ni(CN)_4]^{2-}$@GO) through π-π stacking, followed by calcination at 700 °C in a N_2 atmosphere and subsequent etching (Fig. 5B a–d) [97]. The fabricated Ni-N_4/GHSs/Fe-N_4 catalyst exhibited excellent bifunctional oxygen-catalytic activity, with a lower E_{gap} of 0.790 V (E_{gap} indicates the potential between the $E_{1/2}$ of the ORR and the $E_{j=10}$ of the OER). The outer Fe-N_4 active centers were mainly conducive to the ORR, and the inner Ni-N_4 active centers facilitated the OER, which was further verified by DFT calculations, as shown in Fig. 5B e–g. Therefore, the rechargeable Zn-air battery driven by the Ni-N_4/GHSs/Fe-N_4 catalyst displayed an exceptional specific capacity of ~ 778 mAh g_{Zn}^{-1}, even better than that of a noble metal-based battery (~ 660 mAh g_{Zn}^{-1}).

3.3 Metal Alloys and Compounds

3.3.1 Metal Alloys for Bifunctional Oxygen Catalysis

As metal-free and metal single-atom catalysts still show insufficient activity toward the OER, carbon-supported metal compounds have been employed as catalysts to achieve sufficient bifunctional ORR and OER catalytic activity and rechargeable Zn-air batteries [33, 100, 101]. Integrating carbon materials and metal alloys/compounds may offer more active sites, good conductivity, and strong tolerance. Thus, carbon-supported metal alloys [102–104] and metal compounds, including oxides [105–108], sulfides [109–111], carbide [112–114], nitrides [115, 116], and phosphide [117–119], have been widely investigated and displayed good rechargeable Zn-air battery performance. For example, $Fe_{0.5}Co_{0.5}$ and $Fe_{0.5}Co_{0.4}Ni_{0.1}$ alloys confined in N-doped CNTs-grafted porous hybrid fibers (FeCo/FeCoNi@NCNTs-HF) showed a low E_{gap} value of 0.747 V. When incorporated into a self-supported flexible rechargeable Zn-air battery, the initial voltage gap between the charge and discharge potentials was 0.76 V. Impressively, the voltage increased by only 0.07 V after a 670 h (1 005 cycles) long-term cycling test [120]. Furthermore, carbides and nitrides as favorable ORR electrocatalysts have also been extensively explored owing to their satisfactory conductivity and corrosion resistance [121]. As shown in Fig. 6A a–d, $Mn_{0.9}Fe_{2.1}C$ embedded in N-doped graphitic carbon ($Mn_{0.9}Fe_{2.1}C$/NC) displayed encouraging ORR ($E_{1/2}$ = 0.780 V) and OER ($E_{j=10}$ = 1.644 V vs. RHE) activities. A rechargeable Zn-air battery assembled with a $Mn_{0.9}Fe_{2.1}C$/NC cathode displayed a high power density of up to 160 mW cm^{-2} and functioned steadily for more than 100 h, as well as being able to power an electronic clock (rated voltage: 1.5 V) for over 12 h [114]. Recently, the bimetal nitride (Co, Fe)$_3$N_2D exhibited a potential of 0.34 V at –2 mA cm^{-2} for the ORR and a lower $E_{j=10}$ of 1.540 V vs. RHE for the OER. When incorporated into a rechargeable Zn-air battery, it showed a maximum power density of 234 mW cm^{-2} and functioned successively for over 300 h at 30 mA cm^{-2} without obvious discharge–charge voltage gap fading [122].

3.3.2 Metal Oxides for Bifunctional Oxygen Catalysis

Moreover, an oxide/hydroxide is also a promising alternative to precious-metal-based ORR catalysts, and a series of NC (e.g., graphene and CNT)-based metal oxide (e.g., Co_3O_4 and CoO) catalysts were reported by the Dai group, all of which displayed ORR activities comparable to that of commercial Pt/C in an alkaline medium [123,

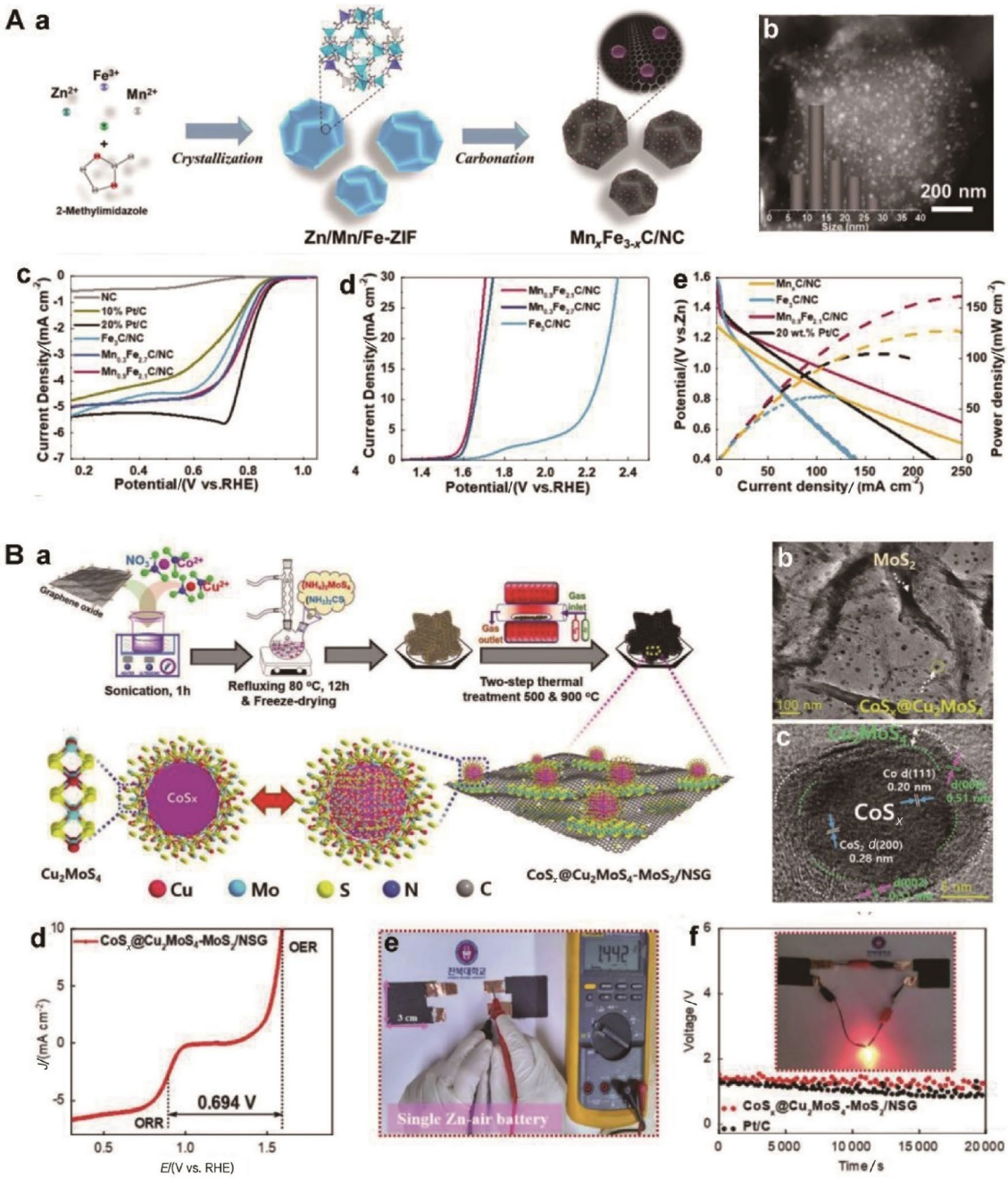

Fig. 6 **A**. **a** Schematic of the sample preparation and **b** TEM image of the $24Mn_xFe_{3-x}NC$ catalyst. **c** ORR and **d** OER LSV curves of different catalysts in 0.1 M KOH. **e** Polarization curves and power densities of Zn-air batteries equipped with different catalysts. **a**–**e** Reproduced with permission from Ref. [114]. Copyright 2019, American Chemical Society. **B. a** Schematic of the synthetic route and **b**, **c** TEM images of the $CoS_x@Cu_2MoS_4$-MoS_2/NSG catalyst. **d** LSV plots of the $CoS_x@Cu_2MoS_4$-MoS_2/NSG catalyst for the ORR and OER in 0.1 M KOH. **e** Cell voltage of a single Zn-air battery. **f** Stability testing of Zn-air batteries driven by the $CoS_x@Cu_2MoS_4$-MoS_2/NSG and Pt/C cathode; the inset shows a photograph of a red light-emitting diode (LED, 5 mm, ≈1.8 V) powered by two tandem Zn-air batteries. **a**–**f** Reproduced with permission from Ref. [109]. Copyright 2020, Wiley–VCH GmbH

124]. Furthermore, most of these metal oxides/hydroxides demonstrated excellent OER activity; thus, carbon-based oxides have achieved an excellent bifunctional oxygen-catalytic process and rechargeable Zn-air battery performance [125, 126]. Representatively, Xie and coworkers fabricated a N-doped graphene-coated ultrathin cobalt oxide (CoO_x) catalyst that showed outstanding bifunctional oxygen-catalytic activity with a low E_{gap} value of 0.704 V. The maximum specific power of the rechargeable Zn-air batteries equipped with this catalyst was as

high as 300 W g_{cat}^{-1} [125]. Compared with metal oxides, metal sulfides normally show improved OER activity due to unsaturated metal centers that can accelerate the adsorption of oxygen-containing intermediates onto catalytic sites [127, 128]. Furthermore, metal phosphides have also been found to exert a favorable effect on oxygen-catalytic activities and durability by influencing the *d*-band structure of the metal [129]. For example, the CoP_x@CNS catalyst exhibited a high $E_{1/2}$ of 0.760 V for the ORR and a low overpotential of 1.516 V vs. RHE at 50 mA cm^{-2} for the OER compared to Co@CNS (1.572 V vs. RHE). The rechargeable Zn-air battery equipped with the CoP_x@CNS cathode demonstrated a high peak power density of 110 mW cm^{-2}. and good work stability for more than 130 h [130].

3.3.3 Heterojunctions for Bifunctional Oxygen Catalysis

Furthermore, carbon-supported multiple-metal compounds also showed an advantage in synergistically increasing the bifunctional ORR/OER activity and battery performance by combining the advantages of each material [33, 131, 132]. As depicted in Fig. 6B a–d, a molybdenum dichalcogenide/N,S-codoped graphene homogeneously distributed with core@shell nanostructured CoS_x@Cu_2MoS_4 catalysts (CoS_x@Cu_2MoS_4-MoS_2/NSG) exhibited an impressive bifunctional oxygen-catalytic activity with an ultra-low E_{gap} of 0.694 V in an alkaline medium. The rechargeable Zn-air battery constructed by using the CoS_x@Cu_2MoS_4-MoS_2/NSG cathode displayed an open-circuit voltage of 1.44 V and excellent cyclic stability (Fig. 6B e–f) [109]. In another reported work, the di-cobalt phosphide (Co_2P)-cobalt nitride (CoN) core–shell nanostructures with double active sites coated on N-doped CNTs (Co_2P/CoN-in-NCNTs) were prepared via straightforward in situ self-template methods and displayed effective Zn-air battery performance, with a prominent working life of more than 96 h [133]. More recently, N,P-co-doped carbon nanofiber (CNF)-coated FeCo alloys and Co_2P (FeCo/Co_2P@NPCF) compounds displayed simultaneously improved ORR and OER activity (E_{gap} = 0.770 V) relative to their counterparts of CNF-coated FeCo alloys (FeCo@CF, 0.86 V) and N,P-co-doped CNF-coated Co_2P (Co_2P@NPCF, 0.94 V). When used as an air cathode in a rechargeable Zn-air battery, these catalysts exhibited outstanding cycling stability, and the discharge–charge voltage gap only decreased from 0.83 to 0.80 V after 642 continuous cycles of testing [134]. Consequently, considerable advancements have been made in carbon-based metal compounds for Zn-air batteries, as listed in Table 2. It is concluded that Co is the best choice and displays better activity for Zn-air batteries among all the transition metal elements (such as Fe, Co, Ni, Cu, and Mn) [135–137].

4 Designing Carbon Supports for Advanced Oxygen Electrodes

4.1 Conventional Carbon Nanomaterials

To date, several commercial carbon substrates, such as carbon black (CB), CNTs, and graphene, have shown great prospects for use in oxygen-catalytic processes owing to their low costs, high surface areas, and good electroconductivity. CNTs feature slender structures that can facilitate the e^- and ion transfer between an electrode and an electrolyte. Graphene is the most popular nanocatalyst because of its fast charge-transport mobility, unique physicochemical performance, flexible modified surface, and remarkable electrochemical stability [125]. Therefore, these materials are suitable for constructing carbon-based air cathodes in Zn-air batteries as a result of heteroatom doping or providing support for other active compounds [69, 102, 115, 125, 138–141].

4.1.1 CB-, CNT-, and Graphene-Based Metal-Free Catalysts for the ORR

Among diverse modification methods, the N doping of carbon is the commonest strategy for improving the ORR activity and Zn-air battery performance of carbon nanomaterials [141–145]. For example, by carbonizing freeze-dried gelatin-KB, a metal-free ORR catalyst of Ketjenblack (KB)-integrated gelatin-derived carbon nanosheets (named GK) was fabricated and exhibited enhanced ORR stability because the incorporated pyridinic N and graphitic N species located near the exposed edge positions markedly facilitated the ORR [141]. The primary Zn-air battery assembled with this catalyst displayed a larger peak power density of 193 mW cm^{-2} than that of a Pt/C-based battery (188 mW cm^{-2}). N-doped graphene and CNTs have also been widely investigated as high-performance ORR catalysts for Zn-air batteries [51, 146–149]. For example, a defect-rich N-doped graphene nanoribbon was fabricated by chemical oxidation and unzipping of CNTs, followed by NH_3 activation at high temperatures. This oxygen catalyst displayed excellent ORR activities, with an $E_{1/2}$ of 0.808 V in alkaline conditions. A primary Zn-air battery driven by this cathode delivered a maximum power density of 151 mW cm^{-2} and outstanding cycling stability over 300 cycles, performing much better than a commercial Pt/C + RuO_2-based battery (126 mW cm^{-2}) [147].

Furthermore, increasing the heteroatom density further improved the oxygen-catalytic performance of carbon-based oxygen catalysts. As shown in Fig. 7 a–b, the Feng group realized a series of high-density B,N-codoped carbon, including 0D carbon spheres, 1D CNTs, and 2D carbon

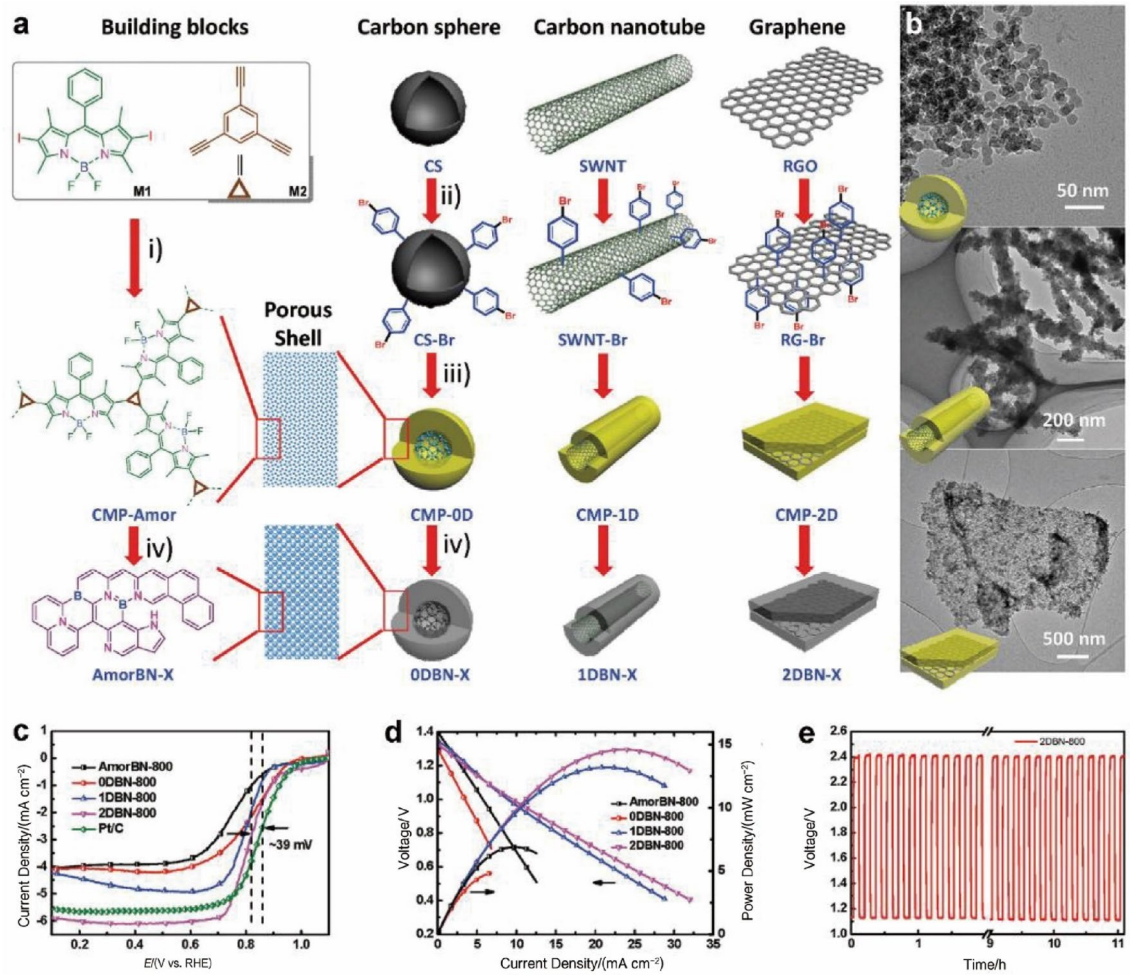

Fig. 7 **a** Dimensionally controlled synthesis of BODIPY-based conjugated CPs and the corresponding BN-X catalysts. **b** TEM images of CP-0D, CP-1D, and CP-2D precursors. **c** LSV curves of various catalysts in 0.1 M KOH. **d** Polarization curve and the corresponding power density plot of assembled Zn-air batteries based on different catalysts. **e** Discharge/charge cycling curve of 2DBN-800. Reproduced with permission from Ref. [150]. Copyright 2015, Wiley–VCH GmbH

nanosheets, by pyrolysis of conjugated polymer-functionalized carbons. Among them, the prepared 2D BN-doped carbon nanosheets exhibit the best ORR catalytic performance ($E_{1/2}$ = 0.810 V, Fig. 7 c). The as-prepared air electrode based on these catalysts showed very stable discharging/charging performance in primary Zn-air batteries (Fig. 7 d–e) [150]. In addition to the codoping of B and N into a carbon matrix, N and S are widely used in bi-heteroatom-doping systems. The Feng group also prepared N,S-codoped porous carbon sheets (N/S-2DPCs) by pyrolysis of S-enriched 2D polymer-functionalized graphene by NH_3 treatment. The N/S ratio of N/S-2DPCs could be well tuned by altering the NH_3 activation time, and N/S-2DPCs-60 manifested the best ORR activity ($E_{1/2}$ = 0.750 V) closest to that of the Pt/C benchmark (0.777 V). When employed as an air cathode in a primary Zn-air battery, outstanding cycling stability for more than 12 h at a current density of 20 mA cm^{-2} was achieved [151].

4.1.2 CB-, CNT-, and Graphene-Based Single-Atom Catalysts for the ORR

Moreover, the decoration of a single-metal atom or metal compounds onto CB, CNT, and graphene catalysts can further improve the ORR activity [80, 152, 153]. For example, a π-conjugated FePc/graphene composite with abundant Fe–N-C centers (*pf*SAC-Fe–X) was designed by means of a pyrolysis-free synthetic method (Fig. 8A a–b) [80]. In an AC HAADF-STEM image, the coordinated single Fe atoms were observed as bright dots and were uniformly distributed on the conductive graphene matrix (Fig. 8A c–d). The results of DFT calculations suggested that the electrons of graphene tended to attach to the FePc sites, leading to a

Table 2 Comparison of the ORR/OER and Zn-air battery performance of carbon-based oxygen catalysts with metal-free heteroatoms, single-metal atoms, and metal alloy and compound sites

Oxygen-catalytic site	Electrocatalyst	ORR /($E_{1/2}$, V)	OER /($E_{j=10}$, V)	E_{gap}/V	Peak power density/(mW cm^{-2})	Specific capacity/(mAh g_{Zn}^{-1})	Stability	Reference
Metal-free heteroatoms	N-CNF	0.800 (0.1 M KOH)				~615	60 h @10 mA cm^{-2}	[58]
	SNBCs	0.850 (0.1 M KOH)			156	348	12 h @0.7 V	[68]
	NPS-G	0.857 (0.1 M KOH)			151	686	20 h @10 mA cm^{-2}	[69]
	GH-BGQD	0.870 (0.1 M KOH)	1.600 (0.1 M KOH)	0.730	112	687	100 h @ 1.23 V	[72]
	P-doped carbon nanosheets	0.850 (0.1 M KOH)	1.595 (0.1 M KOH)	0.745			1000 cycles @10 mA cm^{-2}	[73]
	NPMC-1000	0.850 (0.1 M KOH)	~1.570 (6.0 M KOH)	0.720	55	735	240 h @2 mA cm^{-2}	[74]
Single-metal atom sites	Fe-N_4 SAs/NPC	0.885 (0.1 M KOH)	1.660 (1.0 M KOH)	0.775	232		36 h @2 mA cm^{-2}	[79]
	SA-Fe-NHPC	0.93 (0.1 M KOH)			266	795.3	240 h @20 mA cm^{-2}	[77]
	3DOM Fe–N–C	0.875 (0.1 M KOH)			235	768.3	100 h @5 mA cm^{-2}	[81]
	Fe-SA-NSFC	0.910 (0.1 M KOH)			247.7	792.1	240 h @10 mA cm^{-2}	[82]
	Co-SAs@NC	0.820 (0.1 M KOH)			105.3	897.1	11.6 h @2 mA cm^{-2}	[84]
	SCoNC	0.910 (0.1 M KOH)	1.54 (0.1 M KOH)	0.630	194	690	20 h @5 mA cm^{-2}	[85]
	Co-POC	0.83 (0.1 M KOH)	1.7 (0.1 M KOH)	0.870	78		200 cycles @2 mA cm^{-2}	[86]
	CoN_4/NG	0.870 (0.1 M KOH)	1.61 (0.1 M KOH)	0.740	115	730	100 h @10 mA cm^{-2}	[87]
	Cu_1/NC-900	0.894 (0.1 M KOH)			213		100 h @5 mA cm^{-2}	[88]
	S-Cu-ISA/SNC	0.918 (0.1 M KOH)			225	735	50 h @10 mA cm^{-2}	[89]
	Mn-SAS/CN	0.910 (0.1 M KOH)			220	780	25 h @10 mA cm^{-2}	[90]
	Zn/CoN-C	0.861 (0.1 M KOH)			230		27.7 h @5 mA cm^{-2}	[93]
	P-O/FeN_4-CNS	0.890 (0.1 M KOH)	1.63 (0.1 M KOH)	0.74	232		450 cycles @25 mA cm^{-2}	[94]
	S,N-Fe/N/C-CNT	0.850 (0.1 M KOH)	1.6 (0.1 M KOH)	0.75	102		100 cycles @5 mA cm^{-2}	[95]
	Fe-NSDC	0.840 (0.1 M KOH)	1.64 (0.1 M KOH)	0.80	225.1	740.8	400 cycles @4 mA cm^{-2}	[96]
	Ni-N_4/GHSs/Fe-N_4	0.830 (0.1 M KOH)	1.62 (0.1 M KOH)	0.79		777.6	600 cycles @10 mA cm^{-2}	[97]
	Fe,Co-SA/CS	0.860 (0.1 M KOH)	1.59 (0.1 M KOH)	0.73	86.65	819.6	300 cycles @5 mA cm^{-2}	[98]
	Fe–NiNC-50	0.850 (0.1 M KOH)	1.57 (1.0 M KOH)	0.72	~220	932.66	100 h @2 mA cm^{-2}	[99]
Metal alloys and compounds	Ni-MnO/rGO aerogels	0.780 (0.1 M KOH)	1.6 (0.1 M KOH)	0.82	123	758	100 cycles @10 mA cm^{-2}	[100]

Table 2 (continued)

Oxygen-catalytic site	Electrocatalyst	ORR /($E_{1/2}$, V)	OER /($E_{j=10}$, V)	E_{gap}/V	Peak power density/(mW cm^{-2})	Specific capacity/(mAh g_{Zn}^{-1})	Stability	Reference
	Ni_3Fe/N–C	0.780 (0.1 M KOH)	1.6 (0.1 M KOH)	0.82		528	420 h @10 mA cm^{-2}	[103]
	Fe_2Ni@NC	0.890 (0.1 M KOH)	1.538 (0.1 M KOH)	0.648	126		500 cycles @10 mA cm^{-2}	[104]
	NiCo/NLG-270	0.820 (0.1 M KOH)	1.57 (0.1 M KOH)	0.75	103	403	40 cycles @2 mA cm^{-2}	[106]
	Co/Co_3O_4@PGS	0.890 (0.1 M KOH)	1.58 (0.1 M KOH)	0.69	118.27		800 h @10 mA cm^{-2}	[107]
	$Zn_{0.4}Ni_{0.6}Co_2O_4$/NCNTs	0.780 (0.1 M KOH)	1.64 (0.1 M KOH)	0.86	109		100 cycles @25 mA cm^{-2}	[108]
	CoS_x@Cu_2MoS_4-MoS_2/NSG	0.900 (0.1 M KOH)	1.5814 (0.1 M KOH)	0.681	40		5.5 h@10 mA cm^{-2}	[109]
	Co_9S_8@N, S-C	0.887(0.1 M KOH)	1.534(0.1 M KOH)	0.647	259	862	660 cycles@10 mA cm^{-2}	[110]
	$Co_{9-x}Ni_xS_8$/NC	0.864(0.1 M KOH)	1.652(0.1 M KOH)	0.788	75		60 h@10 mA cm^{-2}	[111]
	FeNC-S-Fe_xC/Fe	0.887(0.1 M KOH)	1.567(0.1 M KOH)	0.68	149.4		42 h@2 mA cm^{-2}	[112]
	$Mn_{0.9}Fe_{2.1}C$/NC	0.780(0.1 M KOH)	1.644(1.0 M KOH)	0.864	160	635	334 h@ 5 mA cm^{-2}	[114]
	Co_4N@NC	0.840(0.1 M KOH)	1.52(0.1 M KOH)	0.68	74.3	769.4	750 h @5 mA cm^{-2}	[116]
	Fe_2P/NPC	0.872(0.1 M KOH)			111.6	654.1	4 h@40 mA cm^{-2}	[117]
	CoP/NP-HPC	0.830(0.1 M KOH)			186		80 h@2 mA cm^{-2}	[118]
	FeCo/FeCoNi@NCNTs-HF	0.850(0.1 M KOH)	1.608(0.1 M KOH)	0.758	156.22	762	240 h@5 mA cm^{-2}	[120]
	Co_2P/CoN-in-NCNTs	0.850(0.1 M KOH)	1.65(0.1 M KOH)	0.80	194.6	649.6	96 h@5 mA cm^{-2}	[133]
	FeCo/Co_2P@NPCF	0.790(0.1 M KOH)	1.56(0.1 M KOH)	0.77	154		107 h@10 mA cm^{-2}	[134]

Fe–C electron path. The oxygen adsorbed only on the Fe atomic sites and provided superior catalytic sites during the ORR. Therefore, the prepared *pf*SAC-Fe exhibited highly efficient ORR properties, with $E_{1/2}$ of 0.910 V and a tolerance for methanol (Fig. 8A e–f). The primary Zn-air battery incorporating *pf*SAC-Fe exhibited a larger specific capacity of 732 mAh g_{Zn}^{-1} and outstanding stability over 300 h (Fig. 8A g). Recently, a hexagonal Fe_2N compound loaded on an NC (Fe_2N/NC) catalyst was obtained through carbonization of a CB, $FeCl_3$, and melamine mixture at 250 °C, followed by NH_3 activation at 700 °C (Fig. 8B a–c). The as-fabricated Fe_2N/NC catalyst, composed of a major Fe_2N phase and Fe-N_4 sites, displayed better ORR activity ($E_{1/2}$ = 0.910 V) than NC (~0.800 V, Fig. 8B d). The peak power density of a primary Zn-air battery equipped with the Fe_2N/NC catalyst as the air cathode reached as high as 155 mW cm^{-2} . (Fig. 8B e). The results of corresponding DFT calculations indicated that the $Fe_2N(\bar{1}\bar{1}1)$ structure had a free energy closer to that of an ideal ORR route than the Fe-N_4 sites at 0.85 V vs. RHE (Fig. 8B f–g), revealing that the excellent ORR activity of Fe_2N/NC could mainly be attributed to the Fe_2N structure rather than to the Fe-N_4 [115].

4.1.3 CB-, CNT-, and Graphene-Based Catalysts for the OER

To date, most of the reported CB-, CNT-, and graphene-based metal-free and single-atom catalysts have only displayed enhanced ORR activities, and good OER performance has rarely been observed. Recently, one study revealed that incorporating electron-withdrawing oxygen atoms into CNTs results in a large positive charge density on adjacent C atoms, resulting in remarkable OOH* adsorption and enhanced OER activity [154]. Therefore, the O/N-codoped CB, CNTs, and graphene substrates have

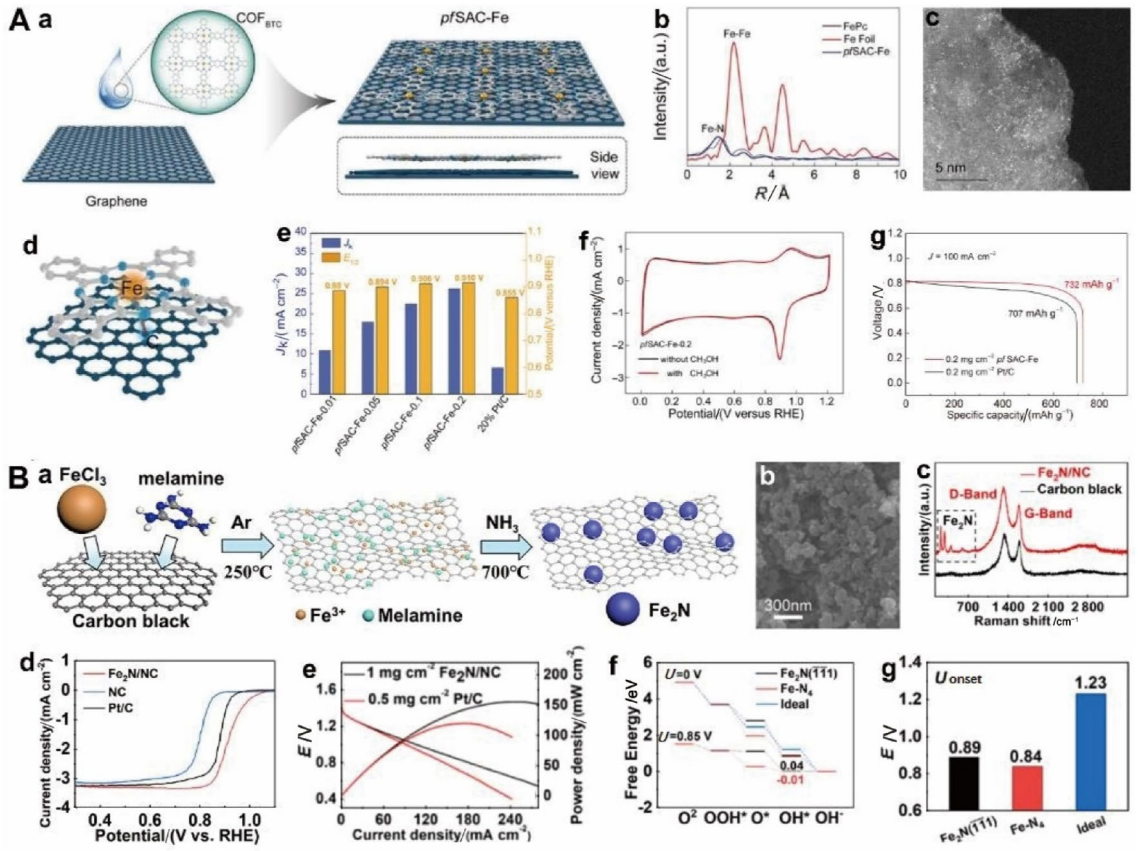

Fig. 8 **A**. **a** Schematic of the preparation process and **b** HAADF-STEM image of the *pf*SAC-Fe electrocatalyst. **c** FT-XANES spectra of *pf*SAC-Fe at the Fe K-edge and **d** simulated structures. **e** Comparison of the $E_{1/2}$ and kinetic current density at 0.850 V vs. RHE of the catalysts. **f** CV curves of *pf*SAC-Fe-0.2 without and with methanol solutions. **g** Comparison of the specific capacities of the Zn-air batteries. **a**–**g** Reproduced with permission from Ref. [80]. Copyright 2020, National Academy of Sciences. **B. a** Schematic preparation of the Fe_2N/NC hybrid and corresponding crystal cell model of hexagonal Fe_2N. **b** SEM image and **c** Raman spectra of the Fe_2N/NC hybrid. **d** ORR LSV profiles of electrocatalysts in a 1.0 M NaOH solution. **e** The power density curves of assembled Zn-air batteries. **f** Free energy diagrams and **g** the corresponding calculated U_{onset}. **a**–**g** Reproduced with permission from Ref. [115]. Copyright 2020, American Chemical Society

been considered as promising candidates in the literature [154, 155, 156]. For example, bifunctional metal-free electrocatalysts of O-functionalized CNTs (OCNTs) were reported by Lu and coworkers, and they displayed good oxygen-catalytic performance, with an $E_{1/2}$ of 0.850 V for the ORR and a low $E_{j=10}$ of 1.546 V for the OER. These OCNTs served as efficient cathode catalysts in a rechargeable Zn-air battery and demonstrated a high peak power density of 130 mW cm^{-2}. Impressively, the discharge–charge voltage of an assembled Zn//OCNT battery manifested negligible fading after 340 h (about 2 040 cycles) of continuous work [154]. Similar results were also realized by Co/N/O triply doped graphene (NGM-Co) with abundant single-atom Co-N_x motifs prepared by dispersing single sites through the structural defects formed in situ during carbonization (Fig. 9A a–b). The as-obtained NGM-Co displayed enhanced bifunctional oxygen-catalytic activity and excellent rechargeable Zn-air battery performance. The equipped rechargeable liquid Zn-air battery showed a high specific capacity of up to 749 mAh g^{-1} and a steady discharge voltage of 1.12 V at 20.0 mA cm^{-2}, which is sufficient to drive a toy vehicle (Fig. 9A c–d). In particular, when this material was incorporated into a flexible rechargeable Zn-air battery, the discharge–charge voltage was stable for over 18 cycles, even under bending (Fig. 9A e–g) [157].

Integrating graphene carbon substrates with other efficient OER species is a highly effective strategy to realize bifunctional oxygen catalysts [108, 124, 125, 157–167]. For example, the Dai group developed a CoO/N-doped CNT (CoO/N-CNT) hybrid for the ORR and NiFe-LDH/CNT for the OER [124]. The rechargeable Zn-air batteries assembled with mixed CoO/N-CNT + NiFe-LDH/CNT catalysts as cathodes displayed excellent charge–discharge stability over 200 cycles. Recently, a rechargeable Zn-air battery driven by N-doped CNTs coated with NiFe particles (NiFe/N-CNT) showed an ultrahigh peak power density of approximately

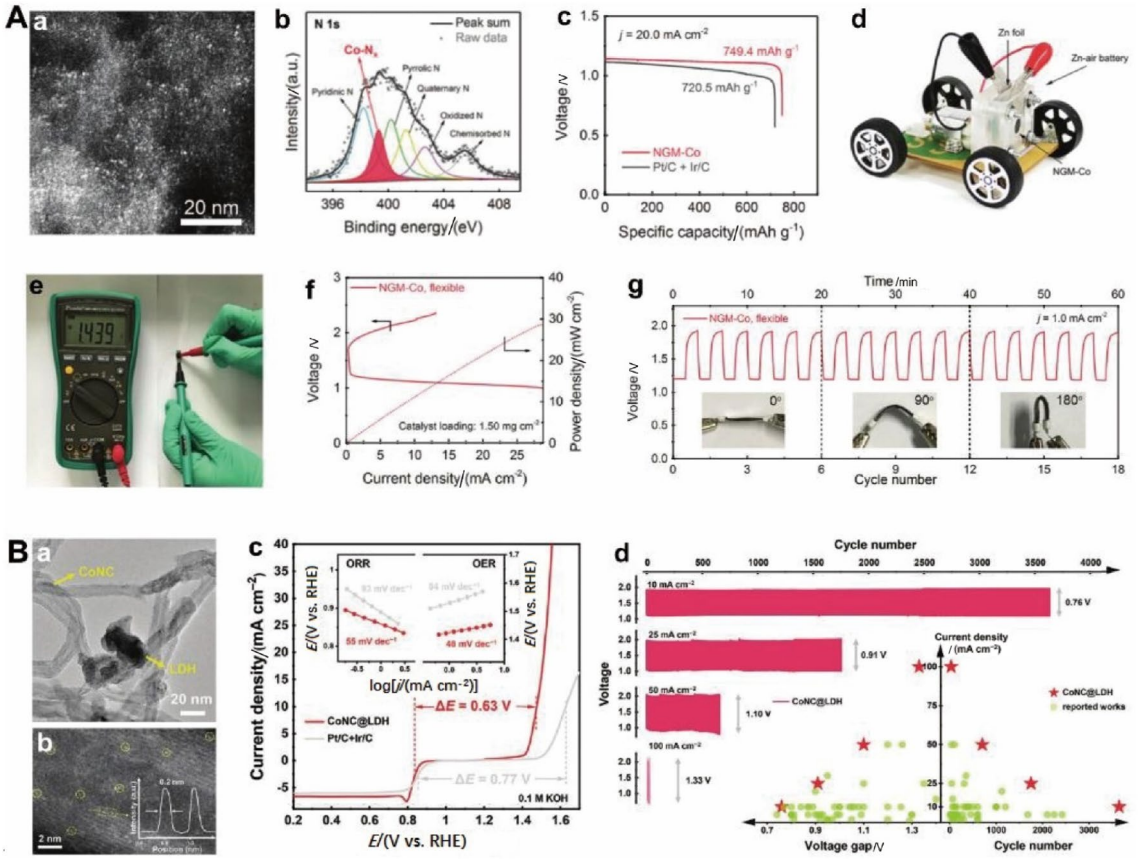

Fig. 9 **A**. **a** HRTEM image and **b** N 1 s XPS spectra of the NGM-Co catalyst. **c** Discharge plots of Zn-air batteries assembled with NGM-Co and Pt/C + Ir/C catalysts at 20.0 mA cm^{-2}. **d** Picture of a toy car powered by one Zn-air battery based on an NGM-Co catalyst. **e** The open-circuit voltage of a solid Zn-air battery. **f** Charge and discharge polarization plots. **g** Galvanostatic discharge–charge cycling profiles at 1.0 mA cm^{-2} under bending. **a**–**g** Reproduced with permission from Ref. [157]. Copyright 2017, Wiley–VCH GmbH. **B. a** TEM and **b** AC HAADF-STEM images of CoNC@LDH. **c** LSV profiles of distinct catalysts in 0.1 M KOH. The inset shows a comparison of Tafel slopes for ORR/OER. **d** Long-term stability evaluations of rechargeable Zn-air batteries. **a**–**d** Reproduced with permission from Ref. [162]. Copyright 2021, Wiley–VCH GmbH

300 mW cm^{-2} and long-life rechargeability for more than 300 cycles [161]. To further prolong the working stability of rechargeable Zn-air batteries, a CNT-based bifunctional catalyst composed of atomically dispersed Co–N-C species with ORR activity integrated with NiFe LDHs with OER activity was fabricated and showed an ultra-low E_{gap} of 0.630 V, far exceeding the Pt/C + Ir/C catalyst (0.77 V) and most of the currently reported catalysts (Fig. 9B a–b) [165, 168, 169]. This type of prepared rechargeable Zn-air batteries exhibited not only a large power density of 173 mW cm^{-2} but also excellent stability (more than 3 600 cycles at 10 mA cm^{-2} without obvious voltage gap fading) (Fig. 9B c) [162]. Afterward, a N-doped graphene substrate coating with an ultrathin CoO_x layer (1 nm-CoO_x/N-RGO) was constructed through a facial ligand-assisted pyrolysis strategy. The 1 nm-CoO_x/N-RGO achieved excellent bifunctional oxygen-catalytic activities with a low E_{gap} of 0.704 V, owing to its improved e^- transfer and abundant active sites. When this material was incorporated into flexible rechargeable Zn-air batteries, good stability for more than 10 h was achieved, even upon bending from 0° to 180° [125].

4.2 Porous Carbon Supports

As discussed above, the ORR process of the Zn-air battery usually presents sluggish kinetics because of poor mass loading and insufficient air/ion diffusion, and it is reported that the catalytic performance of an air cathode relies not only on the intrinsic catalytic active sites but also on their assembled nanostructures, especially the porous structures [71, 170]. Therefore, in addition to the inherent activities of catalysts, the porous structure design should be considered in the fabrication of high-performance carbon-based oxygen catalysts. Recently, 3D porous carbon-based oxygen catalysts exhibited excellent advantages in Zn-air batteries due to accelerated reactant diffusion in their pores,

their enlarged electrode/electrolyte contact area, and their promising potential in reliable, portable, and flexible devices [100]. Generally, the 3D porous structures of carbon-based catalysts incorporate a multilevel porous configuration over one length scale from micropores to mesopores and macropores. The micropores are favored for the exposure of catalytic centers, while the meso- and macropores benefit fluent mass transportation [171]. Therefore, ideal carbon-based oxygen catalysts should possess both mesoporous and macroporous architectures to achieve high oxygen-catalytic efficiency.

4.2.1 3D Graphene Aerogels

To date, most of the reported porous carbon-based oxygen catalysts used in Zn-air batteries were derived from graphene-based aerogels [72, 100, 172], the assembly of low-dimensional carbon materials [173–179], or the direct synthesis of carbon materials by chemical vapor deposition (CVD) [51, 146, 180, 181]. For instance, a 3D porous graphene aerogel-loaded Ni/MnO (Ni-MnO/rGO) catalyst was prepared by the sol–gel process followed by pyrolysis and displayed bifunctional oxygen-catalytic activity (E_{gap} = 0.820 V) similar to that of Pt/C + RuO_2 catalysts (0.770 V). The rechargeable Zn-air battery assembled with this porous catalyst exhibited better cycling stability for more than 100 cycles than a Pt/C + RuO_2-assembled Zn-air battery [100]. Recent work showed that the interconnected ordered macropores of carbon matrices further enhanced the mass transport efficiency and resulted in more exposed active sites than micro-/mesoporous carbon. Therefore, an air cathode of hierarchical porous N,P-doped carbon aerogel with ordered macropores and coated FeP/Fe_2O_3 compounds was fabricated by freeze-drying and subsequent pyrolysis (Fig. 10A a–d) and displayed an $E_{1/2}$ (0.838 V) very similar to that of commercial Pt/C (0.819 V) for the ORR and a lower onset potential than benchmark RuO_2 for the OER (1.430 V) in an alkaline medium [172]. When incorporated into an aqueous rechargeable Zn-air battery, this material exhibited a high peak power density of 130 mW cm^{-2} and excellent charge–discharge cycle stability for more than 200 h. Encouragingly, based on the alkaline poly(vinyl alcohol) (PVA) gel electrolyte, the peak power density of a freestanding flexible Zn-air battery can also reach up to 40 mW cm^{-2}.

4.2.2 Low-Dimensional Carbon Assembled 3D Structures

A typical example of integrating 1D CNTs with other low-dimensional materials to prepare 3D catalysts is the fabrication of a 3D freestanding film from a Ni-centered hollow MOF/GO precursor (Fig. 10B a–c) by the Wang group [175]. During the pyrolysis process, MOFs were prepared by wrapping a 1D N-CNT carbon shell around Ni nanoparticles cores, followed by connection to 2D rGO to from a heteronanostructure. Their synergistic effect endows the resulting 3D catalyst with superior oxygen-catalytic activities, with an $E_{1/2}$ of 0.875 V for the ORR and $E_{j=10}$ of 1.490 V for the OER. When this material was applied as the cathode in a rechargeable Zn-air battery, a high peak power density (~ 117 mW cm^{-2}), specific capacity (706 mAh g^{-1}), and energy density (841 Wh kg^{-1}) were obtained.

4.2.3 3D Carbon Synthesized by the CVD Method

Moreover, the CVD strategy has been extensively applied to the controllable preparation of various carbon nanocatalysts, such as CNTs and graphene, by the transport of gaseous precursors followed by deposition on substrates or templates. As shown in Fig. 10C a–b, 3D bicontinuous mesoporous N-doped graphene (N-MG-800) catalysts were prepared by CVD of triethylene glycol in the presence of NH_3 and served as metal-free ORR catalysts [146]. N-MG-800 showed a mesopore size of approximately 25 nm (Fig. 10C c) and a high specific surface area of up to 1 015 m^2 g^{-1}, endowing N-MG-800 with a high N-doping content of up to 5.83 At% (At% means the atomic percentage), with 3.86 At% of the desired pyridinic N, and excellent ORR activity comparable to that of a Pt/C catalyst. Thus, the assembled primary Zn-air battery displayed a maximum power density of 270 mW cm^{-2} and good operational durability over 10 h in an alkaline medium.

4.3 Organic Precursor-Derived Carbon

Compared with the conventional commercial carbon support method, the direct carbonization of organic precursors, including metal-free polymers, metal-coordinated hybrids and polymers, and metal–organic frameworks (MOFs), has the advantages of (a) tunable meso-/microporous structures and (b) a wide selection of active metallic sites and doped heteroatoms. In the following sections, these three types of precursor-derived oxygen catalysts for Zn-air batteries are discussed in detail.

4.3.1 Polymer-Derived Metal-Free Carbon

Polymers containing only heteroatoms in their backbones are usually investigated as precursors for heteroatom-doped carbon catalysts. Polymer-derived metal-free carbon–oxygen catalysts with low cost and various nanostructures have attracted increasing attention and are considered promising candidates in air cathodes of Zn-air batteries for the ORR [182–184]. For example, chitosan, a linear polysaccharide with a N content of approximately 7%, was used to fabricate NC oxygen catalysts. A representative porous NC catalyst

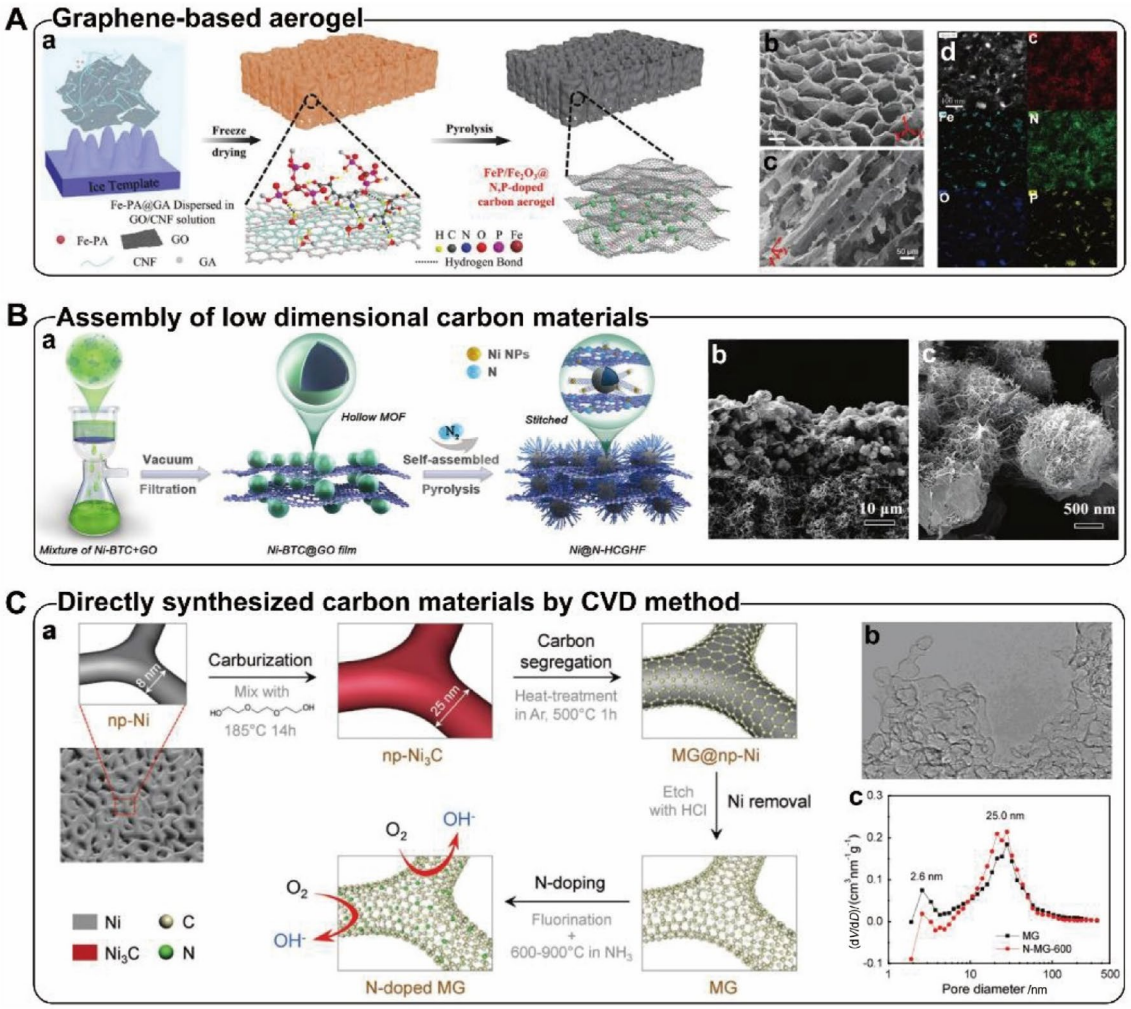

Fig. 10 **A**. **a** Diagram illustrating the preparation of FeP/Fe_2O_3@NPCA. **b**, **c** SEM image, **d** HAADF-STEM images and energy-dispersive X-ray spectroscopy mapping of FeP/Fe_2O_3@NPCA. **a**–**d** Reproduced with permission from Ref. [172]. Copyright 2020, Wiley–VCH GmbH. **B. a** Synthesis process and **b**, **c** cross-sectional SEM images of Ni@N-HCGHF. **a**–**c** Reproduced with permission from Ref. [175]. Copyright 2020, Wiley–VCH GmbH. **C. a** Schematic fabrication of N-MG-800 by CVD. **b** TEM image of N-MG-800. **c** Pore size distributions of MG and N-MG-600. **a**–**d** Reproduced with permission from Ref. [146]. Copyright 2018, Wiley–VCH GmbH

was obtained by molten salt pyrolysis using chitosan as a precursor and exhibited superior ORR activity, with $E_{1/2}$ of 0.860 V, compared to commercial Pt/C (0.84 V) in an alkaline medium. When this material was applied as an air cathode in a primary Zn-air battery, a maximum power density of 178 mW cm^{-2} and high charge–discharge cycling stability over 50 h were achieved [182]. Recently, a porous N-doped carbon (NPC) catalyst with a high specific surface area of up to 1 900 m^2 g^{-1} was obtained by carbonizing glucose in the presence of cyanuric acid and ammonia chloride. The resultant NPC-1000 displayed excellent bifunctional ORR and OER activities, with an E_{gap} of 0.720 V, similar to that of Pt/C + RuO_2 catalysts (~ 0.80 V), which enabled the assembly of a rechargeable Zn-air battery with NPC-1000. After 300 cycles for 50 h, the potential gap of this battery remained near 0.85 V without obvious change [183].

Furthermore, conductive polymers, such as polyaniline (PANI), polypyrrole (PPy), and polythiophene (PTh), with desired optoelectronic features, have also been regarded as ideal metal-free carbon–oxygen catalyst precursors for the ORR and Zn-air batteries due to their abundant carbon/heteroatom sources, augmented asymmetrical atomic spin density, and possibly higher conductivity than that of traditional polymer-derived carbon materials [185]. Additionally, it is easy to construct porous nanostructures of these polymers, thus facilitating mass transport and air/electrolyte diffusion. The hard-templating method has been widely used to construct porous structures of polymer-derived carbons for the ORR and Zn-air batteries

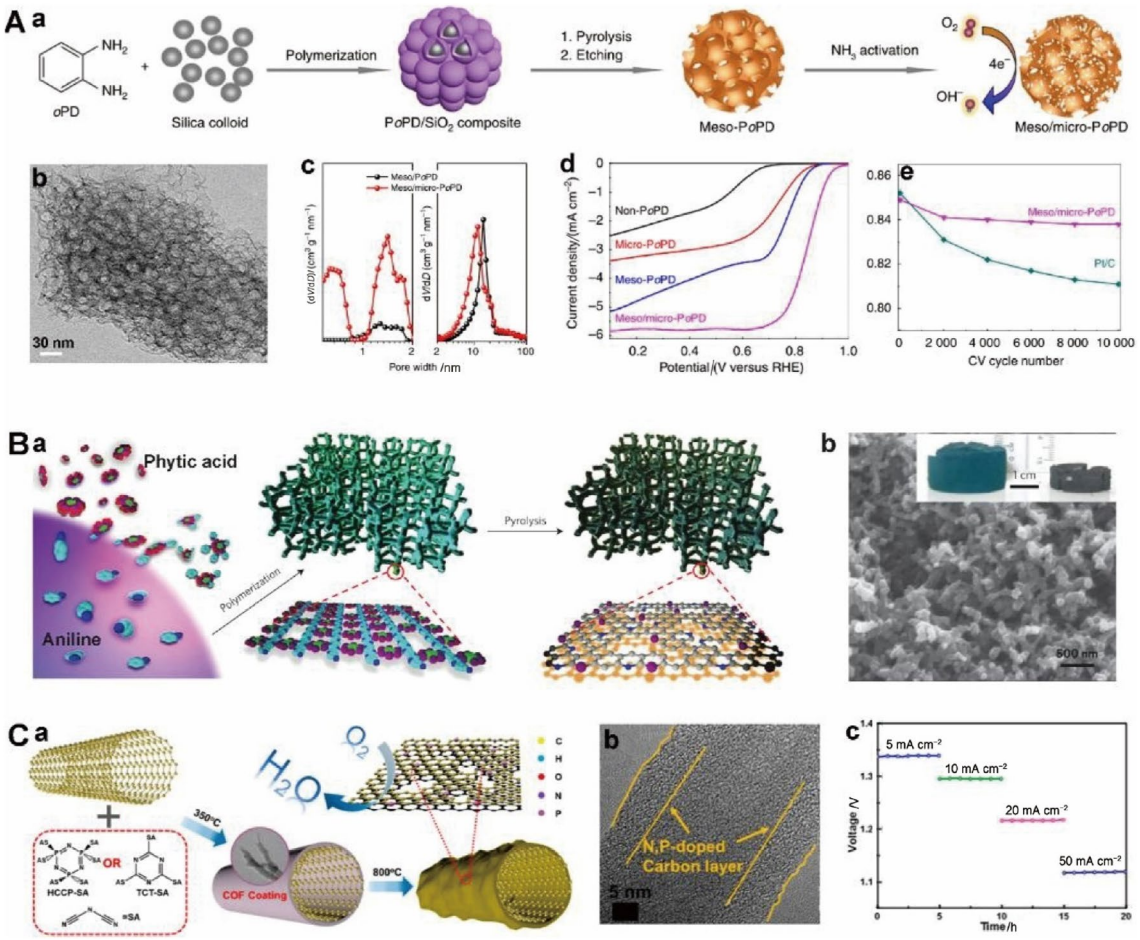

Fig. 11 **A. a** Schematic of the fabrication process and **b** TEM image of meso-/micro-P*o*PD. **c** Pore size distribution and **d** ORR polarization curves of different catalysts. **e** The stability of meso-/micro-P*o*PD and Pt/C. **a**–**e** Reproduced with permission from Ref. [187]. Copyright 2014. Nature Publishing Group. **B. a** Preparation of the NPMC electrocatalysts. **b** SEM images of NPMC-1000; the inset shows pictures of the PANI aerogel gel before (left) and after (right) carbonization. **a**–**b** Reproduced with permission from Ref. [74]. Copyright 2015, Nature Publishing Group. **C. a** Schematic of the fabrication process and **b** TEM image of N/P-co-doped porous carbon obtained at 800 °C. **c** Discharge curves at various current densities. **a**–**c** Reproduced with permission from Ref. [192]. Copyright 2017, American Chemical Society

[186–188]. As shown in Fig. 11A a–d, through pyrolysis of *o*-phenylenediamine with SiO_2 colloids, followed by etching and NH_3 activation, a meso-/micro-P*o*PD catalyst with a hierarchically porous structure and N doping was fabricated. Impressively, the primary Zn-air battery driven by the meso-/micro-P*o*PD displayed superior stability for 60 h, making it superior to meso-P*o*PD and Pt/C [187]. Instead of the hard-templating method, a self-templated aniline-phytic acid composite was used to fabricate a N/P-co-doped mesoporous carbon foam (NPMC)(Fig. 11B a–b). The resultant NPMC-1000 with a large surface area (1 663 $m^2\ g^{-1}$) and abundant N/P doping facilitated mass diffusion during catalysis, resulting in excellent ORR activity ($E_{1/2} = 0.850$ V) and enhanced OER activity. The rechargeable Zn-air battery based on the NPMC-1000 catalyst achieved encouraging cycling stability for 30 h at 5 mA cm^{-2} and 180 discharge/charge cycles over a period of 30 h [74].

Recently developed covalent-organic frameworks (COFs) with *p*-conjugated and precisely customized architectures and adjustable pore sizes have provided a novel perspective to fabricating the porous carbon–oxygen catalysts [189–192]. For example, a naphthalene-based COF-derived N/S-co-doped porous carbon (CPN-NS) catalyst with a large surface area of 1 116 $m^2\ g^{-1}$ was designed (Fig. 11C a–b) and displayed excellent ORR activity, with an $E_{1/2}$ of 0.868 V [189]. In addition, a N/P-codoped porous carbon catalyst was fabricated by pyrolysis of N/P-containing COF-coated CNTs. The N/P-codoped catalyst showed excellent primary Zn-air battery performance in terms of a high peak power density (255 mW cm^{-2}) and discharge stability over 20 h (Fig. 11C c) [192].

4.3.2 Metal-Coordinated Hybrids and Polymer-Derived Carbon

Although much effort has been made to explore metal-free carbon-based oxygen catalysts, the sluggish kinetics of the oxygen-involving electrochemistry still significantly limit their performance in Zn-air batteries, especially in the OER process. The introduction of metal ions is regarded as an effective strategy to dramatically decrease the kinetic barrier and facilitate electrocatalytic kinetics [193]. In recent years, metal-coordinated hybrids and polymers, which contain well-distributed coordination metal species in polymeric hybrids or frameworks, have been widely used to fabricate M-NC and carbon-supported metal compounds.

In particular, metal–phenolic hybrid-derived catalysts are receiving dramatically increasing attention owing to their strong binding ability to various metal species.[110, 194–198] Tannic acid, a natural organic ligand with abundant phenolic hydroxyl groups, can self-assemble into a cross-linked porous polyphenolic framework and coordinate with different metal ions [199]. For example, a N/S-co-doped carbon aerogel loaded with a Fe–Ni alloy (Fe–Ni ANC@NSCA) was realized by pyrolysis of a chelate of tannic acid, PANI, Fe^{3+} and Ni^{2+} ions (Fig. 12A a–c). Benefiting from the synergistic effects of the N_4-Fe–O-Ni-N_4 sites, the prepared Fe–Ni ANC@NSCA displayed a balance between the adsorption of reactants and the desorption of products. Thus, the Fe–Ni ANC@NSCA showed excellent bifunctional oxygen-catalytic activity, with an E_{gap} of 0.599 V (Fig. 12A d), far exceeding that of the commercial Pt/C + RuO_2 catalyst. Accordingly, the rechargeable Zn-air battery based on this catalyst delivered a peak power density of 140 mW cm^{-2} and extremely good stability over 500 h at 5 mA cm^{-2} (Fig. 12A e) [195]. Through a one-pot thermolysis reaction of Fe(II) salts, TA, and disodium hydrogen phosphate, a N/P-codoped carbon with well-dispersed metal phosphide nanoparticles (FeP_x) and Fe–N-C sites (FeP_x/Fe–N-C/NPC) was constructed. The synergistic effect again boosted the bifunctional oxygen-catalytic performance and resulted in a smaller E_{gap} of 0.695 V. The prepared rechargeable Zn-air battery exhibited cycling stability for 33 h and less voltage gap fading [197].

Dopamine (DA), which contains both a rigid catechol group and a flexible methylene amino group, is a more promising candidate for constructing M-NC catalysts [153, 200–203]. As an example, a layered metal–organic precursor of DA-intercalated iron(III) chloride hexahydrate, which shows a well-defined layered structure and good flexibility/processability, was reported by our group. This novel metal–organic precursor not only can be used to construct M-N_x-doped 2D microporous carbon nanosheets (NFe/CNs-700–800-NH_3) but also can be incorporated into other templates to construct hierarchically porous M-N_x-doped carbon catalysts (meso-/micro-FeCo-N_x-CN) (Fig. 12B a–d) [200, 204]. The prepared NFe/CNs-700–800-NH_3 catalyst showed excellent ORR properties, with an $E_{1/2}$ of 0.863 V (Fig. 12B e). Therefore, the assembled primary Zn-air battery exhibited a higher specific capacity of 750 mAh g^{-1} than a Pt/C battery at a large discharge current density of 100 mA cm^{-2}. Furthermore, the 2D hierarchically porous meso-/micro-FeCo-N_x-CN catalyst showed excellent ORR/OER activity (E_{gap} = 0.780 V) and stability; thus, the assembled rechargeable Zn-air battery presented superior cycle stability during a long-time charge/discharge process at a current density of 20 mA cm^{-2} (Fig. 12B f–h).

COFs with transition metal-binding groups, such as bipyridyl [19], porphyrin [86, 205, 206], and phthalocyanine [79, 207–211], were also investigated as metal-coordinated polymeric precursors for effective ORR and OER catalysts in Zn-air batteries [212, 213]. For example, a Fe–N-doped mesoporous carbon catalyst was fabricated by carbonizing the SiO_2-templated bipyridine-containing COF (mC-TpBpy-Fe) (Fig. 13A a–d). The obtained mC-TpBpy-Fe displayed markedly improved mass transfer efficiency and enhanced accessibility of the active centers, resulting in better ORR activity ($E_{1/2}$ = 0.845 V) than C-TpBpy-Fe (0.804 V) without any mesoporous structure (Fig. 13A e). A primary Zn-air battery driven by this catalyst exhibited a peak power density of ~81 mW $cm.^{-2}$ and discharging stability over 70 h (Fig. 13A f) [19]. A triazine covalent-organic framework (PTCOF) incorporated with Co nanoparticles (CoNP-PTCOF), which showed well-defined active sites and pores, was readily prepared under mild conditions, and such materials with modulated electronic structures have been investigated as bifunctional electrocatalysts for the ORR and OER. A Zn-air battery assembled with bifunctional CoNP-PTCOF exhibited a smaller E_{gap} of 0.830 V than PTCOF (1.12 V) and better durability for 720 cycles than a battery containing commercial Pt/C and RuO_2 [214]. A metal (Fe and Ni)-phthalocyanine-based COF has also emerged as a promising precursor for preparing N-doped carbon-coated FeNi catalysts for bifunctional oxygen catalysts (Fig. 13B a, c). The resultant FeNi-COP-800 displayed a lower E_{gap} of 0.827 V than Fe-COP-800 and Ni-COP-800 (Fig. 13B b). Impressively, the rechargeable Zn-air battery prepared with a FeNi-COP-800 cathode showed the best cycling performance with a low voltage change (decreased from the initial 55.8% to 52.9%) after 175 h, where the loss of voltaic efficiency was only 2.9% (Fig. 13B e) [210].

4.3.3 MOF-Derived Carbon

MOFs are crystalline porous materials consisting of inorganic moieties (metal ions or metal oxo clusters) and organic linkers (rigid, semi-rigid, or flexible ligands) with well-defined structures and large specific surface areas.

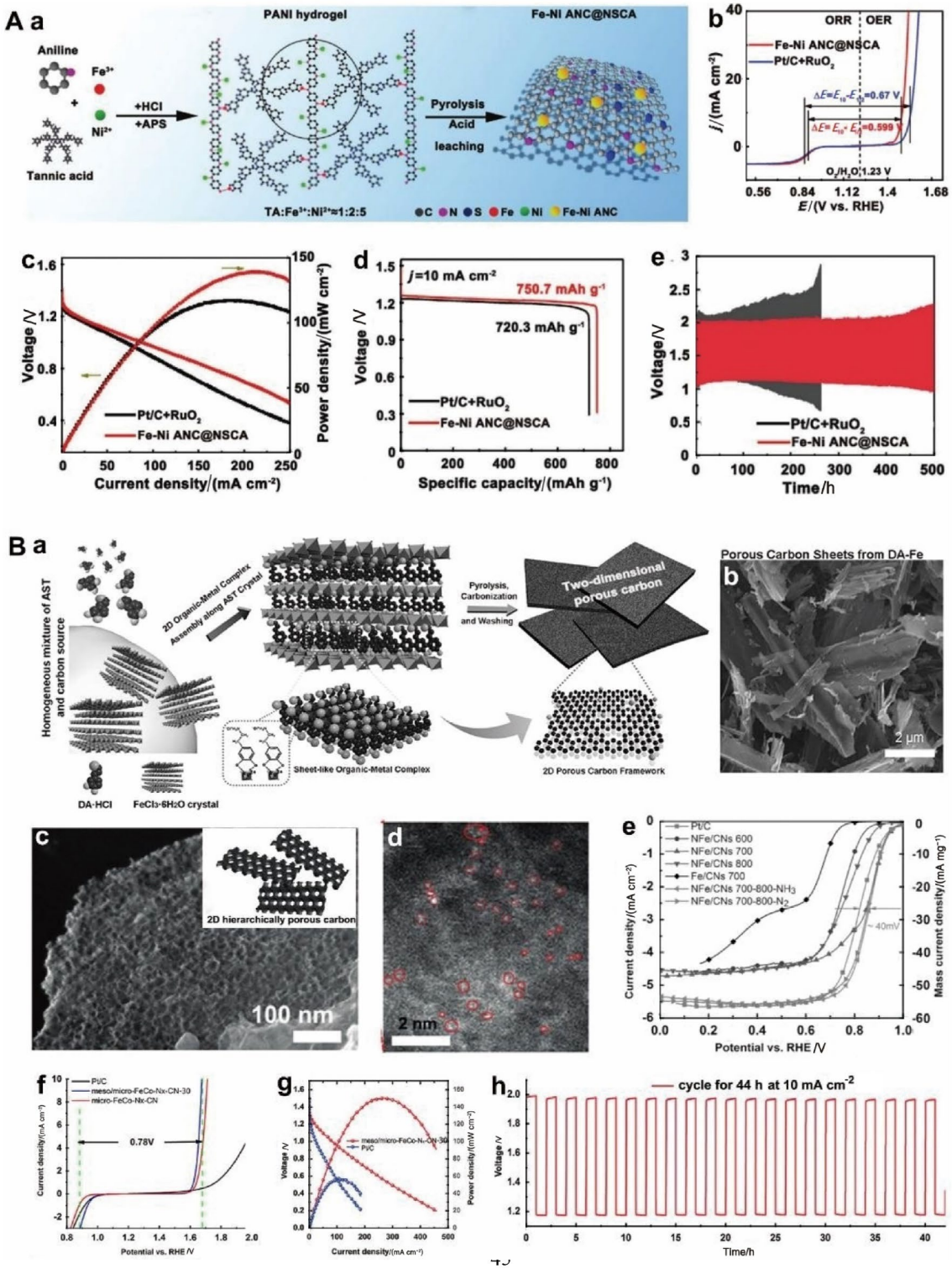

This unique coordination structure of MOF precursors can not only inhibit the aggregation or formation of large metal nanoparticles, resulting in the uniform distribution of metal doping throughout the carbon-based matrix, but also produce abundant hierarchical pores with the decomposition of organic ligands during pyrolysis. Furthermore, the diversity of metal ions and organic linkers with different organic groups and structures can lead to a variety of MOF-derived nanostructured carbon materials [215]. Because of these advantages, MOF-derived carbon materials as emerging ORR or bifunctional oxygen catalysts have attracted

◂**Fig. 12** **A**. **a** Schematic of the synthesis route of the Fe–Ni ANC@NSCA catalyst. **b** LSV curves of Fe–Ni ANC@NSCA and Pt/C + RuO_2. **c** Discharge polarization and power density curves. **d** Specific capacity plots. **e** Stability testing curves of Zn-air batteries assembled with Fe–Ni ANC@NSCA and Pt/C + RuO_2. Reproduced with permission from Ref. [195]. Copyright 2021, Wiley–VCH GmbH. **B**. **a** Synthesis of 2D microporous carbon nanosheets. **b** SEM image of porous carbon sheets from DA-Fe. **c** SEM and **d** HAADF-STEM images of meso-/micro-FeCo-N_x-CN. **e** ORR LSV curves of NFe/CNs-700–800-NH_3 and other counterparts. **f** Comparison of E_{gap} values of different catalysts. **g** Discharge plots and corresponding power density of Zn-air batteries assembled by using meso-/micro-FeCo-N_x-CN and Pt/C. **h** Long-time charge and discharge curves of meso-/micro-FeCo-N_x-CN. **a**, **b**, **e** Reproduced with permission from Ref. [200]. Copyright 2017, Wiley–VCH GmbH. **c**, **d**, **f**–**h** Reproduced with permission from Ref. [204]. Copyright 2018, Wiley–VCH GmbH

widespread interest for use in Zn-air batteries [130, 136, 216–223].

4.3.3.1 MOF-Derived Single-Atom-Decorated Carbon Zeolitic imidazole frameworks (ZIFs) as a representative MOF series were synthesized by strong bonding between imidazole derivatives and transition metals, especially Zn(II) and Co(II) ions [85, 224–231]. Metal-doped ZIF-8 (Zn) precursors are promising candidates for the fabrication of porous NC and single-atom-doped porous NC catalysts since the melting and escape of Zn at high temperatures prevent the agglomeration of other nanoparticles [89, 232–236]. For example, a hierarchical porous (micro-meso-macropore) NC catalyst (N-HPC) with trace Fe was fabricated by pyrolysis of the assembled ZIF-8 and rGO by means of foam copper impregnated with a ferrous acetate solution [234]. Benefitting from the N-doped, hierarchically porous, and noncovalently joined N-deficient/N-rich heterostructures, the N-HPCs manifested improved adsorption for oxygen intermediates and facilitated electron transfer; thus, a high $E_{1/2}$ of 0.920 V for the ORR in a 0.1 M KOH solution was achieved. A primary Zn-air battery assembled using a N-HPC cathode catalyst showed a high power density of 158 mW cm^{-2}, far exceeding that of the benchmark Pt/C-based battery (108 mW cm^{-2}). Furthermore, a MOF-derived defect-rich NC can be directly applied as a carbon support for loading single atoms. For instance, a single Cu atom-doped defect-rich NC was also realized by pyrolysis of commercial copper(I) oxide (Cu_2O) powder with a ZIF-8-derived NC near the melting temperature of Cu_2O (1 500 K). As shown in Fig. 14A a–c, the as-synthesized Cu ISAS/NC electrocatalyst presented outstanding ORR performance, with an $E_{1/2}$ of 0.920 V (Fig. 14A d). When applied as an air cathode in a primary Zn-air battery, it demonstrated an outstanding power density of 280 mW cm^{-2}, greater than that of a Pt/C-based Zn-air battery (200 mW cm^{-2}, Fig. 14A e) [236]. Recently, the introduction of dual-atom sites has proved to be an effective way to further improve oxygen-catalytic activities [237, 238]. For example, 2D ultrathin porous NC nanosheets with adjacent Fe-N_4 and Mn-N_4 sites (FeMn-DSAC) were converted by molten salt-assisted pyrolysis of Fe/ZIF-8@Mn/GM composites. Such Fe–Mn dual-sites and 2D porous structures displayed outstanding bifunctional ORR and OER performance, with a low E_{gap} of 0.713 V, compared to other structures such as Fe-SAC, Mn-SAC, and even noble metal-based Pt/C + Ir/C (0.724 V). A flexible rechargeable Zn-air battery assembled with this catalyst exhibited a high specific capacity of 734 mAh g^{-1} at room temperature; surprisingly, the 86% specific capacity could be maintained even at the ultra-low temperature of − 40 °C [91].

4.3.3.2 MOF-Derived Metal Compound-Decorated Carbon Moreover, MOFs can also be used to fabricate carbon-based compounds with bifunctional oxygen-catalytic activity for use in rechargeable Zn-air batteries [136, 217, 239–243]. For example, a kind of double-shell nanocages (NC@Co-NGC DSNCs) with NC as the inner shell and Co–N-doped graphitic carbon as the outer shell was prepared through the pyrolysis of core–shell ZIF-8@ZIF-67. The as-prepared NC@Co-NGC DSNCs showed a lower E_{gap} of 0.820 V than single-shell nanocages (Co-NGC DSNCs) in alkaline electrolytes. A rechargeable Zn-air battery driven by these catalysts exhibited an excellent charge and discharge stability over 56 h at a current density of 10 mA cm^{-2} [240]. Later, the Chen group prepared NC nanorods loaded with a Fe–Ni-Co metal/metal phosphide catalyst (FeNiCo@NC-P) by pyrolysis of the dual-MOF complex Fe_2Ni_MIL-88@ZnCo-ZIF, followed by phosphatization. The hierarchically porous FeNiCo@NC-P exhibited a lower E_{gap} of 0.700 V than its counterparts FeNi@C-P and Co@NC-P; therefore, the assembled rechargeable Zn-air battery realized long-time stability for 130 h without obvious voltage gap fading at a current density of 10 mA cm^{-2} [217]. Recently, a series of bimetallic compounds (e.g., FeCo, FeNi, and CoNi) encapsulated in hollow NC nanocubes were fabricated by pyrolysis of DA-coated MOFs in an NH_3 atmosphere (Fig. 14B a–c). In particular, the FeCo-NPs/NC composite displayed excellent bifunctional ORR and OER activities, with an ultra-low E_{gap} of 0.670 V (Fig. 14B d). When incorporated into an all-solid-state rechargeable Zn-air battery, this composite exhibited a large power density (~77 mW cm^{-2}) and excellent cycling stability for 32 h, with little potential gap fading at a current density of 1 mA cm^{-2}, even when bent from 0° to 180° [243].

4.3.3.3 MOF-Derived 3D Porous Carbon To further enhance the mass diffusion properties of MOF-derived carbon catalysts, a 3D macroporous nanostructure was designed by pyrolysis of SiO_2- or PS-templated MOFs [81, 225, 244, 245]. For example, ordered macroporous carbon (ZOMC) with abundant Co–N-C sites prepared from a ZIF-67-coated silica assembly displayed better bifunctional oxygen-catalytic activity than the benchmark

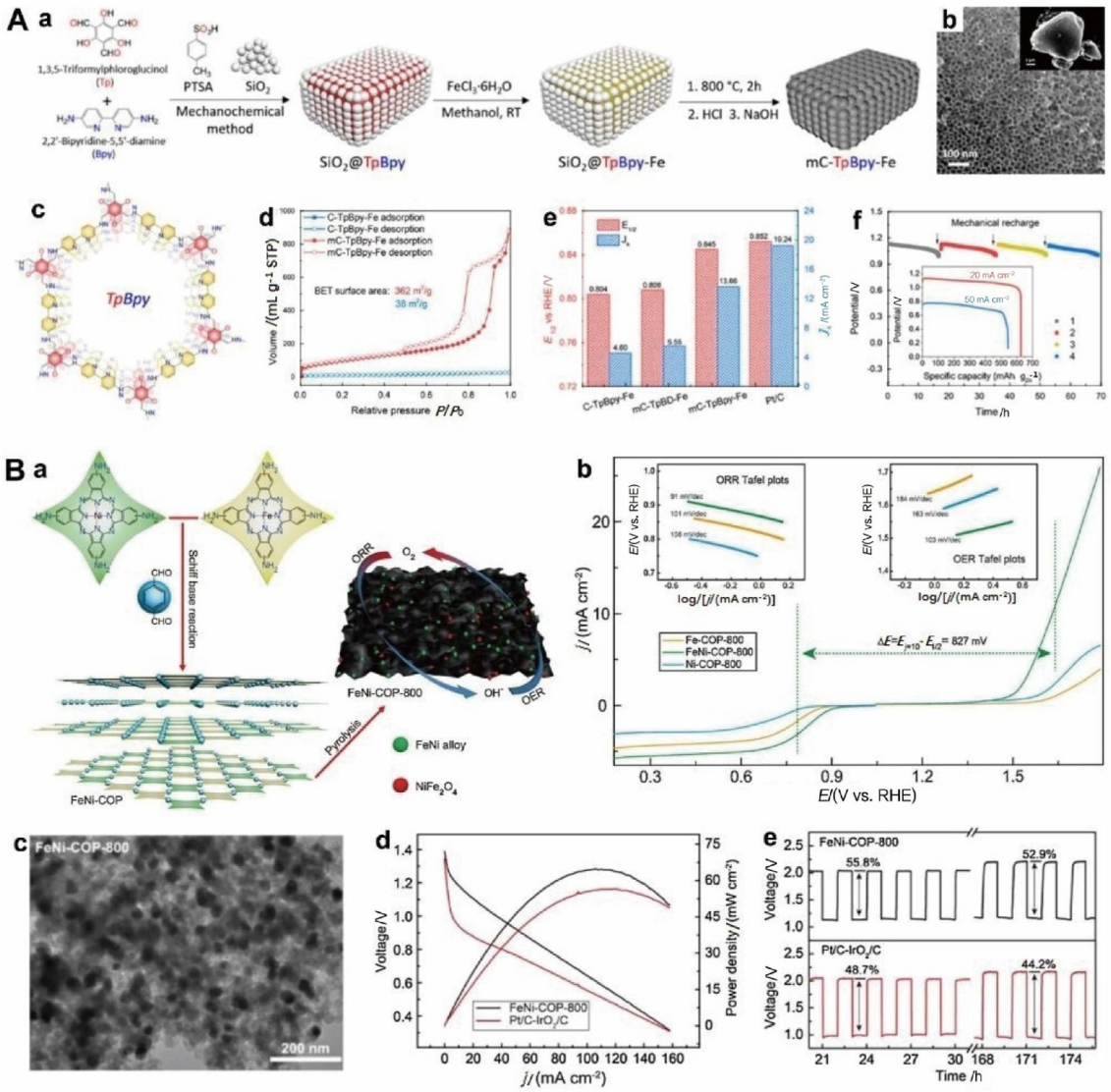

Fig. 13 **A**. **a** Schematic illustration of the preparation of mC-TpBpy-Fe. **b** SEM image of mC-TpBpy-Fe. **c** Structural diagram of TpBpy exhibiting the bipyridine coordination sites available in the COF backbone. **d** N_2 adsorption–desorption isotherms of catalysts. **e** Comparison of the $E_{1/2}$ and the kinetic current of the ORR catalysts at 0.800 V. **f** Discharge curve of a primary Zn-air battery driven by mC-TpBpy-Fe at a current density of 20 mA cm^{-2}. **a**–**f** Reproduced with permission from Ref. [19]. Copyright 2019, American Chemical Society. **B. a** Schematic diagram of the synthesis of FeNi-COP-800. **b** LSV curves of different catalysts for the ORR and the OER; the inset shows the corresponding Tafel plots. **c** TEM image of FeNi-COP-800. **d** Discharge polarization and power density plots of FeNi-COP-800- and Pt/C + IrO_2/C-based Zn-air batteries. **e** Charge–discharge cycle plots of assembled Zn-air batteries with FeNi-COP-800 and Pt/C + IrO_2/C. **a**–**e** Reproduced with permission from Ref. [210]. Copyright 2019, Elsevier B.V

Pt/C catalyst [225]. Thus, a rechargeable Zn-air battery equipped with the ZOMC cathode achieved a high power density of up to 221 mW cm^{-2} and operated for more than 160 h. A trimodal-porous carbon dispersed with Fe and Ni sites (Fe/Ni-N_x/OC) was synthesized by combining PS templates with Fe,Ni-doped-ZIF-8 ((Fe, Ni)-ZiF-8@PS) [245]. This unique porous configuration and the coexisting Fe-N_4 and Ni-N_4 active centers endowed Fe/Ni-N_x/OC with exceptional ORR activity ($E_{1/2}$ = 0.938 V, Fig. 15A. When applied as an air cathode in a primary Zn-air battery, Fe/Ni-N_x/OC displayed a large peak power density of 148 mW cm^{-2}. Furthermore, the self-templating method is another important way to construct 3D micro-/mesoporous carbon-based oxygen catalysts via the in situ pyrolysis of organics and the release of small molecules [239, 246]. As an example, the Xu group obtained 3D ordered open carbon cages with micro-/mesopores via direct pyrolysis of the morphology-controlled Fe(III)-doped core@shell Zn@Co-MOFs precursor (Fig. 15B a–c). Such open carbon cages endowed the resultant CoFe20@CC with supe-

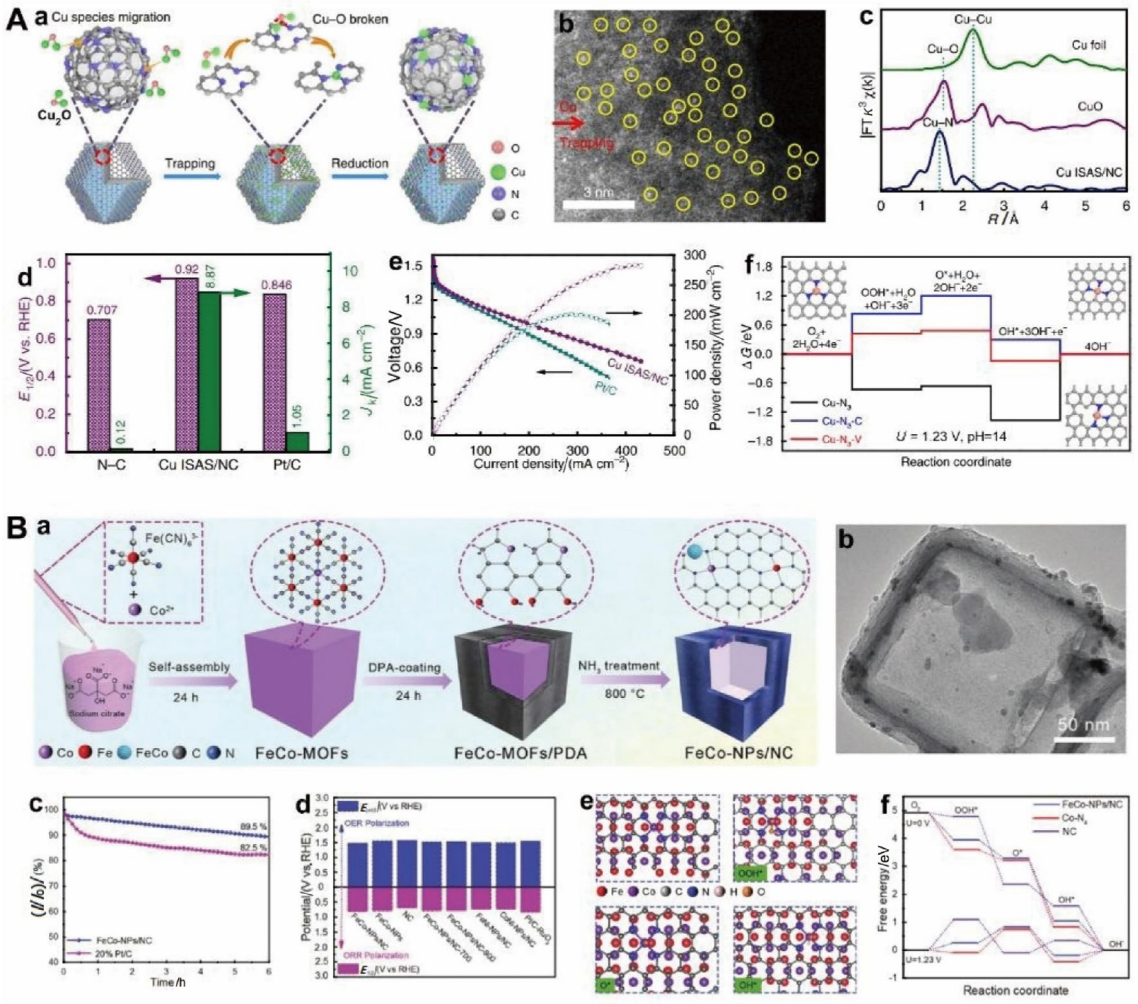

Fig. 14 **A**. **a** The synthetic procedure of isolated Cu active centers, **b** AC HAADF-STEM image of the Cu ISAS/N–C catalyst, the single Cu atoms are marked with yellow circles. **c** FT-EXAFS spectra in *k* space of the Cu ISAS/N–C catalyst. **d** $E_{1/2}$ and kinetic current density (j_k) of different catalysts. **e** Polarization and power density profiles. **f** Free energy diagram of three desired models (inset) for the ORR. **a**–**f** Reproduced with permission from Ref. [236]. Copyright 2019, Nature Publishing Group. **B. a** Schematic diagram of the fabrication process and **b** TEM image of FeCo-NPs/NC. **c** Durability of FeCo-NPs/NC and Pt/C for ORR. **d** Comparisons of $E_{1/2}$ and $E_{j\ =\ 10}$ of various catalysts. **e** Illustration of the adsorption of oxygen intermediates on FeCo-NPs/NC. **f** Free energy plots of the ORR at $U = 0$ and 1.230 V. **a**–**f** Reproduced with permission from Ref. [243]. Copyright 2021, Wiley–VCH GmbH

rior bifunctional catalytic activities for the ORR and OER, comparable to those of noble metal-based RuO_2 and Pt/C catalysts. When this material was applied as a cathode in rechargeable Zn-air batteries, a substantially elongated lifetime for 400 cycles (130 h) was achieved, and a negligible voltage loss was observed (Fig. 15B d) [239].

Based on the above discussion, considerable progress has been made in the design of carbon supports for advanced oxygen electrodes, as listed in Table 3. Conventional carbon nanomaterials exhibit excellent ORR activities and stabilities when incorporated into primary Zn-air batteries. Surface functionalization, heteroatom doping, and defect engineering are commonly used strategies to augment the oxygen-catalytic activities and realize rechargeable performance. Although most of the porous carbon supports and organic precursor-derived carbon electrodes have realized satisfactory bifunctional oxygen activities and rechargeable performance, there are still challenges in achieving a high energy density and durability for practical applications. Therefore, the development of high-power Zn-air batteries for practical applications will be discussed in the following section.

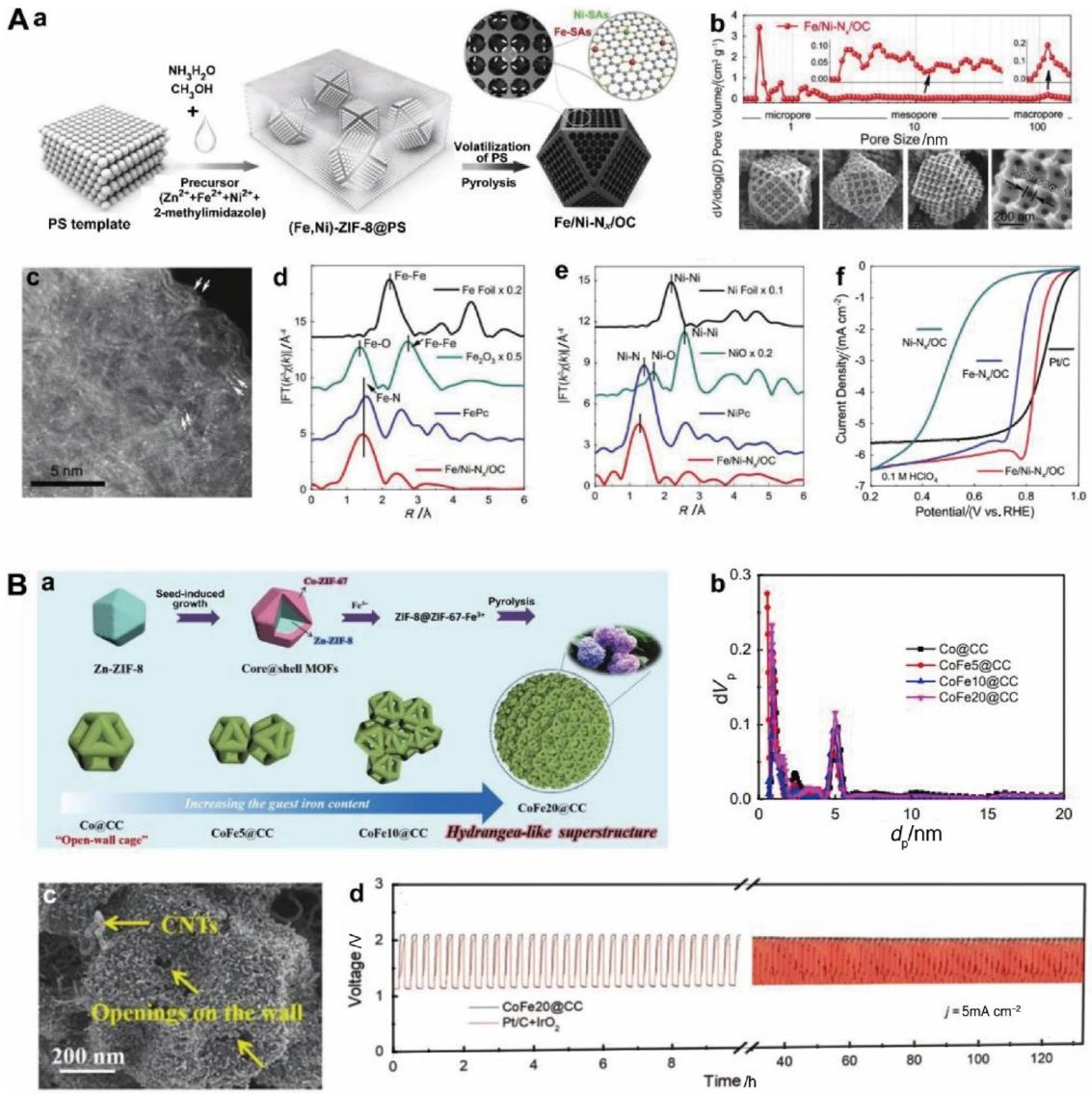

Fig. 15 **A**. **a** Schematic diagram of the synthesis process, **b** pore size distributions (top) and SEM images (bottom), **c** HAADF-STEM image of Fe/Ni-N_x/OC. FT-EXAFS spectra of Fe/Ni-N_x/OC and reference materials at **d** the Fe K-edge and **e** the Ni K-edge. **f** ORR LSV curves of different catalysts in 0.1 M KOH. **a**–**f** Reproduced with permission from Ref. [245]. Copyright 2020, Wiley–VCH GmbH. **B. a** Schematic diagram of the fabrication of porous CN-based oxygen catalysts through the self-template pyrolysis strategy. **b** Pore size distributions of different precursors. **c** SEM image of CoFe20@CC. **d** Discharge–charge cycling test of CoFe20@CC and Pt/C-IrO_2 at 5 mA cm^{-2}. **a**–**d** Reproduced with permission from Ref. [239]. Copyright 2019, Wiley–VCH GmbH

5 Representative Applications of Nanostructured Carbon-Based Electrodes for Zn-Air Batteries

5.1 Flexible Zn-Air Batteries

Over the years, flexible Zn-air batteries have received increased attention in wearable electronics due to their large theoretical energy density, aesthetic versatility, and easy incorporation into irregular geometric surfaces [247, 248]. Although the preparation of diverse advanced flexible Zn-air batteries has been attempted, along with consecutive promotion in design strategies and assembly technologies [249], the development of specifically functionalized electrodes that exhibit a combination of superior flexibility, safety, comfort, and excellent battery performance remains a considerable challenge [249]. The first obstacle hindering the preparation of flexible Zn-air batteries is achieving air cathode flexibility. Accordingly, carbon-based cathodes with good conductivity, stability, and easily constructed porous structures, such as CNT paper, CNF cloth, graphene or porous graphene film, and carbon foam, have shown

Table 3 ORR/OER and Zn-air battery performance of electrocatalysts with different carbon supports

Support	Electrocatalyst	ORR/($E_{1/2}$, V)	OER/($E_{j=10}$, V)	E_{gap}/V	Peak power density/ (mW cm^{-2})	Specific capacity/ (mAh g_{Zn}^{-1})	Stability	Reference
Conventional carbon nanomaterial	DN-UGNR	0.808(0.1 M KOH)	1.742(0.1 M KOH)	0.934	151		300 cycles @5 mA cm^{-2}	[147]
	2D BNC-800	0.81(0.1 M KOH)			14.6		11 h@20 mA cm^{-2}	[150]
	N/S-2DPCs-60	0.75(0.1 M KOH)			0.69		12 h@20 mA cm^{-2}	[151]
	*pf*SAC-Fe-0.2	0.91(0.1 M KOH)			123.43	732	300 h@5 mA cm^{-2}	[80]
	OCNTs	0.850(1.0 M KOH)	1.546(1.0 M KOH)	0.696	130		340 h@5 mA cm^{-2}	[154]
	CoNC@LDH	0.84(0.1 M KOH)	1.47(0.1 M KOH)	0.63	173	800	3600 cycles@10 mA cm^{-2}	[162]
Porous carbon supports	Ni-MnO/rGO aerogels	0.78(0.1 M KOH)	1.6(0.1 M KOH)	0.82	123	758	100 cycles @10 mA cm^{-2}	[100]
	FeP/Fe_2O_3@NPCA	0.838(0.1 M KOH)	1.632	0.79	130	767	160 h@5 mA cm^{-2}	[172]
	Co/CNFs (1000)	0.896(0.1 M KOH)	1.55(1.0 M KOH)	0.654	163	~690	200 h@15 mA cm^{-2}	[173]
	CoS_x/Co-NC-800	0.80(0.1 M KOH)	1.54(0.1 M KOH)	0.74	103	770.4	200 h@2 mA cm^{-2}	[174]
	Ni@N-HCGHF	0.875(0.1 M KOH)	1.49(1.0 M KOH)	0.615	117.1	706	20 h@10 mA cm^{-2}	[175]
	CoFe/N-GCT	0.79(0.1 M KOH)	1.67(0.1 M KOH)	0.88	203		267 h@10 mA cm^{-2}	[176]
	$CoIn_2S_4$/S-rGO	0.82(0.1 M KOH)	1.6(0.1 M KOH)	0.78	133	745	50 h@10 mA cm^{-2}	[177]
	$NiCo_2S_4$@g-C_3N_4-CNT	0.76(0.1 M KOH)	1.56(1.0 M KOH)	0.8	142	493.0	110 h@10 mA cm^{-2}	[178]
	S-GNS/$NiCo_2S_4$	0.88(0.1 M KOH)	1.56(0.1 M KOH)	0.68	216.3		100 h@10 mA cm^{-2}	[179]
	Ni,N-codoped np-graphene	0.845(0.1 M KOH)	1.5(1.0 M KOH)	0.655	83.8		43 h@2 mA cm^{-2}	[180]
	N-Mo-holey G	0.85(0.1 M KOH)	1.53(1.0 M KOH)	0.68	83		88 h@2 mA cm^{-2}	[181]
Organic precursor-derived carbon supports	NPC-1000	0.91(0.1 M KOH)	1.63(0.1 M KOH)	0.72	50	641.6	50 h@1 mA cm^{-2}	[183]
	meso/micro-P*o*PD	0.85(0.1 M KOH)				~630	100 h@10 mA cm^{-2}	[187]
	Fe–Ni ANC@NSCA	0.891(0.1 M KOH)	1.49(1.0 M KOH)	0.599	140.3	750.7	500 h@5 mA cm^{-2}	[195]
	FeP_x/Fe–N-C/NPC	0.86(0.1 M KOH)	1.555(1.0 M KOH)	0.695		739	33.3 h@20 mA cm^{-2}	[197]
	meso/micro-FeCo-N_x-CN-30	0.886(0.1 M KOH)	1.67(0.1 M KOH)	0.784	150		42.5 h@10 mA cm^{-2}	[204]
	mC-TpBpy-Fe	0.845(0.1 M KOH)			~81	~625	70 h@20 mA cm^{-2}	[19]
	CoNP-PTCOF	0.85(0.1 M KOH)	1.68(0.1 M KOH)	0.83	53	796.9	120 h@10 mA cm^{-2}	[214]

Table 3 (continued)

Support	Electrocatalyst	ORR/($E_{1/2}$, V)	OER/($E_{j=10}$, V)	E_{gap}/V	Peak power density/ (mW cm^{-2})	Specific capacity/ (mAh g_{Zn}^{-1})	Stability	Reference
	FeNi-COP-800	0.803(0.1 M KOH)	1.63(0.1 M KOH)	0.827	64		175 h@5 mA cm^{-2}	[210]
	N-HPCs	0.92 (0.1 M KOH)			158	829	100 h@5 mA cm^{-2}	[234]
	FeMn-DSAC	0.922(0.1 M KOH)	1.605(0.1 M KOH)	0.713	184	734	80 h@2 mA cm^{-2}	[91]
	Cu ISAS/NC	0.92 (0.1 M KOH)			280	~736	45 h@20 mA cm^{-2}	[236]
	NC@Co-NGC DSNC	0.82(0.1 M KOH)	1.64(0.1 M KOH)	0.82	109		56 h@10 mA cm^{-2}	[240]
	FeNiCo@ NC-P	0.84 (0.1 M KOH)	1.54 (0.1 M KOH)	0.7	112	807	135 h@10 mA cm^{-2}	[217]
	FeCo-NPs/NC	0.82 (0.1 M KOH)	1.49 (1.0 M KOH)	0.67	77	751.6	32 h @1 mA cm^{-2}	[243]
	ZOMC	0.85(0.1 M KOH)	1.56(0.1 M KOH)	0.71	221.1	795.3	160 h @5 mA cm^{-2}	[225]
	Fe/Ni-N_x/OC	0.938(0.1 M KOH)	1.668(1.0 M KOH)	0.73	148	712	310 h@20 mA cm^{-2}	[245]
	CoFe20@CC	0.86(0.1 M KOH)	1.516(0.1 M KOH)	0.656	190.37	787.9	130 h@5 mA cm^{-2}	[239]

promise in applications in flexible Zn-air batteries [72, 180, 250, 251]. Currently, the available flexible carbon-based air cathodes have been mainly constructed by two methods: (i) spraying technique (spraying electrocatalyst ink onto flexible porous current collectors) and (ii) in situ fabrication (in situ preparation of electrocatalysts/current collectors incorporated into free-supporting electrodes).

Spraying is a common method to design flexible electrodes coated with the desired electrocatalysts as long as the electrocatalyst powder can be prepared. Various impressive works related to this method have been reported. Recently, a fabricated N-doped CNT/rGO composite prepared by pyrolyzing MOFs grown on rGO nanosheets exhibited excellent ORR propertied with an $E_{1/2}$ of 0.850 V, which is very similar to that of noble metal-based catalysts [252]. After being sprayed onto a carbon cloth, the N-CNT/rGO catalyst was applied to construct an excellent air cathode for use in flexible primary Zn-air batteries. Impressively, when the resulting battery was studied in various bending states, the loaded battery still displayed a small voltage gap and steady charge/discharge potentials. In another representative work, a 2D multilayer mesoporous Co_3O_4/N-rGO catalyst was fabricated via facile solvothermal and oxidation treatment and displayed excellent electrochemical performance with a lower E_{gap} value of 0.930 V than that of a commercial Pt/C catalyst (1.16 V) [126]. As shown in Fig. 16A, after being sprayed onto Toray carbon fibers (the red circle), this Co_3O_4/N-rGO was knitted into a fiber-shaped rechargeable Zn-air battery with a desirable length and woven into clothing to power various portable products, such as smart glass, wearable sensors, and electronic devices. Nevertheless, the flexibility of oxygen electrodes obtained via spraying mainly depends on the flexibility of the conductive substrates, of which CNTs and graphene showed more favorable deformability than CNF cloth. Furthermore, certifying the strong interaction between the electrocatalyst and current collector is a considerable challenge during the spraying technique. Moreover, the usage of conductive substrates improves the total weight. All of these factors are critical to improving the cycling stability, rate capability, and energy density of the battery. Therefore, developing another synthetic method to maintain both satisfactory interactions and flexibility is necessary.

The in situ construction strategy of free-supporting electrocatalysts aims to solve the above-mentioned issues inherent to the spraying technique. Generally, the construction of free-supporting electrocatalyst involves an elaborate configuration and comparatively complicated post-processing. According to the literature to date, freestanding air cathodes with high catalytic sites and unique microstructures can be synthesized via three general methods or their combinations: the hydrothermal growth, solvothermal method, electrospinning, or CVD [12]. The resulting composite free-supporting cathode electrocatalyst was fairly flexible and exhibited satisfactory catalytic activities even under various deformation conditions. A typical example is that a flexible freestanding air cathode of oxygenated cobalt vanadium selenide (O-$Co_xV_{1-x}Se_2$)

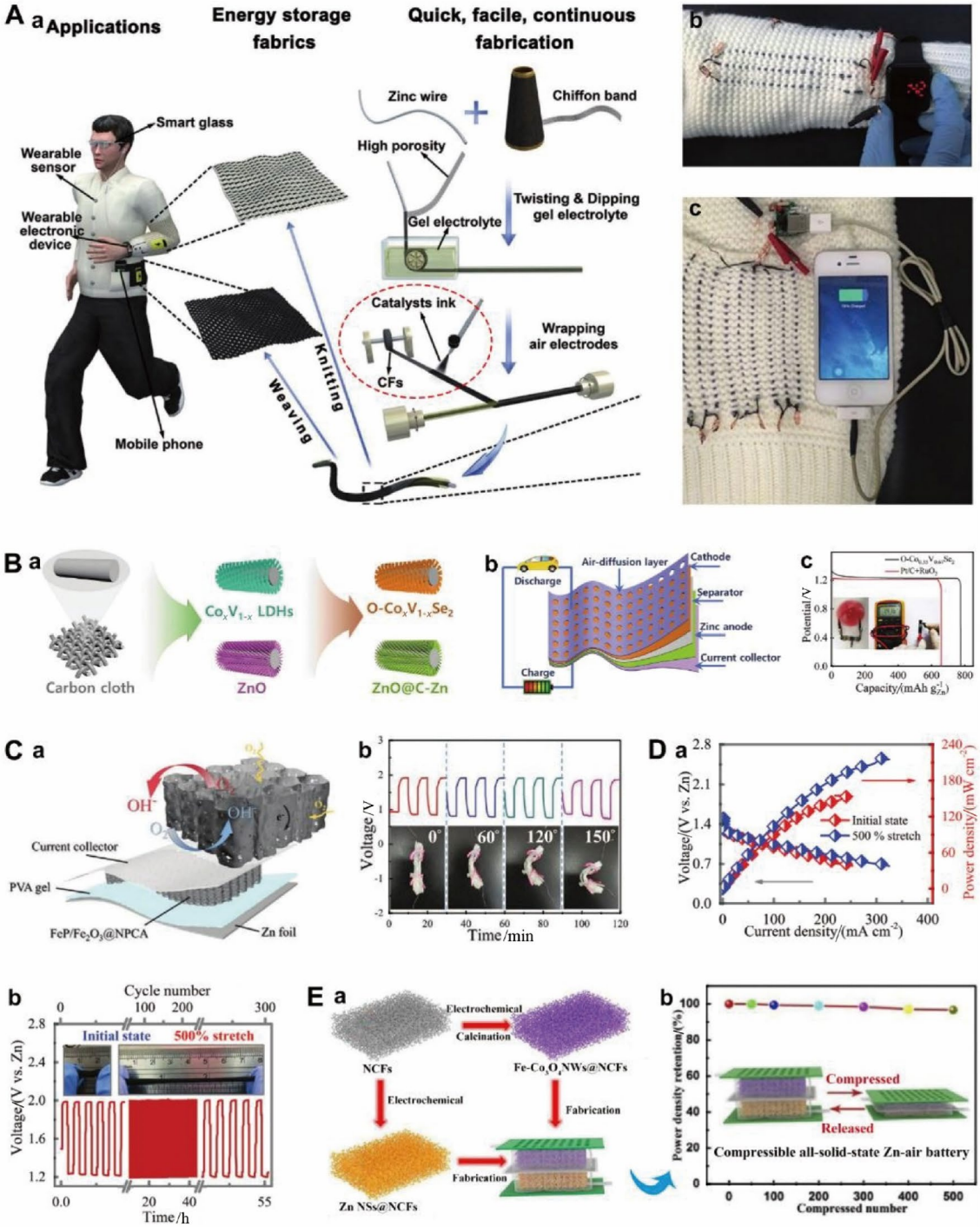

Fig. 16 **A. a** Preparation of a flexible fiber-shaped Zn-air battery. **b** Photographs of an LED watch and **c** iPhone 4 s powered by this battery. **a**–**c** Reproduced with permission from Ref. [126]. Copyright 2018, Wiley–VCH GmbH. **B. a** Preparation, **b** assembly, and **c** discharge plots of a flexible Zn-air battery. **a**–**c** Reproduced with permission from Ref. [253]. Copyright 2020, Wiley–VCH GmbH. **C. a** Schematic of the material configuration and **b** charge/discharge cycling curve of a flexible Zn-air battery. **a**–**b** Reproduced with permission from Ref. [172]. Copyright 2020, Wiley–VCH GmbH. **D. a** Polarization and power density plots and **b** the corresponding cycling profile of stretchable Zn-air batteries. **a**–**b** Reproduced with permission from Ref. [254]. Copyright 2019, Wiley–VCH GmbH. **E. a** Preparation and **b** power density retention (%) of a squeezable Zn-air battery. **a**–**b** Reproduced with permission from Ref. [251]. Copyright 2019, Elsevier B.V

grew directly on carbon fiber cloth (CFC) via hydrothermal-assisted selenization (Fig. 16B a). In addition, a CFC-based anode composed of porous 3D ZnO@C-Zn nanorods was also obtained. When poly(vinyl alcohol) (PVA)/KOH was utilized as the gel electrolyte, the fabricated flexible rechargeable Zn-air battery (Fig. 16B b) displayed an excellent specific capacity of 775 mAh g_{Zn}^{-1}, far exceeding that of a Pt/C-RuO_2 assembled Zn-air battery (Fig. 16B c) [253]. Furthermore, CNFs covered with single Co (or Ni) atoms and NC flakes (named M SA@NCF/CNF) were fabricated by self-assembled growth of ZIF on polyacrylonitrile (PAN) nanofibers and subsequent pyrolysis and etching. The assembled flexible rechargeable Zn-air battery displayed outstanding stability under different deformation states could supply power for three light-emitting diodes (LEDs) simultaneously [250]. However, the extremely compact fibrous configuration led to decreased air/electrolyte penetrability and incompetent air diffusion for ideal battery applications. Simultaneously, the loading contents of the electrocatalysts were also restricted by the small specific surface area of the carbon cloth. Currently, these restrictions can be alleviated by constructing 3D porous carbon aerogels through directional freeze-casting and subsequent pyrolysis, promoting the catalysis reactions at the interface and resulting higher electroconductibility by the absence of polymer additives [172]. For example, a flexible rechargeable Zn-air battery driven by FeP/Fe_2O_3 nanoparticle-decorated N,P-doped carbon aerogel catalyst cathodes showed a remarkable specific capacity and cyclability under various deformation conditions (Fig. 16C) [172].

In addition, stretchability is another intrinsic feature of flexible Zn-air batteries that can be achieved by designing both stretchable electrodes and gel polymer electrolytes (GPEs). Based on a metal Zn spring, a CNT paper-loaded catalyst, and 1 200% stretchable GPEs, a stretchable fiber Zn-air battery was constructed and showed excellent waterproofness, ambient adaptive capacity, and catalytic performance, even under 500% stretching (Fig. 16D) [254]. On the other hand, compressible performance was also achieved in a carbon-based rechargeable Zn-air battery, and displayed a tiny alteration in power density which was observed after 500 deformation cycles (Fig. 16E) [251]. The cathode and anode were, respectively, fabricated by electroplating Fe-Co_3O_4 nanowires and Zn nanosheets on 3D porous N-doped carbon foam (NCF).

5.2 High-Power Zn-Air Batteries

Zn-air batteries have shown promising potential as alternatives to energy storage devices; some basic parameters are used to estimate the properties of energy storage systems, such as power density (mW cm^{-2}), specific capacity (mAh g_{Zn}^{-1}), cycle life, safety, and cost. There are two major weaknesses of Zn-air batteries: the short life span when recharged electrically and Zn anode dendrite generation resulting in short circuits and shedding of Zn. However, these factors do not affect primary Zn-air batteries because their Zn anodes can be mechanically replaced by new Zn metal. In 1999, the Electric Fuel Ltd. Co. developed a mechanically rechargeable Zn-air battery for military use and a fleet of electric vehicles [255]. Thereafter, various studies have focused on how to reduce the high overpotential in the cathode reaction and offer a high power density by constructing novel catalysts and optimizing air electrode structures, and the previous sections have discussed many carbon-based oxygen electrodes for Zn-air batteries. In particular, 2D Ni-doped CoO nanosheets with abundant micro-/nanostructures exhibit favorable O_2 diffusion, enhanced catalytic activation, and improved native ORR performance at the catalytic center by Ni doping. Integration of CB substrates as air cathodes in primary Zn-air batteries resulted in an ultrahigh power density (377 mW cm^{-2}, Fig. 17A a), and integrated all-solid-state coin cells can be used to power an iPhone 7 mobile phone (Fig. 17A b–d) [256].

Although considerable effort has been made in developing cathode catalysts, the electrolytes are also bottleneck factors that highly restrict the power density and working life of Zn-air batteries. Optimizing Zn-air batteries as a whole is essential for further performance improvement, and some researchers have always been devoted to developing novel electrolytes. For example, Song and coworkers produced a kind of GPE gel electrolyte via multistep cross-linking reactions involving PVA, GO, and poly(acrylic acid) [257]. The resultant PVAA-GO GPE displayed much greater performance than previously reported PVA electrolytes in terms of ionic conductivity, mechanical strength, and water-retaining properties, which endows rechargeable Zn-air batteries with a minimal charge potential of 1.69 V, a superb energy efficiency of up to 73%, and a life-span working stability over 200 h, even under various severe working conditions. For example, a series of cable and sandwich forms of Zn-air batteries have been, respectively, incorporated into clothing for charging of smartwatches (Fig. 17B), and a sandwich from of rechargeable Zn-air batteries has been incorporated into commercial electroluminescence devices.

The above-mentioned endeavors to promote the performance of Zn-air batteries have concentrated on designing bifunctional cathode catalysts or increasing the Zn anode lifetime via the development of improved electrode structures or electrolyte additives. However, formidable challenges remain in the preparation of secondary Zn-air batteries. Recent studies have reported that near-neutral electrolytes could inhibit the generation of Zn dendrite and carbonates [258, 259]. Thus, based on a CB cathode,

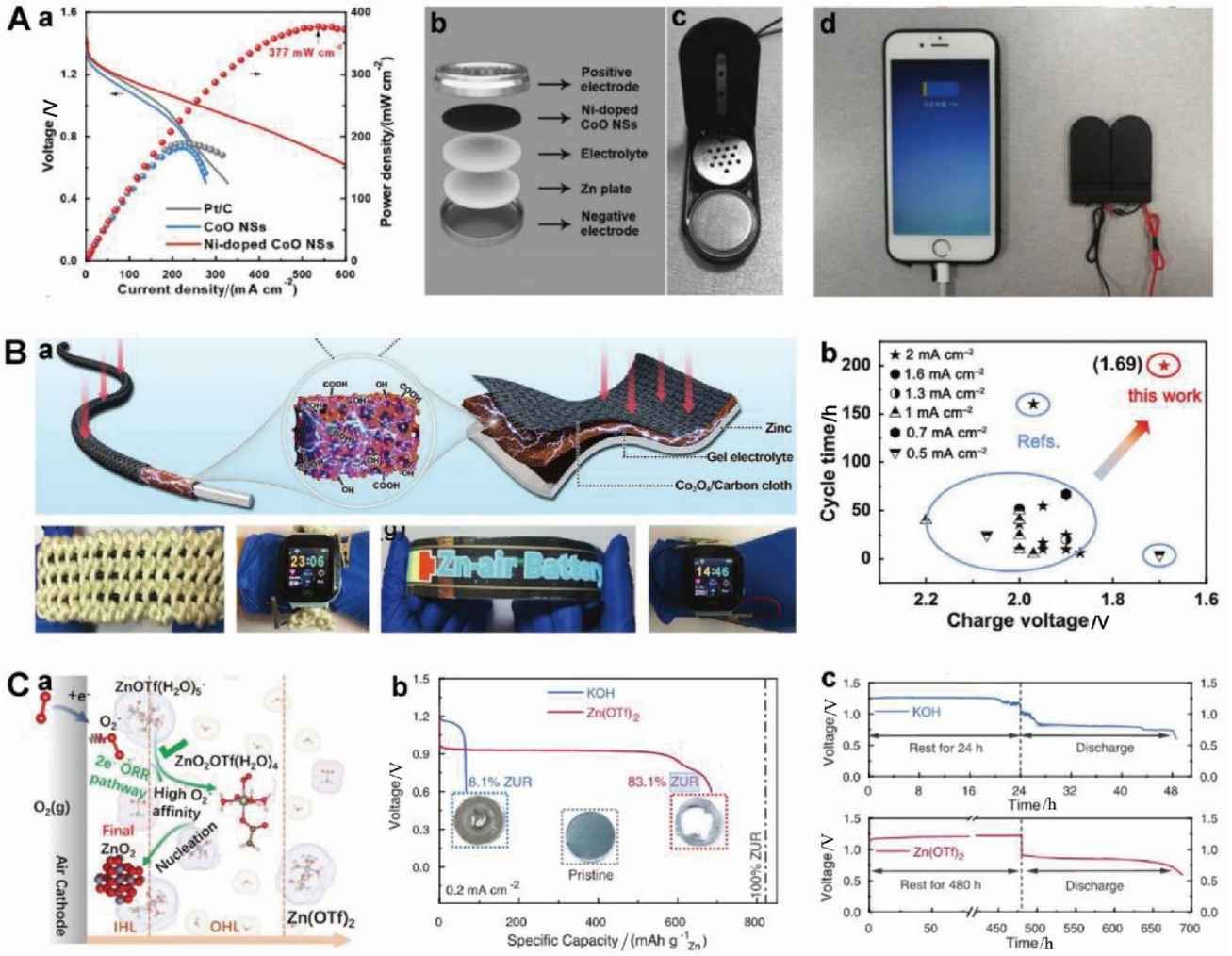

Fig. 17 **A**. **a** Polarization curves and power density plots of integrated batteries using different catalysts as air electrodes. **b** Schematic of the structure and photographs of **c** a button-like Zn-air battery and **d** an iPhone 7 powered by 4 series-connected cells. **a**–**d** Reproduced with permission from Ref. [256]. Copyright 2018, Wiley–VCH GmbH. **B.** **a** Top: schematic of the structure of the cable and sandwich forms of Zn-air batteries using PVAA-GO GPE. Bottom: corresponding photographs of connected cells used to power a commercial smartwatch. **b** Comparison of the cycle time and charge potential of the sandwich form of KI-PVAAGO-based Zn-air batteries with other batteries. **a**–**b** Reproduced with permission from Ref. [257]. Copyright 2020, Wiley–VCH GmbH. **C.** **a** Schematic diagram of the reaction procedures in the IHL and the outer Helmholtz layer (OHL). **b** Galvanostatic discharge plots of Zn-air batteries, different electrolytes, and the corresponding Zn utilization ratios (ZURs). The insets show photographs of a pristine Zn anode and after discharge in distinct electrolytes. **c** Storage of Zn-air batteries using distinct electrolytes. **a**–**c** Reproduced with permission from Ref. [4]. Copyright 2021, National Academy of Sciences

a Zn metal anode, and a nonalkaline zinc trifluoromethanesulfonate ($Zn(OTf)_2$) electrolyte, Sun and coworkers developed a Zn-O_2/ZnO_2 complex that underwent a 2e$^-$/O_2 pathway as a result of its water-poor and Zn^{2+}-rich inner Helmholtz layer (IHL) on the air cathode induced by the hydrophobic trifluoromethanesulfonate anions (OTf^-) (Fig. 17C a). This endowed the assembled rechargeable Zn-air full battery with an efficiently reversible redox reaction process, and the battery exhibited outstanding cycling properties in ambient air despite its simple configuration (Fig. 17C b–c). This different interface structure regulated by electrolyte features blazed a new path for electrochemical irreversibility and allowed the realization of secondary Zn-air batteries [4].

6 Conclusions and Perspectives

Nanostructured carbon-based electrodes with different oxygen-catalytic sites and carbon supports appear to be promising catalysts for efficient Zn-air batteries because of their many advantages compared to traditional metal/metal oxide and noble metal-based catalysts, such as larger surface areas, efficient oxygen-catalytic centers, hierarchically porous matrices, superior durability, and low cost. In this timely review, we have provided a comprehensive summary of the recent advances in synthesizing nanostructured carbon-based electrodes to prepare efficient Zn-air batteries, especially in tailoring the oxygen-catalytic sites and designing carbon supports. In this review, we focus on versatile synthetic strategies, characterization methods, and an in-depth understanding of the relationships between oxygen-catalytic sites/nanostructures and the oxygen electrode performance. In addition, we have highlighted the current development of flexible and high-power Zn-air batteries to illustrate their application potential in exploiting scalable, bendable, and wearable power supplies. Finally, a thorough discussion of current primary challenges and future perspectives on the rational design of nanostructured carbon-based oxygen electrodes has been given; we believe that the investigation of oxygen-catalytic carbon electrodes for Zn-air batteries is still in an early stage, and enormous challenges must be solved.

(a) As for Carbon-Based Oxygen Electrodes

The synthetic cost of carbon electrodes is a critical issue for commercial use. Based on the calculation in an earlier review, carbon nanomaterials (i.e., CBs, CNTs, graphene) and related catalysts exhibit higher conductivity and a lower cost per mass and volume than many catalysts [260]. However, further optimization of the catalytic performance by introducing heteroatoms, porosity, or porous structures would increase the cost of such carbon catalysts, which may increase the final price to even more than that of commercial Pt/C. Therefore, more effort should be devoted to decreasing the cost of carbon nanomaterial-based electrocatalysts. As for the organic precursor (i.e., metal-free polymer, metal-coordinated hybrid and polymer, and MOF)-derived carbon catalysts, the high cost of the organic molecules and the synthetic processes may also be substantial barriers preventing their commercialization. On the other hand, pyrolysis of precursors to afford large-scale and low-cost carbon-based catalysts is also necessary for practical applications of carbon electrodes.

In addition to considering the scale-up production, the well-defined oxygen-catalytic sites, controllable morphology, and optimized porosities should also be taken into account to balance the performance of electrical conductivity, cycling stability, and mass/air transport. Generally, carbon supports with high-density functional groups or edge sites can endow the anchored catalytic sites with better dispersion and smaller sizes. Furthermore, carbon with different porosities can increase the number of catalytic centers to improve the electrocatalytic activities of carbon electrodes. Further tuning of the configuration of carbon, the heteroatom-doping level, and the degree of graphitization of carbon electrodes is essential for increasing the intrinsic activity of catalytic sites and improving the transport issues. However, the controlled engineering of catalytic sites in carbon electrodes does not seem to be an easy task to achieve. Therefore, organic precursors with well-defined and tailorable structures, particularly those with N/P/S-doping, constitute a powerful toolbox to design tailor-made carbon electrodes for Zn-air batteries. Furthermore, an in-depth understanding of structure-performance relationships involved in Zn-air batteries has become feasible thanks to the elaborate structural control achieved in recent sophisticated studies.

For flexible electrodes, many of the currently synthesized carbon electrodes show promising potential for the fabrication of flexible Zn-air batteries in the form of cable or sandwich structures. However, more effort should be committed to improving the Zn-air batteries' properties in terms of energy density, cycling life, and fast charging, as well as the ionic conductivity of flexible carbon electrodes. In addition, enormous challenges related to the low-cost, lightweight, and flexible carbon electrodes that can be applied in flexible and wearable commercial devices on a large scale remain to be addressed.

(b) Concerning the Development of Electrolytes

The oxygen catalysis process occurs at the solid (active catalysts)–liquid (electrolytes)–gas (O_2) three-phase interface; thus, the mutual contraction of electrolytes with O_2 dissolved on the surface of the electrode is closely related to the efficiency of the reaction. Furthermore, the wettability of the electrode can affect the contact between the electrolyte and the electrode. Therefore, in addition to regulating oxygen-catalytic sites and designing nanostructured carbon-based electrodes, the properties of electrolytes should also be recognized as key points for future Zn-air battery fabrication. Generally, the widely researched alkaline liquid electrolytes possess the advantages of low toxicity, high ionic conductivity, nonflammability, and low cost. However, the problems associated with corrosion, evaporation, leakage, a narrow electrochemical stability window, and restrictions in miniaturization cannot be ignored. Moreover, carbonate precipitation (e.g., K_2CO_3 or $KHCO_3$) and the generation

of Zn dendrites are expected to decrease battery capacity. An increasing number of studies have reported that near-neutral electrolytes can inhibit the generation of Zn dendrites and that carbonates show better stability and reversibility in ambient environments [4, 258, 259]. Therefore, near-neutral electrolytes could be one of the promising future research directions.

Polymer electrolytes, including gel polymer, solid polymer, and composite polymer electrolytes, exhibit good film-forming features, excellent mechanical strength, and desired flexibility and are favorable for future devices [261, 262]. Gel polymers are widely used in flexible Zn-air batteries because of their high conductivity and simple preparation. Nevertheless, compared to liquid Zn-air batteries, flexible Zn-air batteries still exhibit a relatively low battery performance due to the high ionic resistance of the gel electrolytes. Furthermore, dehydration is a serious problem for gel electrolytes, reducing their ability to stay wet for a long time and thus decreasing their chemical durability, ion conductivity, and performance [23, 263]. Therefore, promising gel electrolytes would require good water retention, high ionic conductivity, and good stability. Currently, much effort is being devoted to these topics, and we believe that developing gel electrolytes could stimulate the commercialization of flexible Zn-air batteries.

(c) In Terms of Battery Configuration

The irreversible deposition and accumulation of ZnO, the formation of Zn dendrites, and the corrosion of high-concentration electrolytes to electrodes are key problems affecting practical applications by reducing cycling stability. To solve these problems, modifications of the composition and surface of Zn electrodes have been suggested as feasible strategies. In addition to the above problems, electrolyte leakage and inconvenient transportation are also critical problems hindering the practical application of liquid Zn-air batteries. Therefore, effort should be devoted to researching flexible Zn-air batteries, especially flexible collectors, flexible electrolytes, and packaging methods. Furthermore, Zn-air batteries currently show excellent application prospects in the grid energy storage, automotive and aerospace, and miniaturized equipment fields; thus, developing low-temperature-resistant batteries that work under extreme conditions should be another research direction of Zn-air batteries in the future.

In conclusion, we believe that this review provides new insights into the design of oxygen-catalytic carbon electrodes and paves the way to engineer efficient, robust, and flexible Zn-air batteries to further the development and prosperity of this emerging field. This review also provides perspectives on a powerful toolbox to design tailor-made carbon electrodes by engineering organic precursors with well-defined structures on the atomic, molecular, and nanoscale levels. More importantly, this review could help readers gain better insight into the advantages, key problems, and further promising solutions of carbon-based oxygen catalysts for Zn-air batteries. Looking into the future, along with the fundamental knowledge breakthroughs in the fabrication of carbon-based catalysts and the technological evolutions of Zn-air batteries devices, we believe that the large-scale production and commercial use of oxygen-catalytic carbon electrodes in Zn-air battery devices will not be far from realization.

Acknowledgements This work was financially supported by the National Key R&D Program of China (2021YFE0205000); the National Natural Science Foundation of China (Nos. 52173133, 51903178, 52161145402); the Science and Technology Project of Sichuan Province (Nos. 2022YFH0042, 2021YFH0135, 2021YJ0554); the China Postdoctoral Science Foundation (2021M692303, 2021M702334), the 1·3·5 Project for Disciplines of Excellence, West China Hospital, Sichuan University (No. ZYJC21047, 2020HXBH126); the Med-X Innovation Programme of the Med-X Center for Materials, Sichuan University (MCM202102); the State Key Laboratory of Polymer Materials Engineering (Grant No. sklpme2022-3-07, sklpme2021-4-02); and Fundamental Research Funds for the Central Universities ("Zero to One" innovative research program: 2021SCU12013). We thank our laboratory members for their generous help.

Author Contributions This manuscript was written through the contributions of all the authors. All the authors have given approval to the final version of the manuscript.

Funding Open Access funding enabled and organized by Projekt DEAL.

Declarations

Conflict of interest The authors declare no conflict of interest.

References

1. Wang, P., Zhao, D.Y., Yin, L.W.: Two-dimensional matrices confining metal single atoms with enhanced electrochemical reaction kinetics for energy storage applications. Energy Environ. Sci. **14**, 1794–1834 (2021). https://doi.org/10.1039/d0ee02651d
2. Pan, F.P., Li, Z., Yang, Z.Z., et al.: Porous FeCo glassy alloy as bifunctional support for high-performance Zn-air battery. Adv.

Energy Mater. **11**, 2002204 (2021). https://doi.org/10.1002/aenm.202002204
3. Yu, J., Li, B.Q., Zhao, C.X., et al.: Seawater electrolyte-based metal-air batteries: from strategies to applications. Energy Environ. Sci. **13**, 3253–3268 (2020). https://doi.org/10.1039/d0ee01617a
4. Sun, W., Wang, F., Zhang, B., et al.: A rechargeable zinc-air battery based on zinc peroxide chemistry. Science **371**, 46–51 (2021). https://doi.org/10.1126/science.abb9554
5. Zhu, X.F., Hu, C.G., Amal, R., et al.: Heteroatom-doped carbon catalysts for zinc-air batteries: progress, mechanism, and opportunities. Energy Environ. Sci. **13**, 4536–4563 (2020). https://doi.org/10.1039/d0ee02800b
6. Zhou, T.P., Zhang, N., Wu, C.Z., et al.: Surface/interface nanoengineering for rechargeable Zn-air batteries. Energy Environ. Sci. **13**, 1132–1153 (2020). https://doi.org/10.1039/c9ee03634b
7. Wan, C.Z., Duan, X.F., Huang, Y.: Molecular design of single-atom catalysts for oxygen reduction reaction. Adv. Energy Mater. **10**, 1903815 (2020). https://doi.org/10.1002/aenm.201903815
8. Wang, Y., Wang, D.S., Li, Y.D.: A fundamental comprehension and recent progress in advanced Pt-based ORR nanocatalysts. SmartMat **2**, 56–75 (2021). https://doi.org/10.1002/smm2.1023
9. Cai, X.Y., Lai, L.F., Lin, J.Y., et al.: Recent advances in air electrodes for Zn-air batteries: electrocatalysis and structural design. Mater. Horiz. **4**, 945–976 (2017). https://doi.org/10.1039/C7MH00358G
10. Yang, J., Qi, G.Q., Bao, R.Y., et al.: Hybridizing graphene aerogel into three-dimensional graphene foam for high-performance composite phase change materials. Energy Storage Mater. **13**, 88–95 (2018). https://doi.org/10.1016/j.ensm.2017.12.028
11. Medenbach, L., Adelhelm, P.: Cell concepts of metal-sulfur batteries (metal = Li, Na, K, Mg): strategies for using sulfur in energy storage applications. Top. Curr. Chem. Cham **375**, 81 (2017). https://doi.org/10.1007/s41061-017-0168-x
12. Zhou, J.W., Cheng, J.L., Wang, B., et al.: Flexible metal–gas batteries: a potential option for next-generation power accessories for wearable electronics. Energy Environ. Sci. **13**, 1933–1970 (2020). https://doi.org/10.1039/d0ee00039f
13. Wang, K., Wu, Y.Y., Cao, X.B., et al.: A Zn–CO_2 flow battery generating electricity and methane. Adv. Funct. Mater. **30**, 1908965 (2020). https://doi.org/10.1002/adfm.201908965
14. Yu, M.Z., Zhou, S., Liu, Y., et al.: Long life rechargeable Li-O_2 batteries enabled by enhanced charge transfer in nanocable-like Fe@N-doped carbon nanotube catalyst. Sci. China Mater. **60**, 415–426 (2017). https://doi.org/10.1007/s40843-017-9021-6
15. Cheng, Y.H., Wang, Y.L., Wang, Q.L., et al.: Hierarchically porous metal-free carbon with record high mass activity for oxygen reduction and Zn-air batteries. J. Mater. Chem. A **7**, 9831–9836 (2019). https://doi.org/10.1039/c9ta02220a
16. Kim, H., Inoishi, A., Ida, S., et al.: Solid-oxide Fe-air rechargeable battery using Fe–Ce(Mn, Fe)O_2 for low temperature operation. J. Mater. Chem. A **4**, 5482–5488 (2016). https://doi.org/10.1039/c5ta10675c
17. Asadi, M., Sayahpour, B., Abbasi, P., et al.: A lithium–oxygen battery with a long cycle life in an air-like atmosphere. Nature **555**, 502–506 (2018). https://doi.org/10.1038/nature25984
18. Zhao, X., Pachfule, P., Li, S., et al.: Bifunctional electrocatalysts for overall water splitting from an iron/nickel-based bimetallic metal-organic framework/dicyandiamide composite. Angew. Chem. Int. Ed. **57**, 8921–8926 (2018). https://doi.org/10.1002/anie.201803136
19. Zhao, X.J., Pachfule, P., Li, S., et al.: Silica-templated covalent organic framework-derived Fe-N-doped mesoporous carbon as oxygen reduction electrocatalyst. Chem. Mater. **31**, 3274–3280 (2019). https://doi.org/10.1021/acs.chemmater.9b00204
20. Zhang, J., Zhang, J., He, F., et al.: Defect and doping co-engineered non-metal nanocarbon ORR electrocatalyst. Nano-Micro Lett **13**, 65 (2021). https://doi.org/10.1007/s40820-020-00579-y
21. Wang, H.F., Tang, C., Zhang, Q.: A review of precious-metal-free bifunctional oxygen electrocatalysts: rational design and applications in Zn-air batteries. Adv. Funct. Mater. **28**, 1803329 (2018). https://doi.org/10.1002/adfm.201803329
22. Huang, Y., Wang, Y., Tang, C., et al.: Atomic modulation and structure design of carbons for bifunctional electrocatalysis in metal-air batteries. Adv. Mater. Deerfield Beach Fla **31**, e1803800 (2019). https://doi.org/10.1002/adma.201803800
23. Liu, H., Xie, W., Huang, Z., et al.: Recent advances in flexible Zn-air batteries: materials for electrodes and electrolytes. Small Methods **6**, e2101116 (2022). https://doi.org/10.1002/smtd.202101116
24. Gu, P., Xu, Y.X., Zhao, Y.F., et al.: Electrocatalysis of rechargeable non-lithium metal-air batteries. Adv. Mater. Interfaces **4**, 1700589 (2017). https://doi.org/10.1002/admi.201700589
25. Tan, P., Chen, B., Xu, H.R., et al.: Flexible Zn- and Li-air batteries: recent advances, challenges, and future perspectives. Energy Environ. Sci. **10**, 2056–2080 (2017). https://doi.org/10.1039/c7ee01913k
26. Chaturvedi, A., Chen, B., Zhang, K.K., et al.: A universal method for rapid and large-scale growth of layered crystals. SmartMat **1**, e1011 (2020). https://doi.org/10.1002/smm2.1011
27. Fu, J., Cano, Z.P., Park, M.G., et al.: Electrically rechargeable zinc-air batteries: progress, challenges, and perspectives. Adv. Mater. **29**, 1604685 (2017). https://doi.org/10.1002/adma.201604685
28. Sun, Y.Y., Sinev, I., Ju, W., et al.: Efficient electrochemical hydrogen peroxide production from molecular oxygen on nitrogen-doped mesoporous carbon catalysts. ACS Catal. **8**, 2844–2856 (2018). https://doi.org/10.1021/acscatal.7b03464
29. Melchionna, M., Fornasiero, P., Prato, M.: The rise of hydrogen peroxide as the main product by metal-free catalysis in oxygen reductions. Adv. Mater. **31**, e1802920 (2019). https://doi.org/10.1002/adma.201802920
30. Li, Y., Dai, H.: Recent advances in zinc-air batteries. Chem. Soc. Rev. **43**, 5257–5275 (2014). https://doi.org/10.1039/c4cs00015c
31. Li, Q., Cao, R.G., Cho, J., et al.: Nanocarbon electrocatalysts for oxygen reduction in alkaline media for advanced energy conversion and storage. Adv. Energy Mater. **4**, 1301415 (2014). https://doi.org/10.1002/aenm.201301415
32. Peng, Y., Lu, B., Chen, S.: Carbon-supported single atom catalysts for electrochemical energy conversion and storage. Adv. Mater.,(2018). https://doi.org/10.1002/adma.201801995
33. Zeng, K., Zheng, X.J., Li, C., et al.: Recent advances in non-noble bifunctional oxygen electrocatalysts toward large-scale production. Adv. Funct. Mater. **30**, 2000503 (2020). https://doi.org/10.1002/adfm.202000503
34. Seh, Z.W., Kibsgaard, J., Dickens, C.F., et al.: Combining theory and experiment in electrocatalysis: insights into materials design. Science (2017). https://doi.org/10.1126/science.aad4998
35. Nørskov, J.K., Rossmeisl, J., Logadottir, A., et al.: Origin of the overpotential for oxygen reduction at a fuel-cell cathode. J. Phys. Chem. B **108**, 17886–17892 (2004). https://doi.org/10.1021/jp047349j
36. Ji, Q.Q., Bi, L., Zhang, J.T., et al.: The role of oxygen vacancies of ABO_3 perovskite oxides in the oxygen reduction reaction. Energy Environ. Sci. **13**, 1408–1428 (2020). https://doi.org/10.1039/d0ee00092b
37. Zhang, J.J.: PEM Fuel Cell Electrocatalysts and Catalyst Layers. Springer, London (2008). https://doi.org/10.1007/978-1-84800-936-3

38. Shi, Q., Zhu, C., Du, D., et al.: Robust noble metal-based electrocatalysts for oxygen evolution reaction. Chem. Soc. Rev. **48**, 3181–3192 (2019). https://doi.org/10.1039/c8cs00671g
39. Rossmeisl, J., Qu, Z.W., Zhu, H.: Electrolysis of water on oxide surfaces. J. Electroanal. Chem. **607**, 83–89 (2007). https://doi.org/10.1016/j.jelechem.2006.11.008
40. Guo, D., Shibuya, R., Akiba, C., et al.: Active sites of nitrogen-doped carbon materials for oxygen reduction reaction clarified using model catalysts. Science **351**, 361–365 (2016). https://doi.org/10.1126/science.aad0832
41. Hunter, M.A., Fischer, J.M.T.A., Yuan, Q.H., et al.: Evaluating the catalytic efficiency of paired, single-atom catalysts for the oxygen reduction reaction. ACS Catal. **9**, 7660–7667 (2019). https://doi.org/10.1021/acscatal.9b02178
42. Kwon, N.H., Kim, M., Jin, X.Y., et al.: A rational method to kinetically control the rate-determining step to explore efficient electrocatalysts for the oxygen evolution reaction. NPG Asia Mater. **10**, 659–669 (2018). https://doi.org/10.1038/s41427-018-0060-3
43. Paul, R., Zhu, L., Chen, H., et al.: Recent advances in carbon-based metal-free electrocatalysts. Adv. Mater. Deerfield Beach Fla **31**, e1806403 (2019). https://doi.org/10.1002/adma.201806403
44. Ghosh, S., Basu, R.N.: Multifunctional nanostructured electrocatalysts for energy conversion and storage: current status and perspectives. Nanoscale **10**, 11241–11280 (2018). https://doi.org/10.1039/c8nr01032c
45. Jiang, J., Sun, F.F., Zhou, S., et al.: Atomic-level insight into super-efficient electrocatalytic oxygen evolution on iron and vanadium co-doped nickel (oxy)hydroxide. Nat. Commun. **9**, 2885 (2018). https://doi.org/10.1038/s41467-018-05341-y
46. Hang, C., Zhang, J., Zhu, J.W., et al.: In situ exfoliating and generating active sites on graphene nanosheets strongly coupled with carbon fiber toward self-standing bifunctional cathode for rechargeable Zn-air batteries. Adv. Energy Mater. **8**, 1703539 (2018). https://doi.org/10.1002/aenm.201703539
47. Gong, K., Du, F., Xia, Z., et al.: Nitrogen-doped carbon nanotube arrays with high electrocatalytic activity for oxygen reduction. Science **323**, 760–764 (2009). https://doi.org/10.1126/science.1168049
48. Ju, Q.J., Ma, R.G., Hu, Y.F., et al.: Highly localized C-N_2 sites for efficient oxygen reduction. ACS Catal. **10**, 9366–9375 (2020). https://doi.org/10.1021/acscatal.0c00474
49. Zhao, Y.S., Wan, J.W., Yao, H.Y., et al.: Few-layer graphdiyne doped with sp-hybridized nitrogen atoms at acetylenic sites for oxygen reduction electrocatalysis. Nat. Chem. **10**, 924–931 (2018). https://doi.org/10.1038/s41557-018-0100-1
50. Liu, J., Song, P., Xu, W.L.: Structure-activity relationship of doped-nitrogen (N)-based metal-free active sites on carbon for oxygen reduction reaction. Carbon **115**, 763–772 (2017). https://doi.org/10.1016/j.carbon.2017.01.080
51. Ito, Y., Qiu, H.J., Fujita, T., et al.: Bicontinuous nanoporous N-doped graphene for the oxygen reduction reaction. Adv. Mater. **26**, 4145–4150 (2014). https://doi.org/10.1002/adma.201400570
52. Chen, L., Du, R., Zhu, J., et al.: Three-dimensional nitrogen-doped graphene nanoribbons aerogel as a highly efficient catalyst for the oxygen reduction reaction. Small **11**, 1423–1429 (2015). https://doi.org/10.1002/smll.201402472
53. Liu, R., Wu, D., Feng, X., et al.: Nitrogen-doped ordered mesoporous graphitic arrays with high electrocatalytic activity for oxygen reduction. Angew. Chem. Int. Ed. **49**, 2565–2569 (2010). https://doi.org/10.1002/anie.200907289
54. Ding, W., Li, L., Xiong, K., et al.: Shape fixing via salt recrystallization: a morphology-controlled approach to convert nanostructured polymer to carbon nanomaterial as a highly active catalyst for oxygen reduction reaction. J. Am. Chem. Soc. **137**, 5414–5420 (2015). https://doi.org/10.1021/jacs.5b00292
55. Jin, H., Zhang, H.M., Zhong, H.X., et al.: Nitrogen-doped carbon xerogel: a novel carbon-based electrocatalyst for oxygen reduction reaction in proton exchange membrane (PEM) fuel cells. Energy Environ. Sci. **4**, 3389 (2011). https://doi.org/10.1039/c1ee01437d
56. Zheng, Y., Jiao, Y., Chen, J., et al.: Nanoporous graphitic-C_3N_4@carbon metal-free electrocatalysts for highly efficient oxygen reduction. J. Am. Chem. Soc. **133**, 20116–20119 (2011). https://doi.org/10.1021/ja209206c
57. Liang, J., Zheng, Y., Chen, J., et al.: Facile oxygen reduction on a three-dimensionally ordered macroporous graphitic C_3N_4/carbon composite electrocatalyst. Angew. Chem. Int. Ed. **51**, 3892–3896 (2012). https://doi.org/10.1002/anie.201107981
58. Liang, H.W., Wu, Z.Y., Chen, L.F., et al.: Bacterial cellulose derived nitrogen-doped carbon nanofiber aerogel: an efficient metal-free oxygen reduction electrocatalyst for zinc-air battery. Nano Energy **11**, 366–376 (2015). https://doi.org/10.1016/j.nanoen.2014.11.008
59. Wu, Z., Liu, R., Wang, J., et al.: Nitrogen and sulfur co-doping of 3D hollow-structured carbon spheres as an efficient and stable metal free catalyst for the oxygen reduction reaction. Nanoscale **8**, 19086–19092 (2016). https://doi.org/10.1039/c6nr06817k
60. Wang, S., Iyyamperumal, E., Roy, A., et al.: Vertically aligned BCN nanotubes as efficient metal-free electrocatalysts for the oxygen reduction reaction: a synergetic effect by co-doping with boron and nitrogen. Angew. Chem. Int. Ed. **50**, 11756–11760 (2011). https://doi.org/10.1002/anie.201105204
61. Jiang, H., Zhu, Y., Feng, Q., et al.: Nitrogen and phosphorus dual-doped hierarchical porous carbon foams as efficient metal-free electrocatalysts for oxygen reduction reactions. Chem. **20**, 3106–3112 (2014). https://doi.org/10.1002/chem.201304561
62. Wang, J., Wu, Z.X., Han, L.L., et al.: Rational design of three-dimensional nitrogen and phosphorus co-doped graphene nanoribbons/CNTs composite for the oxygen reduction. Chin. Chem. Lett. **27**, 597–601 (2016). https://doi.org/10.1016/j.cclet.2016.03.011
63. Fu, S.F., Zhu, C.Z., Song, J.H., et al.: Nitrogen and fluorine-codoped carbon nanowire aerogels as metal-free electrocatalysts for oxygen reduction reaction. Chem. Eur. J. **23**, 10460–10464 (2017). https://doi.org/10.1002/chem.201701969
64. Qiu, Y., Xin, L., Jia, F., et al.: Three-dimensional phosphorus-doped graphitic-C_3N_4 self-assembly with NH_2-functionalized carbon composite materials for enhanced oxygen reduction reaction. Langmuir **32**, 12569–12578 (2016). https://doi.org/10.1021/acs.langmuir.6b02498
65. Zou, X., Wang, L., Yakobson, B.I.: Mechanisms of the oxygen reduction reaction on B- and/or N-doped carbon nanomaterials with curvature and edge effects. Nanoscale **10**, 1129–1134 (2018). https://doi.org/10.1039/c7nr08061a
66. Wang, Y., Jiao, M., Song, W., et al.: Doped fullerene as a metal-free electrocatalyst for oxygen reduction reaction: a first-principles study. Carbon **114**, 393–401 (2017). https://doi.org/10.1016/j.carbon.2016.12.028
67. Wang, J.M., Hao, J., Liu, D., et al.: Porous boron carbon nitride nanosheets as efficient metal-free catalysts for the oxygen reduction reaction in both alkaline and acidic solutions. ACS Energy Lett. **2**, 306–312 (2017). https://doi.org/10.1021/acsenergylett.6b00602
68. Kim, M.J., Park, J.E., Kim, S., et al.: Biomass-derived air cathode materials: pore-controlled S, N-co-doped carbon for fuel cells and metal-air batteries. ACS Catal. **9**, 3389–3398 (2019). https://doi.org/10.1021/acscatal.8b03730
69. Zheng, X.J., Wu, J., Cao, X.C., et al.: N-, P-, and S-doped graphene-like carbon catalysts derived from onium salts with

enhanced oxygen chemisorption for Zn-air battery cathodes. Appl. Catal. B Environ. **241**, 442–451 (2019). https://doi.org/10.1016/j.apcatb.2018.09.054
70. Zhao, S., Wang, D.W., Amal, R., et al.: Carbon-based metal-free catalysts for key reactions involved in energy conversion and storage. Adv. Mater. **31**, e1801526 (2019). https://doi.org/10.1002/adma.201801526
71. Paul, R., Du, F., Dai, L., et al.: 3D heteroatom-doped carbon nanomaterials as multifunctional metal-free catalysts for integrated energy devices. Adv. Mater. **31**, e1805598 (2019). https://doi.org/10.1002/adma.201805598
72. Tam, T.V., Kang, S.G., Kim, M.H., et al.: Novel graphene hydrogel/B-doped graphene quantum dots composites as trifunctional electrocatalysts for Zn-air batteries and overall water splitting. Adv. Energy Mater., 1900945 (2019). https://doi.org/10.1002/aenm.201900945
73. Lei, W., Deng, Y.P., Li, G.R., et al.: Two-dimensional phosphorus-doped carbon nanosheets with tunable porosity for oxygen reactions in zinc-air batteries. ACS Catal. **8**, 2464–2472 (2018). https://doi.org/10.1021/acscatal.7b02739
74. Zhang, J.T., Zhao, Z.H., Xia, Z.H., et al.: A metal-free bifunctional electrocatalyst for oxygen reduction and oxygen evolution reactions. Nat. Nanotechnol. **10**, 444–452 (2015). https://doi.org/10.1038/nnano.2015.48
75. Chen, Y.J., Ji, S.F., Zhao, S., et al.: Enhanced oxygen reduction with single-atomic-site iron catalysts for a zinc-air battery and hydrogen-air fuel cell. Nat. Commun. **9**, 5422 (2018). https://doi.org/10.1038/s41467-018-07850-2
76. Zang, W.J., Sumboja, A., Ma, Y.Y., et al.: Single Co atoms anchored in porous N-doped carbon for efficient zinc-air battery cathodes. ACS Catal. **8**, 8961–8969 (2018). https://doi.org/10.1021/acscatal.8b02556
77. Chen, G.B., Liu, P., Liao, Z.Q., et al.: Zinc-mediated template synthesis of Fe-N-C electrocatalysts with densely accessible Fe-N_x active sites for efficient oxygen reduction. Adv. Mater. **32**, 1907399 (2020). https://doi.org/10.1002/adma.201907399
78. Zhou, L., Zhou, P., Zhang, Y., et al.: 3D star-like atypical hybrid MOF derived single-atom catalyst boosts oxygen reduction catalysis. J. Energy Chem. **55**, 355–360 (2021). https://doi.org/10.1016/j.jechem.2020.06.059
79. Pan, Y., Liu, S., Sun, K., et al.: A bimetallic Zn/Fe polyphthalocyanine-derived single-atom Fe-N_4 catalytic site: a superior trifunctional catalyst for overall water splitting and Zn-air batteries. Angew. Chem. Int. Ed. **57**, 8614–8618 (2018). https://doi.org/10.1002/anie.201804349
80. Peng, P., Shi, L., Huo, F., et al.: A pyrolysis-free path toward superiorly catalytic nitrogen-coordinated single atom. Sci. Adv. **5**, 2322 (2019). https://doi.org/10.1126/sciadv.aaw2322
81. Zhang, X.B., Han, X., Jiang, Z., et al.: Atomically dispersed hierarchically ordered porous Fe-N-C electrocatalyst for high performance electrocatalytic oxygen reduction in Zn-Air battery. Nano Energy **71**, 104547 (2020). https://doi.org/10.1016/j.nanoen.2020.104547
82. Zhou, Y.Z., Tao, X.F., Chen, G.B., et al.: Multilayer stabilization for fabricating high-loading single-atom catalysts. Nat. Commun. **11**, 5892 (2020). https://doi.org/10.1038/s41467-020-19599-8
83. Wang, Q., Shang, L., Sun-Waterhouse, D., et al.: Engineering local coordination environments and site densities for high-performance Fe-N-C oxygen reduction reaction electrocatalysis. SmartMat **2**, 154–175 (2021). https://doi.org/10.1002/smm2.1033
84. Han, X., Ling, X., Wang, Y., et al.: Generation of nanoparticle, atomic-cluster, and single-atom cobalt catalysts from zeolitic imidazole frameworks by spatial isolation and their use in zinc-air batteries. Angew. Chem. Int. Ed. **58**, 5359–5364 (2019). https://doi.org/10.1002/anie.201901109
85. Wu, J.B., Zhou, H., Li, Q., et al.: Densely populated isolated single Co-N site for efficient oxygen electrocatalysis. Adv. Energy Mater. **9**, 1900149 (2019). https://doi.org/10.1002/aenm.201900149
86. Li, B.Q., Zhao, C.X., Chen, S., et al.: Framework-porphyrin-derived single-atom bifunctional oxygen electrocatalysts and their applications in Zn-air batteries. Adv. Mater. **31**, e1900592 (2019). https://doi.org/10.1002/adma.201900592
87. Yang, L., Shi, L., Wang, D., et al.: Single-atom cobalt electrocatalysts for foldable solid-state Zn-air battery. Nano Energy **50**, 691–698 (2018). https://doi.org/10.1016/j.nanoen.2018.06.023
88. Wu, W.J., Liu, Y., Liu, D., et al.: Single copper sites dispersed on hierarchically porous carbon for improving oxygen reduction reaction towards zinc-air battery. Nano Res. **14**, 998–1003 (2021). https://doi.org/10.1007/s12274-020-3141-x
89. Shang, H.S., Zhou, X.Y., Dong, J.C., et al.: Engineering unsymmetrically coordinated Cu-S_1N_3 single atom sites with enhanced oxygen reduction activity. Nat. Commun. **11**, 3049 (2020). https://doi.org/10.1038/s41467-020-16848-8
90. Han, X., Zhang, T.Y., Chen, W.X., et al.: Mn-N_4 oxygen reduction electrocatalyst: operando investigation of active sites and high performance in zinc-air battery. Adv. Energy Mater. **11**, 2002753 (2020). https://doi.org/10.1002/aenm.202002753
91. Cui, T.T., Wang, Y.P., Ye, T., et al.: Engineering dual single-atom sites on 2D ultrathin N-doped carbon nanosheets attaining ultra-low-temperature zinc-air battery. Angewandte Chemie Int. Ed. **61**, e202115219 (2022). https://doi.org/10.1002/anie.202115219
92. Wei, W., Shi, X.M., Gao, P., et al.: Well-elaborated, mechanochemically synthesized Fe-TPP⊂ZIF precursors (Fe-TPP = tetraphenylporphine iron) to atomically dispersed iron-nitrogen species for oxygen reduction reaction and Zn-air batteries. Nano Energy **52**, 29–37 (2018). https://doi.org/10.1016/j.nanoen.2018.07.033
93. Lu, Z., Wang, B., Hu, Y., et al.: An isolated zinc-cobalt atomic pair for highly active and durable oxygen reduction. Angew. Chem. Int. Ed. **58**, 2622–2626 (2019). https://doi.org/10.1002/anie.201810175
94. Sun, H., Liu, S., Wang, M., et al.: Updating the intrinsic activity of a single-atom site with a P-O bond for a rechargeable Zn-air battery. ACS Appl. Mater. Interfaces **11**, 33054–33061 (2019). https://doi.org/10.1021/acsami.9b11337
95. Chen, P., Zhou, T., Xing, L., et al.: Atomically dispersed iron-nitrogen species as electrocatalysts for bifunctional oxygen evolution and reduction reactions. Angew. Chem. Int. Ed. **56**, 610–614 (2017). https://doi.org/10.1002/anie.201610119
96. Zhang, J., Zhang, M., Zeng, Y., et al.: Single Fe atom on hierarchically porous S, N-codoped nanocarbon derived from porphyra enable boosted oxygen catalysis for rechargeable Zn-air batteries. Small **15**, e1900307 (2019). https://doi.org/10.1002/smll.201900307
97. Chen, J., Li, H., Fan, C., et al.: Dual single-atomic Ni-N_4 and Fe-N_4 sites constructing Janus hollow graphene for selective oxygen electrocatalysis. Adv. Mater. **32**, e2003134 (2020). https://doi.org/10.1002/adma.202003134
98. Jose, V., Hu, H., Edison, E., et al.: Modulation of single atomic co and Fe sites on hollow carbon nanospheres as oxygen electrodes for rechargeable Zn-air batteries. Small Methods **5**, e2000751 (2021). https://doi.org/10.1002/smtd.202000751
99. Zhu, X.F., Zhang, D.T., Chen, C.J., et al.: Harnessing the interplay of Fe-Ni atom pairs embedded in nitrogen-doped carbon for bifunctional oxygen electrocatalysis. Nano Energy **71**, 104597 (2020). https://doi.org/10.1016/j.nanoen.2020.104597
100. Fu, G.T., Yan, X.X., Chen, Y.F., et al.: Boosting bifunctional oxygen electrocatalysis with 3D graphene aerogel-supported Ni/

MnO particles. Adv. Mater. **30**, 1704609 (2018). https://doi.org/10.1002/adma.201704609
101. Wang, H.F., Tang, C., Wang, B., et al.: Bifunctional transition metal hydroxysulfides: room-temperature sulfurization and their applications in Zn-air batteries. Adv. Mater. **29**, 1702327 (2017). https://doi.org/10.1002/adma.201702327
102. Zeng, S., Lv, B., Qiao, J., et al.: PtFe alloy nanoparticles confined on carbon nanotube networks as air cathodes for flexible and wearable energy devices. ACS Appl. Nano Mater. **2**, 7870–7879 (2019). https://doi.org/10.1021/acsanm.9b01865
103. Fu, G.T., Cui, Z.M., Chen, Y.F., et al.: Ni_3Fe-N doped carbon sheets as a bifunctional electrocatalyst for air cathodes. Adv. Energy Mater. **7**, 1601172 (2017). https://doi.org/10.1002/aenm.201601172
104. Zhu, J.B., Xiao, M.L., Li, G.R., et al.: A triphasic bifunctional oxygen electrocatalyst with tunable and synergetic interfacial structure for rechargeable Zn-air batteries. Adv. Energy Mater. **10**, 1903003 (2020). https://doi.org/10.1002/aenm.201903003
105. Mu, C., Mao, J., Guo, J., et al.: Rational design of spinel cobalt vanadate oxide Co_2VO_4 for superior electrocatalysis. Adv. Mater. **32**, e1907168 (2020). https://doi.org/10.1002/adma.201907168
106. Wang, X.R., Liu, J.Y., Liu, Z.W., et al.: Identifying the key role of pyridinic-N–Co bonding in synergistic electrocatalysis for reversible ORR/OER. Adv. Mater. **30**, e1800005 (2018). https://doi.org/10.1002/adma.201800005
107. Jiang, Y., Deng, Y.P., Fu, J., et al.: Zn-air batteries: interpenetrating triphase cobalt-based nanocomposites as efficient bifunctional oxygen electrocatalysts for long-lasting rechargeable Zn-air batteries. Adv. Energy Mater. **8**, 1870068 (2018). https://doi.org/10.1002/aenm.201870068
108. Wang, X.T., Ouyang, T., Wang, L., et al.: Surface reorganization on electrochemically-induced Zn-Ni-Co spinel oxides for enhanced oxygen electrocatalysis. Angew. Chem. Int. Ed. **59**, 6492–6499 (2020). https://doi.org/10.1002/anie.202000690
109. Nguyen, D.C., Tran, D.T., Doan, T.L.L., et al.: Rational design of core@shell structured CoS_x @Cu_2MoS_4 hybridized MoS_2/N, S-codoped graphene as advanced electrocatalyst for water splitting and Zn-air battery. Adv. Energy Mater. **10**, 1903289 (2020). https://doi.org/10.1002/aenm.201903289
110. Lyu, D.D., Yao, S.X., Ali, A., et al.: N, S codoped carbon matrix-encapsulated Co_9S_8 nanoparticles as a highly efficient and durable bifunctional oxygen redox electrocatalyst for rechargeable Zn-air batteries. Adv. Energy Mater. **11**, 2101249 (2021). https://doi.org/10.1002/aenm.202101249
111. Cai, Z.C., Yamada, I., Yagi, S.: ZIF-derived $Co_{9-x}Ni_xS_8$ nanoparticles immobilized on N-doped carbons as efficient catalysts for high-performance zinc-air batteries. ACS Appl. Mater. Interfaces **12**, 5847–5856 (2020). https://doi.org/10.1021/acsami.9b19268
112. Qiao, Y.Y., Yuan, P.F., Hu, Y.F., et al.: Sulfuration of an Fe-N-C catalyst containing Fe_xC/Fe species to enhance the catalysis of oxygen reduction in acidic media and for use in flexible Zn-air batteries. Adv. Mater. **30**, 1804504 (2018). https://doi.org/10.1002/adma.201804504
113. Yang, Z.K., Zhao, Z.W., Liang, K., et al.: Synthesis of nanoporous structured iron carbide/Fe-N-carbon composites for efficient oxygen reduction reaction in Zn-air batteries. J. Mater. Chem. A **4**, 19037–19044 (2016). https://doi.org/10.1039/c6ta08050b
114. Lin, C., Li, X.P., Shinde, S.S., et al.: Long-life rechargeable Zn-air battery based on binary metal carbide armored by nitrogen-doped carbon. ACS Appl. Energy Mater. **2**, 1747–1755 (2019). https://doi.org/10.1021/acsaem.8b01865
115. Lou, Y.W., Liu, J.J., Liu, M., et al.: Hexagonal Fe_2N coupled with N-doped carbon: crystal-plane-dependent electrocatalytic activity for oxygen reduction. ACS Catal. **10**, 2443–2451 (2020). https://doi.org/10.1021/acscatal.9b03716
116. Ge, H.Y., Li, G., Shen, J., et al.: Co_4N nanoparticles encapsulated in N-doped carbon box as tri-functional catalyst for Zn-air battery and overall water splitting. Appl. Catal. B Environ. **275**, 119104 (2020). https://doi.org/10.1016/j.apcatb.2020.119104
117. Chen, L.L., Zhang, Y., Dong, L., et al.: Honeycomb-like 3D N-, P-codoped porous carbon anchored with ultrasmall Fe_2P nanocrystals for efficient Zn-air battery. Carbon **158**, 885–892 (2020). https://doi.org/10.1016/j.carbon.2019.11.073
118. Wang, Y.X., Wu, M.J., Li, J., et al.: In situ growth of CoP nanoparticles anchored on (N, P) co-doped porous carbon engineered by MOFs as advanced bifunctional oxygen catalyst for rechargeable Zn-air battery. J. Mater. Chem. A **8**, 19043–19049 (2020). https://doi.org/10.1039/d0ta06435a
119. Li, H., Li, Q., Wen, P., et al.: Colloidal cobalt phosphide nanocrystals as trifunctional electrocatalysts for overall water splitting powered by a zinc-air battery. Adv. Mater. **30**, 1705796 (2018). https://doi.org/10.1002/adma.201705796
120. Wang, Z., Ang, J., Zhang, B., et al.: FeCo/FeCoNi/N-doped carbon nanotubes grafted polyhedron-derived hybrid fibers as bifunctional oxygen electrocatalysts for durable rechargeable zinc-air battery. Appl. Catal. B **254**, 26–36 (2019). https://doi.org/10.1016/j.apcatb.2019.04.027
121. Chen, L.L., Zhang, Y., Liu, X., et al.: Bifunctional oxygen electrodes of homogeneous Co_4N nanocrystals@N-doped carbon hybrids for rechargeable Zn-air batteries. Carbon **151**, 10–17 (2019). https://doi.org/10.1016/j.carbon.2019.05.063
122. Deng, Y.P., Jiang, Y., Liang, R.L., et al.: Dynamic electrocatalyst with current-driven oxyhydroxide shell for rechargeable zinc-air battery. Nat. Commun. **11**, 1952 (2020). https://doi.org/10.1038/s41467-020-15853-1
123. Liang, Y.Y., Li, Y.G., Wang, H.L., et al.: Co_3O_4 nanocrystals on graphene as a synergistic catalyst for oxygen reduction reaction. Nat. Mater. **10**, 780–786 (2011). https://doi.org/10.1038/nmat3087
124. Li, Y.G., Gong, M., Liang, Y.Y., et al.: Advanced zinc-air batteries based on high-performance hybrid electrocatalysts. Nat. Commun. **4**, 1805 (2013). https://doi.org/10.1038/ncomms2812
125. Zhou, T., Xu, W., Zhang, N., et al.: Ultrathin cobalt oxide layers as electrocatalysts for high-performance flexible Zn-air batteries. Adv. Mater. **31**, e1807468 (2019). https://doi.org/10.1002/adma.201807468
126. Li, Y.B., Zhong, C., Liu, J., et al.: Zinc-air batteries: atomically thin mesoporous Co_3O_4 layers strongly coupled with N-rGO nanosheets as high-performance bifunctional catalysts for 1D knittable zinc-air batteries. Adv. Mater. **30**, 1870027 (2018). https://doi.org/10.1002/adma.201870027
127. Anantharaj, S., Ede, S.R., Sakthikumar, K., et al.: Recent trends and perspectives in electrochemical water splitting with an emphasis on sulfide, selenide, and phosphide catalysts of Fe Co, and Ni: a review. ACS Catal. **6**, 8069–8097 (2016). https://doi.org/10.1021/acscatal.6b02479
128. Han, H., Kim, K.M., Choi, H., et al.: Parallelized reaction pathway and stronger internal band bending by partial oxidation of metal sulfide-graphene composites: important factors of synergistic oxygen evolution reaction enhancement. ACS Catal. **8**, 4091–4102 (2018). https://doi.org/10.1021/acscatal.8b00017
129. Parra-Puerto, A., Ng, K.L., Fahy, K., et al.: Supported transition metal phosphides: activity survey for HER, ORR, OER, and corrosion resistance in acid and alkaline electrolytes. ACS Catal. **9**, 11515–11529 (2019). https://doi.org/10.1021/acscatal.9b03359
130. Hou, C.C., Zou, L., Wang, Y., et al.: MOF-mediated fabrication of a porous 3D superstructure of carbon nanosheets decorated with ultrafine cobalt phosphide nanoparticles for efficient electrocatalysis and zinc-air batteries. Angew. Chem. Int. Ed. **59**, 21360–21366 (2020). https://doi.org/10.1002/anie.202011347

131. Tabassum, H., Mahmood, A., Zhu, B.J., et al.: Recent advances in confining metal-based nanoparticles into carbon nanotubes for electrochemical energy conversion and storage devices. Energy Environ. Sci. **12**, 2924–2956 (2019). https://doi.org/10.1039/c9ee00315k
132. Tian, Y., Xu, L., Li, M., et al.: Interface engineering of CoS/CoO@N-doped graphene nanocomposite for high-performance rechargeable Zn-air batteries. Nano-Micro Lett. **13**, 3 (2020). https://doi.org/10.1007/s40820-020-00526-x
133. Guo, Y.Y., Yuan, P.F., Zhang, J.N., et al.: Co_2P-CoN double active centers confined in N-doped carbon nanotube:heterostructural engineering for trifunctional catalysis toward HER, ORR, OER, and Zn-air batteries driven water splitting. Adv. Funct. Mater. **28**, 1805641 (2018). https://doi.org/10.1002/adfm.201805641
134. Shi, Q., Liu, Q., Ma, Y., et al.: High-performance trifunctional electrocatalysts based on FeCo/Co_2P hybrid nanoparticles for zinc-air battery and self-powered overall water splitting. Adv. Energy Mater. **10**, 1903854 (2020). https://doi.org/10.1002/aenm.201903854
135. Wang, Y., Cao, Q., Guan, C., et al.: Recent advances on self-supported arrayed bifunctional oxygen electrocatalysts for flexible solid-state Zn-air batteries. Small **16**, e2002902 (2020). https://doi.org/10.1002/smll.202002902
136. Zhang, M.D., Dai, Q.B., Zheng, H.G., et al.: Novel MOF-derived Co@N-C bifunctional catalysts for highly efficient Zn-air batteries and water splitting. Adv. Mater. **30**, 1705431 (2018). https://doi.org/10.1002/adma.201705431
137. Cao, X.Y., Deng, J.P., Pan, K.: Electrospinning Janus type CoO_x/C nanofibers as electrocatalysts for oxygen reduction reaction. Adv. Fiber Mater. **2**, 85–92 (2020). https://doi.org/10.1007/s42765-020-00033-z
138. Fu, J., Hassan, F.M., Zhong, C., et al.: Defect engineering of chalcogen-tailored oxygen electrocatalysts for rechargeable quasi-solid-state zinc-air batteries. Adv. Mater. **29**, 1702526 (2017). https://doi.org/10.1002/adma.201702526
139. Tang, Y., Lei, Y., Tong, K., et al.: Fe, N-doped graphene-wrapped carbon black nanoparticles as highly efficient catalyst towards oxygen reduction reaction. Appl. Surf. Sci. **545**, 148981 (2021). https://doi.org/10.1016/j.apsusc.2021.148981
140. Liu, J., Jiang, L.H., Tang, Q.W., et al.: Amide-functionalized carbon supports for cobalt oxide toward oxygen reduction reaction in Zn-air battery. Appl. Catal. B Environ. **148**(149), 212–220 (2014). https://doi.org/10.1016/j.apcatb.2013.10.058
141. Nam, G., Park, J., Kim, S.T., et al.: Metal-free Ketjenblack incorporated nitrogen-doped carbon sheets derived from gelatin as oxygen reduction catalysts. Nano Lett. **14**, 1870–1876 (2014). https://doi.org/10.1021/nl404640n
142. Yi, S.J., Qin, X., Liang, C., et al.: Insights into $KMnO_4$ etched N-rich carbon nanotubes as advanced electrocatalysts for Zn-air batteries. Appl. Catal. B Environ. **264**, 118537 (2020). https://doi.org/10.1016/j.apcatb.2019.118537
143. Wei, P., Li, X., He, Z., et al.: Porous N, B co-doped carbon nanotubes as efficient metal-free electrocatalysts for ORR and Zn-air batteries. Chem. Eng. J. **422**, 130134 (2021). https://doi.org/10.1016/j.cej.2021.130134
144. Song, R.L., Cao, X.T., Zhou, X.S., et al.: N-doped graphene supported on N-rGO nanosheets as metal-free oxygen reduction reaction electrocatalysts for Zn-air batteries. New J. Chem. **45**, 21716–21724 (2021). https://doi.org/10.1039/d1nj04258k
145. Fan, F., Zhou, H., Yan, R., et al.: Anchoring Fe-N-C sites on hierarchically porous carbon sphere and CNT interpenetrated nanostructures as efficient cathodes for zinc-air batteries. ACS Appl. Mater. Interfaces **13**, 41609–41618 (2021). https://doi.org/10.1021/acsami.1c10510
146. Han, J., Huang, G., Wang, Z., et al.: Low-temperature carbide-mediated growth of bicontinuous nitrogen-doped mesoporous graphene as an efficient oxygen reduction electrocatalyst. Adv. Mater. **30**, e1803588 (2018). https://doi.org/10.1002/adma.201803588
147. Zhang, J., Sun, Y., Zhu, J., et al.: Ultranarrow graphene nanoribbons toward oxygen reduction and evolution reactions. Adv. Sci. **5**, 1801375 (2018). https://doi.org/10.1002/advs.201801375
148. Lai, L.F., Potts, J.R., Zhan, D., et al.: Exploration of the active center structure of nitrogen-doped graphene-based catalysts for oxygen reduction reaction. Energy Environ. Sci. **5**, 7936 (2012). https://doi.org/10.1039/c2ee21802j
149. Li, Y.G., Zhou, W., Wang, H.L., et al.: An oxygen reduction electrocatalyst based on carbon nanotube–graphene complexes. Nat. Nanotechnol. **7**, 394–400 (2012). https://doi.org/10.1038/nnano.2012.72
150. Zhuang, X., Gehrig, D., Forler, N., et al.: Conjugated microporous polymers with dimensionality-controlled heterostructures for green energy devices. Adv. Mater. **27**, 3789–3796 (2015). https://doi.org/10.1002/adma.201501786
151. Su, Y.Z., Yao, Z.Q., Zhang, F., et al.: Sulfur-enriched conjugated polymer nanosheet derived sulfur and nitrogen co-doped porous carbon nanosheets as electrocatalysts for oxygen reduction reaction and zinc-air battery. Adv. Funct. Mater. **26**, 5893–5902 (2016). https://doi.org/10.1002/adfm.201602158
152. Guo, J.: The synthesis and synergistic catalysis of iron phthalocyanine and its graphene-based axial complex for enhanced oxygen reduction. Nano Energy **46**, 347–355 (2018). https://doi.org/10.1016/j.nanoen.2018.02.026
153. Liu, Y.L., Chen, F.J., Ye, W., et al.: High-performance oxygen reduction electrocatalyst derived from polydopamine and cobalt supported on carbon nanotubes for metal-air batteries. Adv. Funct. Mater. **27**, 1606034 (2017). https://doi.org/10.1002/adfm.201606034
154. Yang, F., Liu, X., Zhang, H., et al.: Boosting oxygen catalytic kinetics of carbon nanotubes by oxygen-induced electron density modulation for advanced Zn-air batteries. Energy Storage Mater. **30**, 138–145 (2020). https://doi.org/10.1016/j.ensm.2020.05.005
155. Yang, R., Xie, J., Liu, Q., et al.: A trifunctional Ni-N/P-O-codoped graphene electrocatalyst enables dual-model rechargeable Zn-CO_2/Zn-O_2 batteries. J. Mater. Chem. A **7**, 2575–2580 (2019). https://doi.org/10.1039/c8ta10958c
156. Li, M., Chen, S., Li, B., et al.: In situ growing N and O co-doped helical carbon nanotubes encapsulated with CoFe alloy as trifunctional electrocatalyst applied in Zn-Air batteries driving water splitting. Electrochim. Acta **388**, 138587 (2021). https://doi.org/10.1016/j.electacta.2021.138587
157. Tang, C., Wang, B., Wang, H.F., et al.: Defect engineering toward atomic Co-N_x-C in hierarchical graphene for rechargeable flexible solid Zn-air batteries. Adv. Mater. **29**, 1703185 (2017). https://doi.org/10.1002/adma.201703185
158. Tan, J.B., He, X., Yin, F., et al.: Fe doped metal organic framework (Ni)/carbon black nanosheet as highly active electrocatalyst for oxygen evolution reaction. Int. J. Hydrog. Energy **45**, 21431–21441 (2020). https://doi.org/10.1016/j.ijhydene.2020.05.230
159. Cheng, H., Li, M.L., Su, C.Y., et al.: Cu-Co bimetallic oxide quantum dot decorated nitrogen-doped carbon nanotubes: a high-efficiency bifunctional oxygen electrode for Zn-air batteries. Adv. Funct. Mater. **27**, 1701833 (2017). https://doi.org/10.1002/adfm.201701833
160. Han, X.P., Wu, X., Zhong, C., et al.: $NiCo_2S_4$ nanocrystals anchored on nitrogen-doped carbon nanotubes as a highly efficient bifunctional electrocatalyst for rechargeable zinc-air batteries. Nano Energy **31**, 541–550 (2017). https://doi.org/10.1016/j.nanoen.2016.12.008
161. Lei, H., Wang, Z., Yang, F., et al.: NiFe nanoparticles embedded N-doped carbon nanotubes as high-efficient electrocatalysts for wearable solid-state Zn-air batteries. Nano Energy **68**, 104293 (2020). https://doi.org/10.1016/j.nanoen.2019.104293

162. Zhao, C.X., Liu, J.N., Wang, J., et al.: A $\Delta E = 0.63$ V bifunctional oxygen electrocatalyst enables high-rate and long-cycling zinc-air batteries. Adv. Mater. **33**, e2008606 (2021). https://doi.org/10.1002/adma.202008606
163. Wang, Z., Huang, J., Wang, L., et al.: Cation-tuning induced d-band center modulation on co-based spinel oxide for oxygen reduction/evolution reaction. Angew. Chem. Int. Ed. **61**, e202114696 (2022). https://doi.org/10.1002/anie.202114696
164. Wei, L., Karahan, H.E., Zhai, S.L., et al.: Amorphous bimetallic oxide-graphene hybrids as bifunctional oxygen electrocatalysts for rechargeable Zn-air batteries. Adv. Mater. **29**, 1701410 (2017). https://doi.org/10.1002/adma.201701410
165. Niu, W.H., Li, Z., Marcus, K., et al.: Surface-modified porous carbon nitride composites as highly efficient electrocatalyst for Zn-air batteries. Adv. Energy Mater. **8**, 1701642 (2018). https://doi.org/10.1002/aenm.201701642
166. Cheng, W.Z., Liang, J.L., Yin, H.B., et al.: Bifunctional iron-phtalocyanine metal-organic framework catalyst for ORR, OER and rechargeable zinc-air battery. Rare Met. **39**, 815–823 (2020). https://doi.org/10.1007/s12598-020-01440-2
167. Zhao, R., Wu, L., Chen, R., et al.: In situ growth of cobalt manganate spinel nanodots on carbon black toward high-performance zinc-air battery: dual functions of 3-aminopropyltriethoxysilane. J. Colloid Interface Sci. **608**, 386–395 (2022). https://doi.org/10.1016/j.jcis.2021.09.151
168. Pei, Z.X., Li, H.F., Huang, Y., et al.: Texturing In situ: N, S-enriched hierarchically porous carbon as a highly active reversible oxygen electrocatalyst. Energy Environ. Sci. **10**, 742–749 (2017). https://doi.org/10.1039/c6ee03265f
169. Meng, Y., Li, J.C., Zhao, S.Y., et al.: Fluorination-assisted preparation of self-supporting single-atom Fe-N-doped single-wall carbon nanotube film as bifunctional oxygen electrode for rechargeable Zn-Air batteries. Appl. Catal. B Environ. **294**, 120239 (2021). https://doi.org/10.1016/j.apcatb.2021.120239
170. Geng, H.Y., Peng, Y., Qu, L.T., et al.: Structure design and composition engineering of carbon-based nanomaterials for lithium energy storage. Adv. Energy Mater. **10**, 1903030 (2020). https://doi.org/10.1002/aenm.201903030
171. Sakai, K., Iwamura, S., Mukai, S.R.: Influence of the porous structure of the cathode on the discharge capacity of lithium-air batteries. J. Electrochem. Soc. **164**, A3075–A3080 (2017). https://doi.org/10.1149/2.0791713jes
172. Wu, K., Zhang, L., Yuan, Y., et al.: An iron-decorated carbon aerogel for rechargeable flow and flexible Zn-air batteries. Adv. Mater. **32**, e2002292 (2020). https://doi.org/10.1002/adma.202002292
173. Yang, Z., Zhao, C., Qu, Y., et al.: Trifunctional self-supporting cobalt-embedded carbon nanotube films for ORR, OER, and HER triggered by solid diffusion from bulk metal. Adv. Mater. **31**, e1808043 (2019). https://doi.org/10.1002/adma.201808043
174. Lu, Q., Yu, J., Zou, X.H., et al.: Self-catalyzed growth of Co, N-codoped CNTs on carbon-encased CoS_x surface: a noble-metal-free bifunctional oxygen electrocatalyst for flexible solid Zn-air batteries. Adv. Funct. Mater. **29**, 1904481 (2019). https://doi.org/10.1002/adfm.201904481
175. Yan, L.T., Xu, Y.L., Chen, P., et al.: Heterostructure films: a freestanding 3D heterostructure film stitched by MOF-derived carbon nanotube microsphere superstructure and reduced graphene oxide sheets: a superior multifunctional electrode for overall water splitting and Zn-air batteries. Adv. Mater. **32**, 2070362 (2020). https://doi.org/10.1002/adma.202070362
176. Liu, X., Wang, L., Yu, P., et al.: A stable bifunctional catalyst for rechargeable zinc-air batteries: iron-cobalt nanoparticles embedded in a nitrogen-doped 3D carbon matrix. Angew. Chem. Int. Ed. **57**, 16166–16170 (2018). https://doi.org/10.1002/anie.201809009
177. Fu, G.T., Wang, J., Chen, Y.F., et al.: Exploring indium-based ternary thiospinel as conceivable high-potential air-cathode for rechargeable Zn-air batteries. Adv. Energy Mater. **8**, 1802263 (2018). https://doi.org/10.1002/aenm.201802263
178. Han, X.P., Zhang, W., Ma, X.Y., et al.: Identifying the activation of bimetallic sites in $NiCo_2S_4$ @g-C_3N_4-CNT hybrid electrocatalysts for synergistic oxygen reduction and evolution. Adv. Mater. **31**, 1808281 (2019). https://doi.org/10.1002/adma.201808281
179. Liu, W.W., Zhang, J., Bai, Z.Y., et al.: Controllable urchin-like $NiCo_2S_4$ microsphere synergized with sulfur-doped graphene as bifunctional catalyst for superior rechargeable Zn-air battery. Adv. Funct. Mater. **28**, 1706675 (2018). https://doi.org/10.1002/adfm.201706675
180. Qiu, H.J., Du, P., Hu, K., et al.: Metal and nonmetal codoped 3D nanoporous graphene for efficient bifunctional electrocatalysis and rechargeable Zn-air batteries. Adv. Mater. **31**, e1900843 (2019). https://doi.org/10.1002/adma.201900843
181. Du, P., Hu, K., Lyu, J., et al.: Anchoring Mo single atoms/clusters and N on edge-rich nanoporous holey graphene as bifunctional air electrode in Zn-air batteries. Appl. Catal. B Environ. **276**, 119172 (2020). https://doi.org/10.1016/j.apcatb.2020.119172
182. Qiao, Y., Kong, F., Zhang, C., et al.: Highly efficient oxygen electrode catalyst derived from chitosan biomass by molten salt pyrolysis for zinc-air battery. Electrochimica Acta **339**, 135923 (2020). https://doi.org/10.1016/j.electacta.2020.135923
183. Chen, S., Chen, S., Zhang, J.T.: Thermal sugar bubbling preparation of N-doped porous carbon for high-performance solid-state Zn-air batteries. Batter. Supercaps **2**, 373–379 (2019). https://doi.org/10.1002/batt.201800105
184. Yang, M.M., Shu, X.X., Zhang, J.T.: A defect-rich N, P co-doped carbon foam as efficient electrocatalyst toward oxygen reduction reaction. ChemCatChem **12**, 4105–4111 (2020). https://doi.org/10.1002/cctc.202000363
185. He, Y., Han, X., Du, Y., et al.: Heteroatom-doped carbon nanostructures derived from conjugated polymers for energy applications. Polymers **8**, E366 (2016). https://doi.org/10.3390/polym8100366
186. Silva, R., Voiry, D., Chhowalla, M., et al.: Efficient metal-free electrocatalysts for oxygen reduction: polyaniline-derived N- and O-doped mesoporous carbons. J. Am. Chem. Soc. **135**, 7823–7826 (2013). https://doi.org/10.1021/ja402450a
187. Liang, H.W., Zhuang, X.D., Brüller, S., et al.: Hierarchically porous carbons with optimized nitrogen doping as highly active electrocatalysts for oxygen reduction. Nat. Commun. **5**, 4973 (2014). https://doi.org/10.1038/ncomms5973
188. Wang, G., Sun, Y., Li, D., et al.: Controlled synthesis of N-doped carbon nanospheres with tailored mesopores through self-assembly of colloidal silica. Angew. Chem. Int. Ed. **54**, 15191–15196 (2015). https://doi.org/10.1002/anie.201507735
189. You, C.H., Jiang, X.W., Wang, X.H., et al.: Nitrogen, sulfur co-doped carbon derived from naphthalene-based covalent organic framework as an efficient catalyst for oxygen reduction. ACS Appl. Energy Mater. **1**, 161–166 (2018). https://doi.org/10.1021/acsaem.7b00045
190. Yang, C., Maenosono, S., Duan, J.G., et al.: COF-derived N, P co-doped carbon as a metal-free catalyst for highly efficient oxygen reduction reaction. ChemNanoMat **5**, 957–963 (2019). https://doi.org/10.1002/cnma.201900159
191. Yang, C., Tao, S., Huang, N., et al.: Heteroatom-doped carbon electrocatalysts derived from nanoporous two-dimensional covalent organic frameworks for oxygen reduction and hydrogen evolution. ACS Appl. Nano Mater. **3**, 5481–5488 (2020). https://doi.org/10.1021/acsanm.0c00786
192. Li, Z., Zhao, W., Yin, C., et al.: Synergistic effects between doped nitrogen and phosphorus in metal-free cathode for zinc-air battery from covalent organic frameworks coated CNT. ACS Appl.

Mater. Interfaces **9**, 44519–44528 (2017). https://doi.org/10.1021/acsami.7b14815
193. Zhang, W.Y., Xu, X.C., Zhang, C.X., et al.: 3D space-confined pyrolysis of double-network aerogels containing in-Fe cyanogel and polyaniline: a new approach to hierarchically porous carbon with exclusive Fe-N_x active sites for oxygen reduction catalysis. Small Methods **1**, 1700167 (2017). https://doi.org/10.1002/smtd.201700167
194. Li, H., Du, K., Xiang, C.S., et al.: Controlled chelation between tannic acid and Fe precursors to obtain N, S co-doped carbon with high density Fe-single atom-nanoclusters for highly efficient oxygen reduction reaction in Zn-air batteries. J. Mater. Chem. A **8**, 17136–17149 (2020). https://doi.org/10.1039/d0ta04210b
195. Li, H., Shu, X., Tong, P., et al.: Fe-Ni alloy nanoclusters anchored on carbon aerogels as high-efficiency oxygen electrocatalysts in rechargeable Zn-air batteries. Small **17**, e2102002 (2021). https://doi.org/10.1002/smll.202102002
196. Wei, X., Zheng, D., Zhao, M., et al.: Cross-linked polyphosphazene hollow nanosphere-derived N/P-doped porous carbon with single nonprecious metal atoms for the oxygen reduction reaction. Angew. Chem. Int. Ed. **59**, 14639–14646 (2020). https://doi.org/10.1002/anie.202006175
197. Qin, Q., Jang, H., Li, P., et al.: A tannic acid-derived N-, P-codoped carbon-supported iron-based nanocomposite as an advanced trifunctional electrocatalyst for the overall water splitting cells and zinc-air batteries. Adv. Energy Mater. **9**, 1803312 (2019). https://doi.org/10.1002/aenm.201803312
198. Xiao, M.L., Xing, Z.H., Jin, Z., et al.: Preferentially engineering FeN_4 edge sites onto graphitic nanosheets for highly active and durable oxygen electrocatalysis in rechargeable Zn-air batteries. Adv. Mater. **32**, 2004900 (2020). https://doi.org/10.1002/adma.202004900
199. Wang, H., Li, X., Jiang, Y., et al.: A universal single-atom coating strategy based on tannic acid chemistry for multifunctional heterogeneous catalysis. Angew. Chem. Int. Ed. **61**, e202200465 (2022). https://doi.org/10.1002/anie.202200465
200. Li, S., Cheng, C., Liang, H.W., et al.: 2D porous carbons prepared from layered organic-inorganic hybrids and their use as oxygen-reduction electrocatalysts. Adv. Mater. **29**, 1700707 (2017). https://doi.org/10.1002/adma.201700707
201. Ai, K., Liu, Y., Ruan, C., et al.: sp^2 C-dominant N-doped carbon sub-micrometer spheres with a tunable size: A versatile platform for highly efficient oxygen-reduction catalysts. Adv. Mater. Deerfield Beach Fla **25**, 998–1003 (2013). https://doi.org/10.1002/adma.201203923
202. Deng, L.B., Qiu, L., Hu, R., et al.: Restricted diffusion preparation of fully-exposed Fe single-atom catalyst on carbon nanospheres for efficient oxygen reduction reaction. Appl. Catal. B Environ. **305**, 121058 (2022). https://doi.org/10.1016/j.apcatb.2021.121058
203. Zhang, Z.Y., Zhao, X.X., Xi, S.B., et al.: Atomically dispersed cobalt trifunctional electrocatalysts with tailored coordination environment for flexible rechargeable Zn-air battery and self-driven water splitting. Adv. Energy Mater. **10**, 2002896 (2020). https://doi.org/10.1002/aenm.202002896
204. Li, S., Cheng, C., Zhao, X., et al.: Active salt/silica-templated 2D mesoporous FeCo-N_x-carbon as bifunctional oxygen electrodes for zinc-air batteries. Angew. Chem. Int. Ed. **57**, 1856–1862 (2018). https://doi.org/10.1002/anie.201710852
205. Cui, K., Wang, Q.T., Bian, Z.N., et al.: Supramolecular modulation of molecular conformation of metal porphyrins toward remarkably enhanced multipurpose electrocatalysis and ultrahigh-performance zinc-air batteries. Adv. Energy Mater. **11**, 2102062 (2021). https://doi.org/10.1002/aenm.202102062
206. Xie, L.S., Zhang, X.P., Zhao, B., et al.: Enzyme-inspired iron porphyrins for improved electrocatalytic oxygen reduction and evolution reactions. Angew. Chem. Int. Ed. **60**, 7576–7581 (2021). https://doi.org/10.1002/anie.202015478
207. Zhong, H., Ly, K.H., Wang, M., et al.: A phthalocyanine-based layered two-dimensional conjugated metal-organic framework as a highly efficient electrocatalyst for the oxygen reduction reaction. Angew. Chem. Int. Ed. **58**, 10677–10682 (2019). https://doi.org/10.1002/anie.201907002
208. Yang, S., Yu, Y., Dou, M., et al.: Two-dimensional conjugated aromatic networks as high-site-density and single-atom electrocatalysts for the oxygen reduction reaction. Angew. Chem. Int. Ed. **58**, 14724–14730 (2019). https://doi.org/10.1002/anie.201908023
209. Ma, Y., Li, J.T., Liao, X.B., et al.: Heterostructure design in bimetallic phthalocyanine boosts oxygen reduction reaction activity and durability. Adv. Funct. Mater. **30**, 2005000 (2020). https://doi.org/10.1002/adfm.202005000
210. Liao, Z.J., Wang, Y., Wang, Q., et al.: Bimetal-phthalocyanine based covalent organic polymers for highly efficient oxygen electrode. Appl. Catal. B Environ. **243**, 204–211 (2019). https://doi.org/10.1016/j.apcatb.2018.10.038
211. Chen, K., Kim, S., Je, M., et al.: Ultrasonic plasma engineering toward facile synthesis of single-atom M-N_4/N-doped carbon (M = Fe, co) as superior oxygen electrocatalyst in rechargeable zinc-air batteries. Nano-Micro Lett **13**, 60 (2021). https://doi.org/10.1007/s40820-020-00581-4
212. Lin, C.Y., Zhang, D.T., Zhao, Z.H., et al.: Covalent organic framework electrocatalysts for clean energy conversion. Adv. Mater. **30**, 1703646 (2018). https://doi.org/10.1002/adma.201703646
213. Lin, C.Y., Zhang, L.P., Zhao, Z.H., et al.: Design principles for covalent organic frameworks as efficient electrocatalysts in clean energy conversion and green oxidizer production. Adv. Mater. **29**, 1606635 (2017). https://doi.org/10.1002/adma.201606635
214. Park, J.H., Lee, C.H., Ju, J.M., et al.: Bifunctional covalent organic framework-derived electrocatalysts with modulated p-band centers for rechargeable Zn-air batteries. Adv. Funct. Mater. **31**, 2101727 (2021). https://doi.org/10.1002/adfm.202101727
215. Liang, Z., Qu, C., Guo, W., et al.: Pristine metal-organic frameworks and their composites for energy storage and conversion. Adv. Mater. **30**, e1702891 (2018). https://doi.org/10.1002/adma.201702891
216. Shinde, S.S., Lee, C.H., Jung, J.Y., et al.: Unveiling dual-linkage 3D hexaiminobenzene metal–organic frameworks towards long-lasting advanced reversible Zn-air batteries. Energy Environ. Sci. **12**, 727–738 (2019). https://doi.org/10.1039/c8ee02679c
217. Ren, D.Z., Ying, J., Xiao, M.L., et al.: Hierarchically porous multimetal-based carbon nanorod hybrid as an efficient oxygen catalyst for rechargeable zinc-air batteries. Adv. Funct. Mater. **30**, 1908167 (2020). https://doi.org/10.1002/adfm.201908167
218. Li, J.J., Xia, W., Tang, J., et al.: MOF nanoleaves as new sacrificial templates for the fabrication of nanoporous Co-N_x/C electrocatalysts for oxygen reduction. Nanoscale Horiz. **4**, 1006–1013 (2019). https://doi.org/10.1039/c9nh00095j
219. Wang, S.G., Qin, J., Meng, T., et al.: Metal-organic framework-induced construction of actiniae-like carbon nanotube assembly as advanced multifunctional electrocatalysts for overall water splitting and Zn-air batteries. Nano Energy **39**, 626–638 (2017). https://doi.org/10.1016/j.nanoen.2017.07.043
220. Zhu, Q.L., Xia, W., Akita, T., et al.: Metal-organic framework-derived honeycomb-like open porous nanostructures as precious-metal-free catalysts for highly efficient oxygen electroreduction.

Adv. Mater. **28**, 6391–6398 (2016). https://doi.org/10.1002/adma.201600979
221. Liu, S., Li, Z.D., Wang, C.L., et al.: Turning main-group element magnesium into a highly active electrocatalyst for oxygen reduction reaction. Nat. Commun. **11**, 938 (2020). https://doi.org/10.1038/s41467-020-14565-w
222. Xiong, W.F., Li, H.F., You, H.H., et al.: Encapsulating metal organic framework into hollow mesoporous carbon sphere as efficient oxygen bifunctional electrocatalyst. Natl. Sci. Rev. **7**, 609–619 (2019). https://doi.org/10.1093/nsr/nwz166
223. Wu, Y.H., Li, Y.W., Gao, J.K., et al.: Recent advances in vacancy engineering of metal-organic frameworks and their derivatives for electrocatalysis. SusMat **1**, 66–87 (2021). https://doi.org/10.1002/sus2.3
224. Wang, T.T., Kou, Z.K., Mu, S.C., et al.: 2D dual-metal zeolitic-imidazolate-framework-(ZIF)-derived bifunctional air electrodes with ultrahigh electrochemical properties for rechargeable zinc-air batteries. Adv. Funct. Mater. **28**, 1705048 (2018). https://doi.org/10.1002/adfm.201705048
225. Douka, A.I., Xu, Y., Yang, H., et al.: A zeolitic-imidazole frameworks-derived interconnected macroporous carbon matrix for efficient oxygen electrocatalysis in rechargeable zinc-air batteries. Adv. Mater. **32**, e2002170 (2020). https://doi.org/10.1002/adma.202002170
226. Zhu, L., Zheng, D., Wang, Z., et al.: A confinement strategy for stabilizing ZIF-derived bifunctional catalysts as a benchmark cathode of flexible all-solid-state zinc-air batteries. Adv. Mater. **30**, e1805268 (2018). https://doi.org/10.1002/adma.201805268
227. Zhou, G.Z., Liu, G.S., Liu, X.B., et al.: 1D/3D heterogeneous assembling body as trifunctional electrocatalysts enabling zinc-air battery and self-powered overall water splitting. Adv. Funct. Mater. **32**, 2107608 (2022). https://doi.org/10.1002/adfm.202107608
228. Wang, Z.H., Jin, H.H., Meng, T., et al.: Fe, Cu-coordinated ZIF-derived carbon framework for efficient oxygen reduction reaction and zinc-air batteries. Adv. Funct. Mater. **28**, 1802596 (2018). https://doi.org/10.1002/adfm.201802596
229. Arafat, Y., Azhar, M.R., Zhong, Y.J., et al.: Advances in zeolite imidazolate frameworks (ZIFs) derived bifunctional oxygen electrocatalysts and their application in zinc-air batteries. Adv. Energy Mater. **11**, 2100514 (2021). https://doi.org/10.1002/aenm.202100514
230. Ban, J.J., Wen, X.H., Xu, H.J., et al.: Dual evolution in defect and morphology of single-atom dispersed carbon based oxygen electrocatalyst. Adv. Funct. Mater. **31**, 2010472 (2021). https://doi.org/10.1002/adfm.202010472
231. Huang, H., Yu, D., Hu, F., et al.: Clusters induced electron redistribution to tune oxygen reduction activity of transition metal single-atom for metal-air batteries. Angew. Chem. Int. Ed. **61**, e202116068 (2022). https://doi.org/10.1002/anie.202116068
232. Geng, Z.G., Liu, Y., Kong, X.D., et al.: N2 electrochemical reduction: Achieving a record-high yield rate of 120.9 μgNH3 mgcat−1 h−1 for N2 electrochemical reduction over Ru single-atom catalysts (adv mater. Adv. Mater. **30**, 1870301 (2018). https://doi.org/10.1002/adma.201870301
233. Chen, Y., Ji, S., Wang, Y., et al.: Isolated single iron atoms anchored on N-doped porous carbon as an efficient electrocatalyst for the oxygen reduction reaction. Angew. Chem. Int. Ed. **56**, 6937–6941 (2017). https://doi.org/10.1002/anie.201702473
234. Kong, F., Cui, X., Huang, Y., et al.: N-doped carbon electrocatalyst: Marked ORR activity in acidic media without the contribution from metal sites? Angew. Chem. Int. Ed. **61**, e202116290 (2022). https://doi.org/10.1002/anie.202116290
235. Xie, X., Peng, L., Yang, H., et al.: MIL-101-derived mesoporous carbon supporting highly exposed Fe single-atom sites as efficient oxygen reduction reaction catalysts. Adv. Mater. **33**, e2101038 (2021). https://doi.org/10.1002/adma.202101038
236. Yang, Z.K., Chen, B.X., Chen, W.X., et al.: Directly transforming copper (I) oxide bulk into isolated single-atom copper sites catalyst through gas-transport approach. Nat. Commun. **10**, 3734 (2019). https://doi.org/10.1038/s41467-019-11796-4
237. Wang, J., Huang, Z., Liu, W., et al.: Design of N-coordinated dual-metal sites: a stable and active Pt-free catalyst for acidic oxygen reduction reaction. J. Am. Chem. Soc. **139**, 17281–17284 (2017). https://doi.org/10.1021/jacs.7b10385
238. Xiao, M., Zhang, H., Chen, Y., et al.: Identification of binuclear Co_2N_5 active sites for oxygen reduction reaction with more than one magnitude higher activity than single atom CoN_4 site. Nano Energy **46**, 396–403 (2018). https://doi.org/10.1016/j.nanoen.2018.02.025
239. Hou, C.C., Zou, L., Xu, Q.: A hydrangea-like superstructure of open carbon cages with hierarchical porosity and highly active metal sites. Adv. Mater. **31**, e1904689 (2019). https://doi.org/10.1002/adma.201904689
240. Liu, S.H., Wang, Z.Y., Zhou, S., et al.: Metal-organic-framework-derived hybrid carbon nanocages as a bifunctional electrocatalyst for oxygen reduction and evolution. Adv. Mater. **29**, 1700874 (2017). https://doi.org/10.1002/adma.201700874
241. Lu, X.F., Chen, Y., Wang, S., et al.: Interfacing manganese oxide and cobalt in porous graphitic carbon polyhedrons boosts oxygen electrocatalysis for Zn-air batteries. Adv. Mater. **31**, e1902339 (2019). https://doi.org/10.1002/adma.201902339
242. Zhong, Y., Pan, Z., Wang, X., et al.: Hierarchical Co_3O_4 nano-micro arrays featuring superior activity as cathode in a flexible and rechargeable zinc-air battery. Adv. Sci. **6**, 1802243 (2019). https://doi.org/10.1002/advs.201802243
243. Xie, D., Yu, D., Hao, Y., et al.: Dual-active sites engineering of N-doped hollow carbon nanocubes confining bimetal alloys as bifunctional oxygen electrocatalysts for flexible metal-air batteries. Small **17**, e2007239 (2021). https://doi.org/10.1002/smll.202007239
244. Yang, M.J., Hu, X.H., Fang, Z.S., et al.: Bifunctional MOF-derived carbon photonic crystal architectures for advanced Zn-air and Li–S batteries: highly exposed graphitic nitrogen matters. Adv. Funct. Mater. **27**, 1701971 (2017). https://doi.org/10.1002/adfm.201701971
245. Zhu, Z., Yin, H., Wang, Y., et al.: Coexisting single-atomic Fe and Ni sites on hierarchically ordered porous carbon as a highly efficient ORR electrocatalyst. Adv. Mater. **32**, e2004670 (2020). https://doi.org/10.1002/adma.202004670
246. Gong, X.F., Zhu, J.B., Li, J.Z., et al.: Self-templated hierarchically porous carbon nanorods embedded with atomic Fe-N_4 active sites as efficient oxygen reduction electrocatalysts in Zn-air batteries. Adv. Funct. Mater. **31**, 2008085 (2021). https://doi.org/10.1002/adfm.202008085
247. Zhang, T.Y., Wang, Z.N., Zhu, A.P., et al.: Flexible, twistable and plied electrode of stainless steel cables@nickel-cobalt oxide with high electrochemical performance for wearable electronic textiles. Electrochim. Acta **348**, 136312 (2020). https://doi.org/10.1016/j.electacta.2020.136312
248. Wu, Z., Wang, Y., Liu, X., et al.: Carbon-nanomaterial-based flexible batteries for wearable electronics. Adv. Mater. **31**, e1800716 (2019). https://doi.org/10.1002/adma.201800716
249. Liu, Q.C., Chang, Z.W., Li, Z.J., et al.: Flexible metal-air batteries: progress, challenges, and perspectives. Small Methods **2**, 1700231 (2018). https://doi.org/10.1002/smtd.201700231
250. Ji, D., Fan, L., Li, L., et al.: Atomically transition metals on self-supported porous carbon flake arrays as binder-free air cathode for wearable zinc-air batteries. Adv. Mater. **31**, e1808267 (2019). https://doi.org/10.1002/adma.201808267

251. Pan, Z.H., Yang, J., Zang, W.J., et al.: All-solid-state sponge-like squeezable zinc-air battery. Energy Storage Mater. **23**, 375–382 (2019). https://doi.org/10.1016/j.ensm.2019.04.036
252. Xu, Y.Y., Deng, P.L., Chen, G.D., et al.: 2D nitrogen-doped carbon nanotubes/graphene hybrid as bifunctional oxygen electrocatalyst for long-life rechargeable Zn-air batteries. Adv. Funct. Mater. **30**, 1906081 (2020). https://doi.org/10.1002/adfm.201906081
253. Nguyen, T.T., Balamurugan, J., Kim, D.H., et al.: Hierarchical 3D oxygenated cobalt vanadium selenide nanosheets as advanced electrode for flexible zinc-cobalt and zinc-air batteries. Small **16**, e2004661 (2020). https://doi.org/10.1002/smll.202004661
254. Ma, L.T., Chen, S.M., Wang, D.H., et al.: Super-stretchable zinc-air batteries based on an alkaline-tolerant dual-network hydrogel electrolyte. Adv. Energy Mater. **9**, 1803046 (2019). https://doi.org/10.1002/aenm.201803046
255. Goldstein, J., Brown, I., Koretz, B.: New developments in the Electric Fuel Ltd. zinc/air system. J. Power Sources **80**, 171–179 (1999). https://doi.org/10.1016/S0378-7753(98)00260-2
256. Li, Y.J., Cui, L., Da, P.F., et al.: Multiscale structural engineering of Ni-doped CoO nanosheets for zinc-air batteries with high power density. Adv. Mater. **30**, e1804653 (2018). https://doi.org/10.1002/adma.201804653
257. Song, Z.S., Ding, J., Liu, B., et al.: Zinc-air batteries: a rechargeable Zn-air battery with high energy efficiency and long life enabled by a highly water-retentive gel electrolyte with reaction modifier. Adv. Mater. **32**, 2070172 (2020). https://doi.org/10.1002/adma.202070172
258. Thomas Goh, F.W., Liu, Z.L., Hor, T.S.A., et al.: A near-neutral chloride electrolyte for electrically rechargeable zinc-air batteries. J. Electrochem. Soc. **161**, A2080–A2086 (2014). https://doi.org/10.1149/2.0311414jes
259. Chen, C.Y., Matsumoto, K., Kubota, K., et al.: Zinc-air batteries: a room-temperature molten hydrate electrolyte for rechargeable zinc-air batteries. Adv. Energy Mater. **9**, 1970086 (2019). https://doi.org/10.1002/aenm.201970086
260. Li, S., Cheng, C., Thomas, A.: Carbon-based microbial-fuel-cell electrodes: from conductive supports to active catalysts. Adv. Mater. **29**, 1602547 (2017). https://doi.org/10.1002/adma.201602547
261. Pan, J., Xu, Y.Y., Yang, H., et al.: Advanced architectures and relatives of air electrodes in Zn-air batteries. Adv. Sci. **5**, 1700691 (2018). https://doi.org/10.1002/advs.201700691
262. Wei, Y.T., Shi, Y.C., Chen, Y., et al.: Development of solid electrolytes in Zn-air and Al-air batteries: from material selection to performance improvement strategies. J. Mater. Chem. A **9**, 4415–4453 (2021). https://doi.org/10.1039/d0ta11068j
263. Chen, P., Zhang, K., Tang, D., et al.: Recent progress in electrolytes for Zn-air batteries. Front. Chem. **8**, 372 (2020). https://doi.org/10.3389/fchem.2020.00372

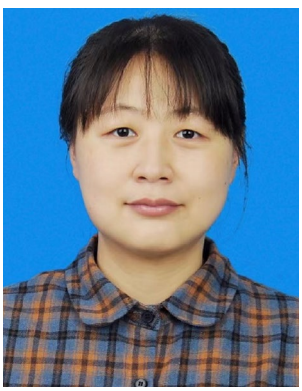

Wenjie Shao is currently a doctoral student at the College of Polymer Science and Engineering, Sichuan University. Her research interest is synthesizing functional nanomaterials related to electrocatalysis in energy conversion, such as water splitting and fuel cells.

Rui Yan received his M.S. degree from Central China Normal University in 2018. He is now a doctoral student at Sichuan University. His research focuses on the high-performance catalyst and the catalytic mechanism in lithium-sulfur batteries.

Mi Zhou is now a full senior experimentalist in the college of biomass science and engineering, Sichuan University. She received her Ph.D. in polymer science and engineering from Sichuan University, China in 2016. Her research interests focus on polymer structure and properties, preparation, and application of biomass polymer material and cellulose nanocomposites.

Lang Ma is now an associate professor at Sichuan University. He obtained his B.S. and Ph.D. degrees from Sichuan University, China, in 2012 and 2016, respectively. His current research interests include the design and fabrication of polymer-functionalized nanomaterials and nanocatalytic materials, and their applications in medical and environmental science fields.

Christina Roth is a trained materials scientist and chair holder at the engineering science faculty of the Universität Bayreuth, where she specializes in electrochemical process engineering. Her research interests are in the areas of fuel cells, redox flow batteries, lithium-ion batteries, and CO_2 electro-reduction, with a focus on operando spectroscopy and dedication towards the structuring of 3D porous electrodes.

Tian Ma is now a postdoctoral research fellow at Sichuan University. She obtained her Ph.D. degree in Chemistry from Jacobs University Bremen in 2019. Her current research interests include the design and fabrication of functionalized polyoxometalates-based/derived catalytic materials, and their applications in electrocatalytic and energy fields, such as water splitting and fuel cells.

Sujiao Cao is a postdoctoral research fellow at Sichuan University. She received her Ph.D. degree from Sichuan University in 2019. Her current research focuses on synthesizing porous carbon based-electrocatalysts and biocatalysts with atomically controlled structures for both medical and energy applications.

Chong Cheng is currently a full professor in the department of polymer science at Sichuan University. He obtained his B.Sc. and Ph.D. from Sichuan University. After a research stay at the University of Michigan, Ann Arbor, USA, he joined the Freie Universität Berlin as an AvH research fellow. His current scientific interests include fabricating advanced low-dimensional materials and organic frameworks for nanomedicines, antibacterial materials, stem cell scaffolds, energy storage devices, and electrocatalysts, especially the cutting-edge catalytic applications of coordination polymers and metal-organic frameworks. He has published over 160 SCI papers, including *Nature Materials, Nature Communications, Science Advances*, and *Advanced Materials*.

Bo Yin received his Bachelor and Ph.D. degrees from the college of polymer science and engineering at Sichuan University in 2002 and 2007, respectively. He now works as a professor at the college of polymer science and engineering at Sichuan University and focuses on polymer engineering and modification, especially in the morphology evolution and control during polymer composite processing and the correlation between polymer composite structure and properties, with applications, lie in various aspects like sensor, nano-generators and shape-memory materials, etc.

Shuang Li received her Bachelor's degree from Sichuan University, Master's degree from Shanghai Jiao Tong University and Ph.D. from Technische Universität Berlin. She has been doing independent research funded by Technische Universität Berlin, UniSysCat, and Deutsche Forschungsgemeinschaft (DFG) from the year of 2019 to 2021. Currently, she is appointed as a full professor in the College of Polymer Science and Engineering at Sichuan University. Her current research focuses on synthesizing metal-organic hybrid precursors for the designing of hybrid catalysts with atomic-scale controlled structures, and their applications in catalysis, including water splitting, fuel cells, CO_2 reductions, and metal-sulfur batteries.